INTERNATIONAL ATOMIC ENERGY AGENCY
UNITED NATIONS EDUCATIONAL, SCIENTIFIC AND CULTURAL ORGANIZATION
INTERNATIONAL CENTRE FOR THEORETICAL PHYSICS
I.C.T.P., P.O. BOX 586, 34100 TRIESTE, ITALY, CABLE: CENTRATOM TRIESTE

H4.SMR/642 - 23

College on Methods and Experimental Techniques in Biophysics

28 September - 23 October 1992

Protein Dynamics

H. FRAUENFELDER
University of Illinois, U.S.A.

From DEBRUNNER – FRAUENFELDER

Physics of Biomolecules

17
CONFORMATIONAL SUBSTATES

Some remarks about history.

Up to now we have treated proteins as if they possessed a unique structure, completely defined by the primary sequence. Theory and experiment both indicate, however, that such a picture is oversimplified. We therefore discuss here the idea of conformational substates. A protein in a given conformation has a well-defined biological function. We will show that it can exist in a large number of structurally slightly different substates even in a given conformation. Here we first summarize the conclusions, then give some simple examples of substates, discuss some of the concepts underlying the study of substates, and finally show how conformational substates can be investigated by X-ray diffraction.

The actual situation in proteins and very likely also in nucleic acids is more complex than discussed in the present chapter and we will return to the problem again later.

1. Theoretical Arguments

A strong indication that proteins may have a highly degenerate ground state comes from the estimate of the fluctuations in internal energy E, entropy S, and volume V. In Appendix B, it is shown that these fluctuations are large.[1] Large fluctuations imply many states accessible at the temperature under consideration.

A second argument for the existence of many substates comes from considering imperfections. In Appendix B, we derive the expression

$$n/N = \exp[\Delta S_p/k_B] \exp(-H_p/k_BT) \qquad (17.1)$$

for the fraction n/N of imperfections in a solid. The first term is larger than 1. In solids, H_p, the enthalpy of creating an imperfection, is of the order of 0.5 eV≙50 kJ/mol and $n/N = 10^{-10}$. In a biomolecule, however, the bonds are much weaker. A typical hydrogen bond is of the order of a few kJ/mol and n/N becomes of the order of 0.1. Thus the number of imperfections in a biomolecule is very large. As we will see, the term "imperfection" is misleading–it is simply substates that we are considering.

A third argument follows the lines of Landau-Lifshitz. The number of states, W, is connected to the entropy of a body by the Boltzmann relation

$$W = \exp(S/k_B). \qquad (17.2)$$

As we will see in the next section,, an amino acid will have a few states with approximately equal energy. Take $W_i \approx 2$–3 for an individual amino acid. Assume that there are N amino acids in the protein. Eq. (17.2) demonstrates that $W = \prod_i w_i$ because entropy is additive. Thus

$$W = (2\text{-}3)^N \approx 10^{50}. \qquad (17.3)$$

A fourth argument is based on folding. A protein may fold in a time that is as short a ms. Computations indicate that the time required to find the lowest energy state is very much longer. A solution to this paradox is to postulate substates. [Levinthal paradox].

We can sum up the arguments by stating that the unique physical characteristics of a biomolecule (small size, strong and weak forces) lead to the existence of many ~~conformational substates. These are states that all have the same biological function, but slighly different structures. In the next section we will look at some of the possible differences.~~

2. Rotational Isomers[2-4]

We discuss here one particular realization of different energy levels in a complex molecule, namely rotational isomers. Consider heme, shown in Fig. 4.9. It can be simplified to the structure in Fig. 17.1.

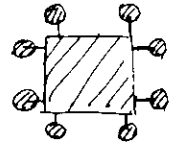

Fig. 17.1 Heme simplified. The central part is planar. A number of groups are attached by single bonds.

conformational substates. Substates have slightly different structures, but perform the same function, but possibly with different rates. We call them **substates** because most proteins perform some function that requires more than two states, for instance hemoglobin with and without bound dioxygen. Each state then can exist in a large number of conformational substates.

The central part can be represented by one planar ring. Attached to it by single bonds are 8 groups. These groups can rotate around single bonds as indicated schematically in Fig. 17.2.

Fig. 17.2 Rotational isomers for a CH_3 group attached to the heme central part.

The potential as a function of the rotation angle ϕ is similar to the one shown in Fig. 17.3 for ethane. In the case of CH_3, there are three minima and three barriers; the minima have equal energies. The other four groups are not as symmetric and the number of minima and their energy values are more difficult to obtain. Still, the basic feature must remain, namely the existence of rotational isomers. Some data for barrier heights are collected in Table 17.1.

Fig. 17.3

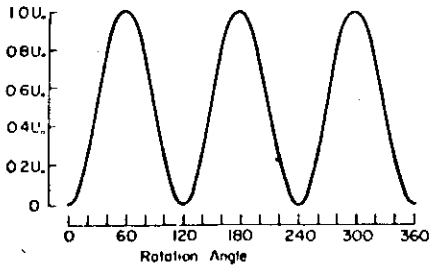

Rotational Potential Energy of Ethane. (C_2H_6)
Drawing of the potential $U = (U_0/2)(1 - \cos 3\phi)$.

Simplify

Table 17.1 Some Barriers to Internal Rotation[a]

Formula	Name	$U^{(3)}$ (kcal/mole)[b]	State
CH_3-CH_3	Ethane	2.875 ± 0.125	Gas
CH_3-CH_2F	Ethyl fluoride	3.33 ± 0.05	Gas
CH_3-CH_2Cl	Ethyl chloride	3.68	Gas
CH_3-CH_2Br	Ethyl bromide	3.68	Gas
CH_3-CH_2I	Ethyl iodide	3.22 ± 0.5	Gas
CF_3-CF_3	Hexafluoroethane	3.92	Gas
CCl_3-CCl_3	Hexachloroethane	10.8	Gas
$CH_3-C\equiv C-CH_3$	Dimethylacetylene	≤0.03	Gas
CH_3-CH_2OH	Ethanol	0.77 - 0.1	Gas
C_2H_5-OH	Ethanol[c]	0.8	Gas
CH_3-SiH_3	Methylsilane	1.70 - 0.1	Gas
CH_3-SiF_3	Methyltrifluorosilane	1.4 ± 0.2	Gas
$(CH_3-)_4Si$	Tetramethylsilane	1.4 ± 0.1	Gas
CH_3-GeH_3	Methylgermane	1.24 ± 0.025	Gas
$(CH_3-)_4Ge$	Tetramethylgermane	0.65	Solid
$(CH_3-)_4Sn$	Tetramethylstannane	0.46	Solid
$(CH_3-)_4Pb$	Tetramethyllead	0.18	Solid
CH_3-NH_2	Methylamine	1.98 0.01	Gas
$(CH_3-)_2NH$	Dimethylamine	3.62 ± 0.05	Gas
$(CH_3-)_3N$	Trimethylamine	4.41 - 0.03	Gas
CH_3-OH	Methanol	1.07 - 0.02	Gas
CH_3-O-CH_3	Dimethyl ether	2.7 ± 0.15	Gas
$(CH_3-)_2SO$	Dimethyl sulfoxide	2.94	Gas
CH_3-SCN	Methyl thiocyanate	1.59 ± 0.08	Gas
CH_3-SeH	Methyl selenol	1.01 ± 0.05	Gas
$(CH_3-)_3B$	Trimethylborane	0	Gas
$(CH_3-)_2Zn$	Dimethylzinc	0	Gas
CH_3-NO_2	Nitromethane[d]	0.00403	Gas
$CH_3-C_6H_5$	Methylbenzene[d]	0.0139	Gas
$C_6H_5CH_2-CH_3$	Ethylbenzene[e]	2.7	Gas
$C_6H_5-C_2H_5$	Ethylbenzene[e]	1.3	Gas
$OHC-NH_2$	Formamide	18 ± 3	Solid

1 kcal/mol = 0.043 eV = 4.18 kJ/mol.

[a] Excerpt from Table II of Lowe (1968).
[b] The definition of $U^{(3)}$ is given in Eq. (21).
[c] The potential form is not molecular symmetry-dictated and is thus an approximation.
[d] $U^{(3)}$ is zero for reasons of symmetry; see below; the value given refers to $U^{(6)}$.

Since each of the eight groups shown for heme can be in a different rotational state, and since two groups (CH_2-CH_2-CO_2) have two more single bonds around which rotations are possible, the number of different states for heme is very large. We can describe each possible configurational state by a configuration coordinate c. The Gibbs energy as a function of the configuration coordinate c then will look about as shown in Fig. 17.4.

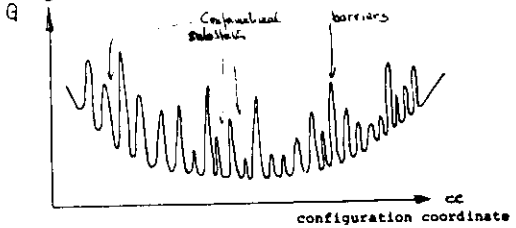

Fig. 17.4 Energy of the heme group as a function of configuration coordinate. (Schematic.)

Heme thus can exist in a large number of configurational states that are different in the rotational position of the side groups.

The number of states in a protein is even larger than in heme. Consider for instance a piece of the backbone, as indicated in Fig. 17.5. Assume that the two C_α atoms at the ends are held fixed at a distance L. The flexibility and the number

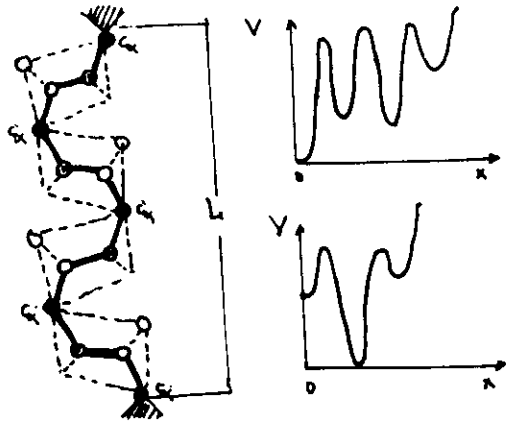

Fig. 17.5 Part of the polypeptide backbone. The endatoms are held fixed at a distance L. Two possible potentials for one particular atom are shown at right.

of states then depend markedly on L.[5] At some distances L, the chain is rather rigid, at others very flexible. To describe the possible states, we draw for each atom a potential energy curve. The shape of the curves will depend on L, on sidechains, and on neighboring chains. The main result is the realization that the total number of quasistationary states for a protein is very large.

3. Conformational Relaxation

The barrier between any two states depends on the particular property that must change. Table 17.1 indicates that for rotations, barrier heights between about 1 and 100 kJ/mol occur. Depending on temperature and on the state of the surrounding, two extreme cases exist:

1. Solid surrounding, low temperature, such that

$$k_B T << G_{barrier} \qquad (17.4)$$

Each protein will then be frozen in a particular conformational substate, with the population of the various substates depending on the temperature at which freezing occurred. The entire system is not in equilibrium.

2. Liquid surrounding, high temperature such that

$$k_B T \geq G_{barrier} \qquad (17.5)$$

Conformational relaxation takes place: each biomolecule changes rapidly from one conformational substate to another, it "breathes". Typical relaxation times can be of the order of ns or faster; any observation that takes longer averages over the entire population.

4. Remarks about the Mössbauer Effect

The effect of conformational substates can be seen in many dynamic experiments, such as NMR, fluorescence, hydrogen exchange, and flash photolysis. Is it also possible to see structural effects? We will show here that such observations are indeed possible. To do so we return to the theory of X-ray diffraction. At the same time, we add some remarks about the Mössbauer effect.

We begin with the simplest case, the emission of a γ ray by a very heavy nucleus fixed rigidly in a lattice, as shown in Fig. 17.5. Since a rigidly fixed nucleus cannot recoil, the emitted photon takes the full transition energy and possesses the natural line width.

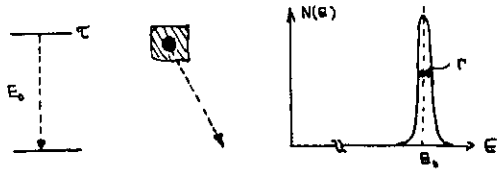

Fig. 17.6 Emission of a γ ray with total transition energy E_0 by a nucleus fixed rigidly in a lattice. The emitted photon has the full energy and natural line width.

The natural line width is given by the uncertainty relation as

$$\Gamma = \hbar/\tau, \qquad (17.6)$$

where τ is the mean life. Classically speaking, the photon is emitted during the time τ and thus is a wave of "length" $c\tau$. The nuclide most often used in Mössbauer experiments, ^{57}Fe, has a transition energy $E_0 = 14.4$ keV and a mean life $\tau = 1.5 \cdot 10^{-7}$ s. The natural line width is $\Gamma = 4.5 \cdot 10^{-9}$ eV, the length $c\tau = 4.5$ m, and $\Gamma/E_0 = 3 \cdot 10^{-13}$.

If the nucleus is not fixed rigidly, but can move in a region of linear dimension $x_{RMS} = \langle x^2 \rangle^{1/2}$, the situation is very different. Part of the wavetrain will originate at one part of this region, another from a different one. The wavetrain will no longer be fully coherent; interference between different parts is reduced or destroyed. The situation is sketched in Fig. 17.7. The problem can be treated classically[6] or quantum mechanically,[7] with essentially the

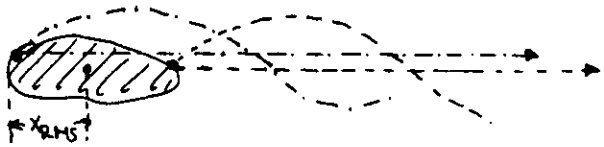

Fig. 17.7 Classical emission of a photon from an extended (vibrating) source. Coherence is partially destroyed.

same result: A certain fraction f of all gamma rays is emitted without energy loss and without line broadening (Mössbauer line); the rest (1-f) is greatly broadened and has energy different from E_0 (Fig. 17.8). The fraction f (called the Lamb-Mössbauer factor) is given by[8-10]

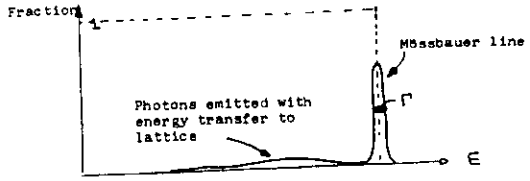

Fig. 17.8 Mössbauer line and γ rays emitted with energy loss.

$$f = \exp(-\langle x^2 \rangle / \lambda^2), \qquad (17.7)$$

Here $\langle x^2 \rangle$ is the mean square displacement of the emitting nucleus in the direction of the gamma ray and $\lambda = \lambda/2\pi$ is the reduced wavelength of the gamma ray. Eq. (17.7) can be understood intuitively, by looking at Fig. 17.7. If $\langle x^2 \rangle \ll \lambda^2$, all photons are emitted from the same point, interference is perfect, and f = 1. If $\langle x^2 \rangle \gg \lambda^2$, very little constructive interference remains and f ≈ 0. Eq. (17.7) is rigorous only for harmonic potentials. We will, nevertheless, use it here for all potentials.

5. The Debye-Waller Factor

We now return to X-ray diffraction. Rereading of the derivation leading to Eq. (10.20) (10.16), the structure factor equation, shows that the derivation implied fixed atoms. We depict the situation in Fig. 17.9a. Atoms, however, move. The problem of temperature motion was taken up as early as 1914 by Debye,[11] and again by Waller.[12] Since then, the problem has been discussed by many authors.[13-17] In Fig. 17.9b, two atoms are shown, each moving

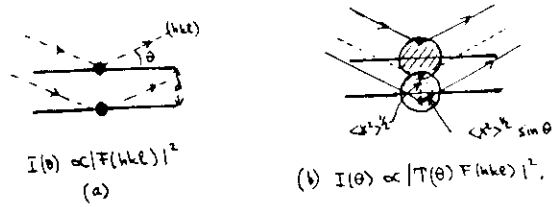

Fig. 17.9 (a) Diffraction from fixed atoms. (b) Atoms vibrate about their equilibrium position.

within a volume characterized by the mean square radius $\langle x^2 \rangle$. The charge density $\rho(\vec{r})$ in Eq. (10.4) must be replaced by

$$\rho(\vec{r}) \rightarrow \int g(\vec{r}') \rho(\vec{r}-\vec{r}') \, d^3r' \qquad (17.8)$$

where $g(\vec{r})$ describes the probability distribution of the atom. Since the Fourier transform of a convolution is equal to the product of the Fourier transforms of the two functions, we obtain the replacement

$$f(\vec{q}) \rightarrow f(\vec{q})\, T(\vec{q}). \qquad (17.9)$$

T(q), the Fourier transform of $g(\vec{r})$, is called the *temperature or Debye-Waller factor*. With Eq. (17.9), Eq. (10.20) becomes

$$I(hk\ell) = \text{const}\; T^2(\vec{r})\, |F(hk\ell)|^2. \qquad (17.10)$$

Assuming isotropic harmonic vibrations about the equilibrium positions, $T(\vec{q})$ can be calculated easily:

$$T(\theta) = \exp(-W(\theta)) \qquad (17.11)$$

$$W(\theta) = 2 \sin^2\theta \, \langle x^2 \rangle / \lambda^2. \qquad (17.12)$$

In the X-ray literature, instead of $\langle x^2 \rangle$ one often quotes

$$B = 8 \pi^2 \langle x^2 \rangle . \qquad (17.13)$$

In proteins many atoms are spread out about their mean positions in a non-harmonic manner. Eq. (17.11) then may be a bad approximation or it may not fit the data at all. The problem has been studied in a few papers,[10,18,19] but much work remains to be done.

The Lamb-Mössbauer factor Eq. (17.7) and the Debye-Waller factor Eq. (17.11) are closely related. In the Mössbauer effect, interference occurs "within one atom" and only $\langle x^2 \rangle$ appears in the exponent. In X-ray diffraction, the X-rays scattered from different atoms interfere and the path difference between two trajectories, for instance the solid and the dashed ones in Fig. 17.9b, is given by $2 \sin^2\theta \langle x^2 \rangle$. Moreover, f describes only emission (or absorption) while X-ray scattering always involves absorption and reemission; the factor T in Eq. (17.10) consequently appears squared.

The determination of $T(\theta)$ and hence $\langle x^2 \rangle$ for each atom in a protein is in principle straightforward. In practice, however, very good diffraction data are required.

6. The Debye-Waller Factor in Proteins[20]

Eq. (17.10) shows that $I(\theta)$ drops with increasing angle because of the decreasing factor F *and* the decreasing $T(\theta)$. Originally, the factor T(r) was considered to arise entirely from the vibrations about the equilibrium positions. In proteins, $\langle x^2 \rangle$ calculated from the measured values of T turned out to be rather large and the unsatisfactory results were blamed on "bad crystals." However, the actual situation is far more interesting than appeared at first.[21] To discuss the problem in a zeroth approximation we ask: What phenomena can contribute to $\langle x^2 \rangle$? After some thinking, we can write

$$\langle x^2 \rangle = \langle x^2 \rangle_c + \langle x^2 \rangle_d + \langle x^2 \rangle_{\lambda d} + \langle x^2 \rangle_v . \qquad (17.14)$$

Here c refers to conformational substates, *d* to diffusion, *λd* to *l*attice *d*isorder, and v to vibrations. The first term comes from the fact that a given atom in a protein can be in many different conformational substates. To the X-rays, the various substates will appear as a larger $\langle x^2 \rangle$. The second term can usually be neglected in X-ray work. If diffusion were important, the X-ray pattern would not be sharp. The third term is caused by imperfections in the crystals and we assume that it is temperature independent and the same for all atoms in the protein. The last term comes from vibrations about the equilibrium position. With Eq. (17.14), $T(\theta)$ in Eq. (17.10) is no longer caused only by temperature motion.

In some favorable cases, X-ray diffraction and Mössbauer effect together permit determination of the conformational distribution. From the X-ray intensities, $\langle x^2 \rangle$ is determined for all atoms in a crystal, if possible at many temperatures. Neglecting diffusion, $\langle x^2 \rangle$ is then given by three terms in Eq. (17.14). If the protein contains an iron atom, the Mössbauer effect can be used to determine the recoilless fraction f. At temperatures where conformational relaxation takes place, $\langle x^2 \rangle$ for the Mössbauer effect contains only two terms, v and c. Lattice disorder is not important, because each iron atom acts independently. Thus from f we can find $\langle x^2 \rangle$ which is given by

$$\langle x^2 \rangle_{Mö} = \langle x^2 \rangle_c + \langle x^2 \rangle_v . \qquad (17.15)$$

Thus $\langle x^2 \rangle_X - \langle x^2 \rangle_{Mö} = \langle x^2 \rangle_{\lambda d}$, the lattice disorder term can be obtained! Once it is known, we can find $\langle x^2 \rangle_{cv} \equiv \langle x^2 \rangle_c + \langle x^2 \rangle_v$ for all atoms. The separation of the conformational and the vibrational term requires measurements over a wide temperature range. However, for the function of a protein, the sum of the two terms is important and not the individual one. We will therefore in the following discuss the behavior of $\langle x^2 \rangle_{cv}$. Before looking at some specific examples we note that computer studies[19] show that the standard evaluation of the Debye-Waller factors gives values for $\langle x^2 \rangle$ that are too small. The actual excursions of atoms in proteins consequently are larger than indicated in the following figures.

A number of proteins have already been explored as discussed above.[20-24] We present here only a few examples from studies of myoglobin. The initial work on

Mb[21] already indicated that protein structural fluctuations are much larger and much more complex than initially anticipated. Fig. 17.10 shows the backbone of Mb. The shaded area gives the region reached by fluctuations. It is defined such that fluctuations have a 1% probability of reaching outside the shaded area. The previous arguments indicate, however, that the evaluation underestimates the motions; the actual displacements may be considerably larger than shown. Fig. 17.10 demonstrates that fluctuations are not uniform as they would be in a solid.

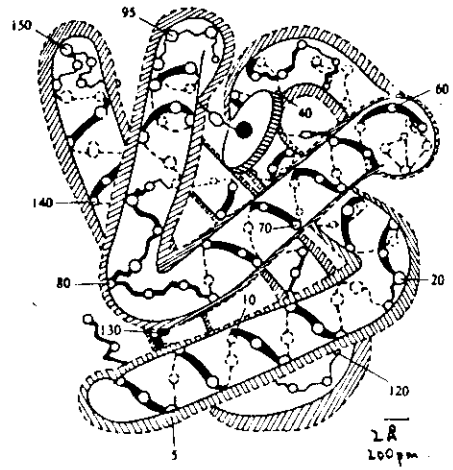

Fig. 17.10 Backbone of myoglobin. The circles indicate the positions of the alpha carbons. Displacements of backbone non-hydrogen atoms have a 1% probability of reaching outside of the shaded region.[21]

in some regions, they are very small, in others, for instance at the corner near 120 (GH corner), they are large.

In Fig. 17.11, the displacements are shown in a different manner. The upper part gives ~~shown~~ $\langle x^2_{cv} \rangle$ at room temperature for the backbone, the lower part shows the largest displacement for each sidechain as a function of residue number.

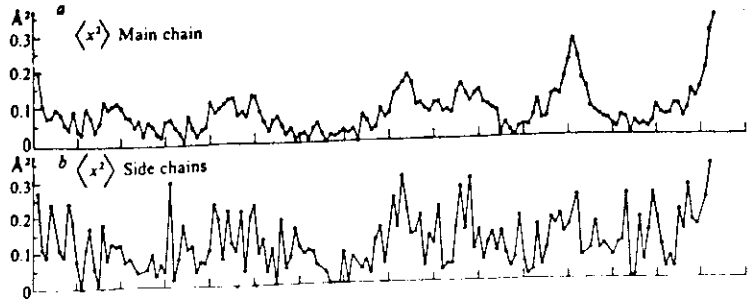

Fig. 17.11 The conformational and vibrational displacement $\langle x^2 \rangle_{cv}$ for myoglobin. The upper part gives the average values for the three mainchain (backbone) atoms C_α, C, N. The lower presents the largest $\langle x^2 \rangle_{cv}$ in each sidechain.[21]

In Fig. 17.12, $\langle x^2 \rangle$ is displayed for the atoms of a particular sidechain, LYS 96, for two related myoglobin forms, Met Fe and Oxy Co. In Met Fe, the iron is in the Fe^{+++} form and no ligand is bound. In Oxy Co, the iron is replaced by a cobalt atom and an oxygen molecule is bound.[25]

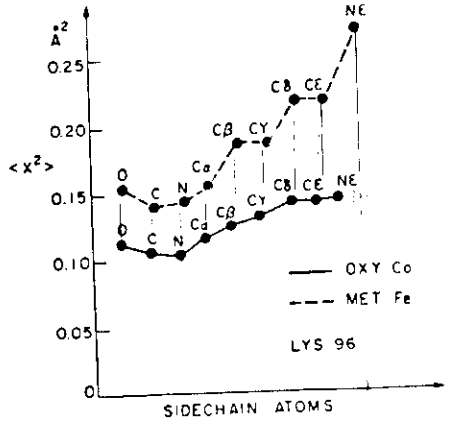

Fig. 17.12 Mean-square displacements for the atoms of LYS 96 for two different myoglobin forms.[25]

More information concerning conformational substates comes from the temperature dependence of $\langle x^2 \rangle$ [21] In a solid, $\langle x^2 \rangle$ has a temperature dependence as shown in Fig. 17.13a. Below the Debye temperature T_D, $\langle x^2 \rangle$ is constant, above TD it has a constant slope with an intercept that goes through zero. In a protein the situation can be very different as suggested in Fig. 17.13b. If substates indeed exist and are frozen at very low temperature, the intercept of the intermediate temperature regime should not pass through zero, but should indicate the value of $\langle x^2 \rangle$ of the substates in the low-temperature limit. At temperatures where transitions among substates can occur, and where substates with higher energies are populated, $\langle x^2 \rangle$ could increase dramatically.

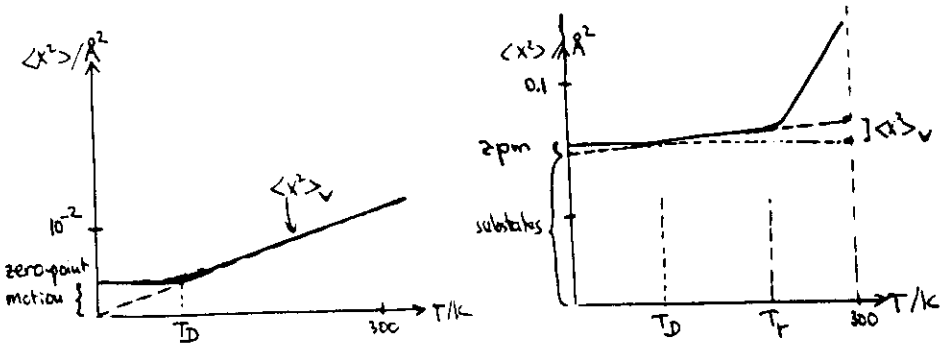

Fig. 17.13 Temperature dependence of $\langle x^2 \rangle$. (a) Debye solid. (b) Protein with substates.

Protein diffraction at low temperatures is not trivial; the crystals can deform or shatter. Two techniques have been developed to avoid this problem. Down to about 200 K, the mother liquor is replaced by a cryoprotectant.[26,27] Protein crystals can be brought to even lower temperatures by shock freezing (plunging it into liquid propane).[28] The low-temperature data indeed display the expected behavior.[20,21,29] The mean square displacements for the backbone of myoglobin at 300 and at 77 K are shown in Fig. 17.14 as example.[29]

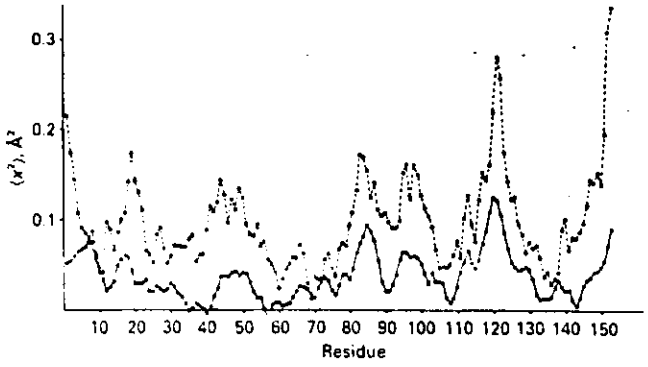

Fig 17.14

Average backbone $\langle x^2 \rangle$ values for myoglobin vs residue number. ●, 80 K; ○, 300 K. The average is taken over the N, C_α, and carbonyl C atoms only, since the $\langle x^2 \rangle$ values of the carbonyl O atoms are usually higher. An $\langle x^2 \rangle_{is}$ of 0.045 Å² has been subtracted from the individual observed $\langle x^2 \rangle$ values. [29]

The results already obtained and shown in part in Figs. 17.10-12 and 16.14 indicate that substates exist and that different parts of a protein display very different spatial fluctuations. The fluctuations are large compared to solids.

Karplus and collaborators have investigated the mean square deviations from equilibrium in some proteins by molecular dynamics calculations.[30] A typical result is shown in Fig. 17.15. The similarity to the experimental data is obvious.

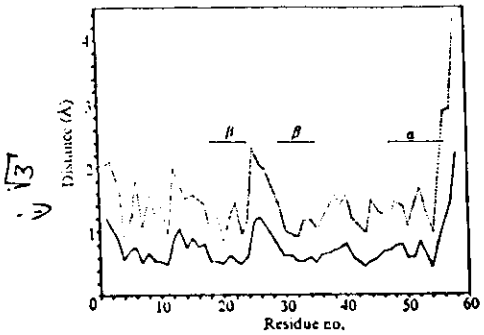

Fig. 17.15

. R.m.s. displacements (——) and maximum displacements (. . . .) of the α carbons, relative to the dynamical average structure.

(McCammon, Gelin, and Karplus[30])

7. Thermal Expansion and Compressibility

X-rays, as we have shown so far, yield the static structure of proteins and provide detailed information about the spatial fluctuations. X-ray diffraction can provide also ~~even more information: it can~~ be used to investigate the thermal expansion and the compressibility of proteins.

For a homogeneous isotropic system, the isothermal compressibility is defined by

$$\beta_T = -\frac{1}{V}\left(\frac{\partial V}{\partial P}\right)_T, \tag{17.16}$$

the linear thermal expansion coefficient by

$$\alpha = \frac{1}{l}\frac{\partial l}{\partial T}. \tag{17.17}$$

Empirically, the two coefficients are connected by the Grüneisen relation,

$$\alpha = \frac{1}{3}\gamma\beta_T c_V. \tag{17.18}$$

Here, l is the linear dimension, V the volume of the system; c_V is the specific heat and γ the Grüneisen parameter.

The overall compressibility and expansion of proteins can be measured by standard techniques.[31,32] For myoglobin, the values are

$$\beta \approx 10^{-10}\ \mathrm{m^2N^{-1}}, \quad \alpha \approx 140\cdot10^{-6}\ \mathrm{K^{-1}}. \tag{17.19}$$

Proteins are, however, not isotropic and homogeneous. X-rays permit the detailed study of compressibility and thermal expansion. To study the differential compressibility, the X-ray structure of a protein is determined at different pressures.[33] To find the expansion coefficient, the structure of a protein is carefully measured at different temperatures.[34,35] The change in the distances among atoms then permits the calculation of α and β, not just for the overall protein, but also for different regions and directions: α and β no longer are scalars, they become tensor fields! The amount of detailed information obtained is staggering and the best method by which to extract meaningful information is not yet obvious. The overall result, however, is clear. The average values of α and β obtained by these X-ray techniques agree with the values (Eq. (17.19)) from standard approaches.

Some data on b are summarized in Fig. 17.16, some data on α are given in Table 17.2.

Table 17.2 Expansion, compressibility, and specific heat, near 300 K.[35]

Substance	β $10^{-6}K^{-1}$	α $10^{-12}m^2N^{-1}$	c_V J/cm^3K
Cu	17.5	7.2	3.4
Mb	115	85	1.8
H_2O	70	450	4.18
Benzene	410	950	1.5

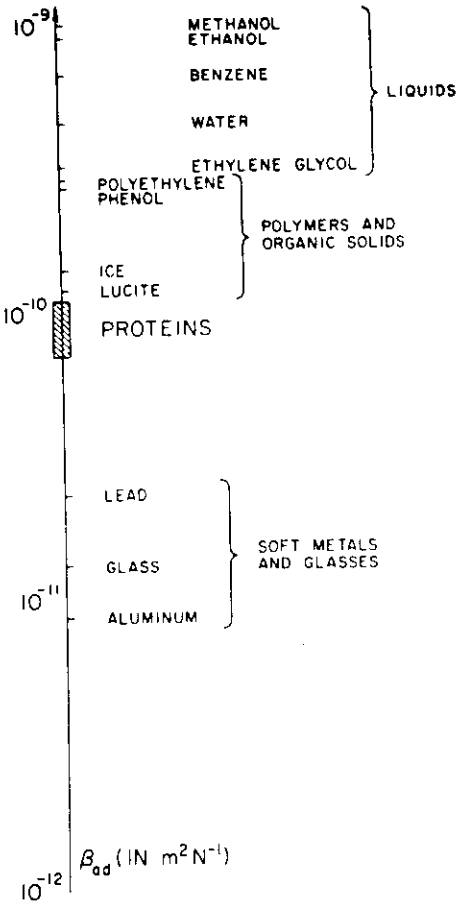

Fig. 17.6 Schematic representation of adiabatic compressibility values for varous substances (ref. 31).

8 Summary

The results emerging from Debye-Waller factor studies and also from detailed structure determinations can be summarized as follows :

A given primary sequence does not lead to a unique tertiary structure, but to a very large number of slightly different structures. The result can be described in different words by saying that a given protein can be in a large number of different conformational substates. Different substates perform the same function, but possibly with different rates. Some may even be inactive.

In some cases, the X-ray data are good enough so that atoms can be seen to occupy different positions. In extreme cases, entire side chains are in different positions. Example : George Phillips MbCO at different pH.

1. A. Cooper, Proc. Natl. Acad. Sci. USA 73, 2740-2741 (1976).
2. B. Wunderlich, *Macromolecular Physics*, Acad. Press, 1973, p. 62.
3. P. J. Flory, *Statistical Mechanics of Chain Molecules*, Wiley, 1969.
4. J. P. Lowe, Progr. Phys. Org. Chem. 6, 1 (1968).
5. B. Gavish, Biophys. Struct. Mechanism 4, 37-52 (1978).
6. F. L. Sh. piro, Soviet Phys. Uspekhi 3, 881 (1961).
7. H. Frauenfelder, *The Mössbauer Effect*, Benjamin, 1962. Mössbauer Spectroscopy, Ed. U. Gonser, Springer, Berlin. I (1975), II (1981).
8. K. S. Singwi and A. Sjölander, Phys. Rev. 120, 1093-1102 (1960).
9. H. J. Lipkin, Ann. Physics NY 26, 115-121 (1964).
10. J. G. Dash, D. P. Johnson, and W. M. Visscher, Phys. Rev. 168, 1087-1094 (1968).
11. P. Debye, Ann. Physik 43, 49 (1914).
12. I. Waller, Z. Physik 17, 398 (1923).
13. F. C. Blake, Rev. Mod. Phys. 5, 169 (1933).
14. A. H. Compton and S. K. Allison, *X-Rays in Theory and Experiment*, Van Nostrand, 1935, p. 437.
15. R. W. James, *Optical Principles of the Diffraction of X-Rays*, London, 1948.
16. B. T. M. Willis and A. W. Pryor, *Thermal Vibrations in Crystallography*, Cambridge Univ. Press, 1975.
17. J. D. Dunitz, *X-Ray Analysis and the Structure of Organic Molecules*, Cornell Univ. Press, 1979.
18. J. A. Krumhansl, *Anharmonicity and Debye-Waller factors in Biomolecules*, Proceedings ~~Conference on~~ Protein Structure, ~~in press~~. Molecular and Electronic Reactivity. Ed. R. Austin et al. Springer, 1987.
19. J. Kuriyan, G. A. Petsko, R. M. Levy, and M. Karplus, *The Effect of Anisotropy and Anharmonicity and Protein Crystallographic Refinement: An Evaluation by Molecular Dynamics*, J. Mol. Biol., ~~submitted~~.
20. G. A. Petsko and D. Ringe, *Fluctuations in Protein Structure from X-Ray Diffraction*. Ann. Rev. Biophys. Bioeng. 13, 331-371 (1984).
21. H. Frauenfelder, G. A. Petsko, and D. Tsernoglou, Nature 280, 558-563 (1979).
22. K. D. Watenpaugh, L. C. Sieker,, and L. H. Jensen, J. Mol. Biol. 138, 615-633 (1980).
23. T. Takano and R. E. Dickerson, in *Interaction between Iron and Protein in Oxygen and Electron Transport* C. Ho, ed., Elsevier, 1981.
24. S. Sheriff, W. A. Hendrickson, R. E. Stenkamp, L. C. Sieker, and L. H. Jensen, Proc. Natl. Acad. Sci. USA 82, 1104-1107 (1985).
25. H. Frauenfelder and G. A. Petsko, Biophys. J.. 32, 465-483 (1980).
26. P. Douzou, G. Hui Bon Hoa, and G. A. Petsko, J. Mol. Biol. 96, 367-380 (1975).
27. G. A. Petsko, J. Mol. Biol. 96, 381-392 (1975).
28. F. Parak, R. L. Mößbauer, W. Hoppe, U. F. Thomanek, and D. Bade, J. de Phys. (Paris) Colloq. C6 37, 703-706 (1976).
29. H. Hartmann, F. Parak, W. Steigemann, G. A. Petsko, D. Ringe Ponzi, and H. Frauenfelder, Proc. Natl. Acad. Sci. USA 79, 4967-4971 (1982).
30. J. A. McCammon, B. R. Gelin, and M. Karplus, Nature 267, 585-590 (1977).
31. B. Gavish, E. Gratton, and C. J. Hardy, Proc. Natl. Acad. Sci. USA 80, 750-754 (1983).
32. H. B. Bull and K. Breese, Biopolymers 12, 2351-2358 (1973).
33. F. M. Richards, ~~in press~~. c.f. Kundrot and F.M. Richards, J. Mol. Biol. 193, 157-170 (1987).
34. D. Ringe, J. Kuriyan, G. A. Petsko, M. Karplus, H. Frauenfelder, R. F. Tilton, and I. D. Kuntz, Trans. Amer. Cryst. Assoc. 20, 109-122 (1984).
35. H. Frauenfelder, H. Hartmann, M. Karplus, I. D. Kuntz, J. Kuriyan, F. Parak, G. A. Petsko, D. Ringe, R. F. Tilton, M. L. Connolly, and N. Max, Biochemistry, ~~in press~~ 24, 1854-1861 (1985).

D. Ringe and G.A. Petsko, Progr. Biophys. moloec. Biol. 45, 197 (1985).

H. Frauenfelder, Int. J. Quantum Chem. 35, 711 (1989).

H. Hartmann, et al., Euro. Biophys. J. 14, 337 (1987)

PART III

THE ENERGY LANDSCAPE OF PROTEINS

The history of physics and chemistry shows that the exploration of energy levels is crucial for understanding physical systems and for discovering physical laws. The measurements of the line spectra in atoms led to the discovery of Balmer's relation, to the Bohr theory of the atom, the Schrödinger and Dirac equations, and quantum electrodynamics. Specific heat experiments revealed the existence of vibrational energy states in solids and of tunnel states in glasses. Nuclear energy levels yielded the essential clues to the building the shell and the collective model. Particle masses and systematics led to the eightfold way, to the quark model, and to quantum chromodynamics. Biomolecules have energy spectra that are exceedingly complex. On the one hand this complexity promises to be a rich source of information. On the other hand, the richness makes the path to an understanding of the energy levels difficult. In the present part, we sketch some of the important tools and describe the major aspects of protein energy levels.

18. SURVEY

18.1 From Nuclei to Proteins

Consider the energy levels of a number of systems. Nuclei, with a characteristic length of a few fm, possess excitation energies of the order of keV to MeV. A typical example is given in Fig. 18.1. The first excited state of the nucleide ^{57}Fe is at 14.4 keV; it has a mean life of 1.4×10^{-7} sec. The spin of the ground state is 1/2, of the first excited state 3/2. In a magnetic field, both ground state and excited state show a Zeeman splitting. In an electric field, the ground state remains degenerate, the excited state splits into two substates. The dominant excitation in atoms is electronic and too well known to be discussed here.

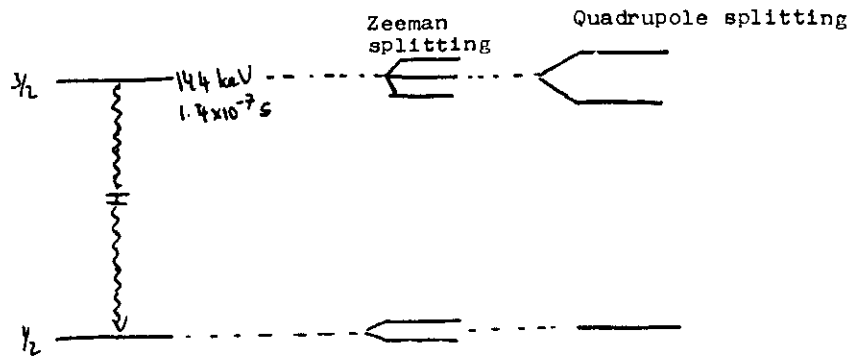

Fig. 18.1 Ground state and first excited state of the nucleide ^{57}Fe.

Diatomic molecules possess three types of excitation, electronic, vibrational, and rotational. The essential features are shown in Fig. 18.2.

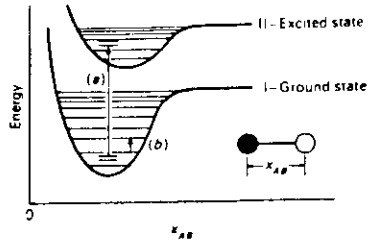

Energy levels for a simple diatomic molecule. The potential energy (heavy curve) is a function of the internuclear distance (X_{AB}). Two electronic states are shown (I and II). They differ in their potential energy and in the position of the minimum, the equilibrium internuclear distance. For each electronic state there are different possible levels of vibrational energy (long, thin lines) and rotational energy (short lines, shown only for two vibrational levels). A possible electronic transition is shown by (a) and a vibrational transition in the electronic ground state by (b).

Fig. 18.2 The energy levels of a diatomic molecule.

In polyatomic molecules, more complex motions can occur. As an important new feature, we mention the existence of tunnel states in the ammonia molecule.[1] The NH_3 is sketched in Fig. 18.3. It can exist in two different arrangements (or substates in our terminology). The degeneracy leads to a

---

1. R. P. Feynman, R. B. Leighton, and M. Sands, The Feynman Lectures on Physics, Addison-Wesley, 1965, Vol. III, Chapter 9.

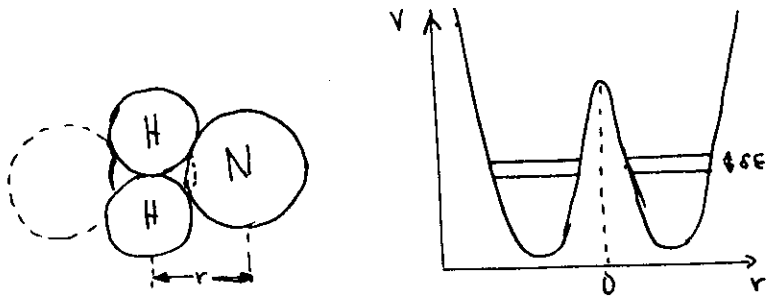

Fig. 18.3 The two substates of the ammonia molecule. The ground state is split into two tunnel states.

splitting of the energy levels. The splitting is caused by the fact that the N atoms can tunnel through the barrier formed by the three H atoms. The tunnel splitting is given by

$$\delta E = 10^{-4} \text{ eV} = 24 \text{ GHz}.$$

In more complex molecules, we can expect more conformational substates, as we have already discussed for the case of heme in Section 17.2.

Solids also show features that are of importance to biomolecules. The specific heat, Eq. (8.26), is classically expected to be independent of temperature. Experimentally, it goes to zero for $T \to 0$. Einstein first explained this observation with discrete energy levels in solids, as indicated in Fig. 18.4a.[2] A typical value of the Einstein energy is 0.1 eV. Debye generalized Einstein's spectrum and a typical Debye spectrum is shown in Fig. 18.4b. A realistic spectrum is shown in Fig. 18.4c. Note that b and c use a different representation from a.

The vibrations in a solid are quantized and called phonons. Phonons are not the only elementary excitations in solids. Plasmons, magnons, polarons, and excitons can also exist.

2. A. Pais, Subtle is the Lord... Clarendon Press, Oxford, 1982, Chapter 20.

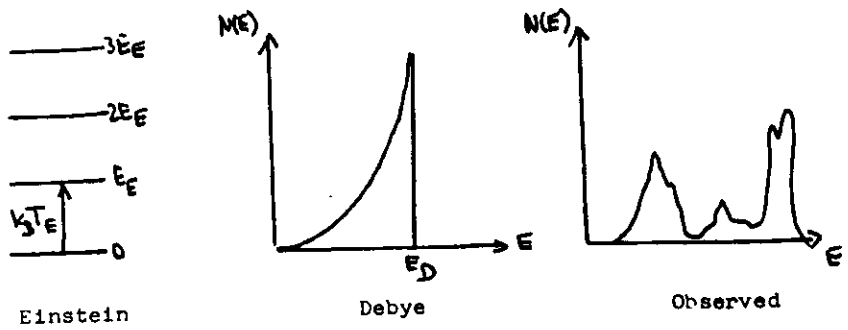

Fig. 18.4 Vibrational spectra in solids.

In proteins, we expect to see most or all of the various excitations and energy levels, from tunnel states to electronic states. A treatment of all possible spectroscopies needed to obtain a complete picture of the energy levels and the excitations in a protein would far exceed the space and time available here. The following chapters are consequently not exhaustive, but should provide a glimpse at the richness of protein spectroscopy. Most of the time we use heme proteins as example. As indicated in Fig. 18.5, all components contribute to the excitations.

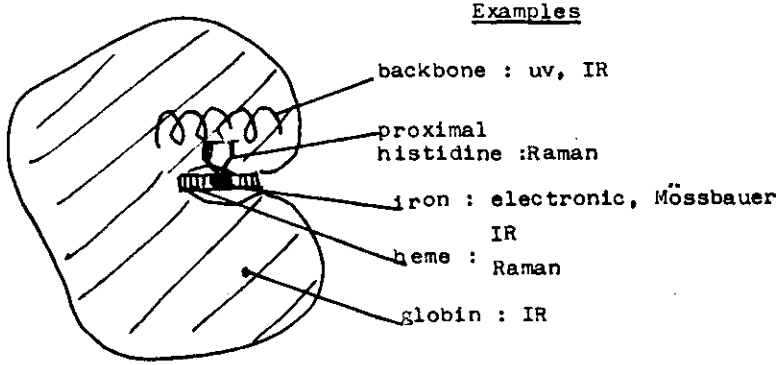

Fig. 18.5 Excitations in a heme protein.

18.2 Units and Typical Energies

In different subfields of physics and chemistry, different units for energy are used and this fact can lead to confusion. We therefore summarize some of the units and conversion factors here. We first note that we can either state the energy per atom or molecule, or per mole. The corresponding Boltzmann factors and the relations are given in Table 18.1. We will

Table 18.1

per molecule	per mole
$\exp(E/k_BT)$	$\exp(E'/RT)$
$E' = N\,E$	
$R = N\,k_B$	
$N = 6.022 \times 10^{23}\ \text{mol}^{-1}$	
$k_B = 1.381 \times 10^{-23}\ \text{J K}^{-1}$	
$R = 8.314\ \text{J mol}^{-1}\ \text{K}^{-1}$	

sometimes switch without warning from "per atom/molecule" to "per mole". No harm should be done! In the chemical literature energies are frequently given in kJ /mol. In atomic physics the electron Volt, eV, is a handy unit; every physicist remembers the binding energy of the first Bohr orbit of the hydrogen atom, -13.6 eV. Spectroscopists either measure energy in terms of frequency, using the Hertz, Hz, or kHz, MHz, GHz as the basic unit, or in terms of wavenumbers, cm^{-1}, i.e. the inverse of the wavelength. These units are related to the energy proper by the following expressions

$$E = h\nu = \hbar\omega = \frac{hc}{\lambda} = \frac{\hbar c}{\chi} \qquad (1)$$

where h is Planck's constant, $\hbar = h/2\pi$, ν is the frequency in Hz (= 1 cycle/sec), ω is angular frequency in radians/sec, c is the speed of light, and λ is the wavelength, $\chi = \lambda/2\pi$, $\hbar c = 197$ eV nm.

Energy can also be expressed in terms of absolute temperature T,

$$E = k_BT \qquad E' = RT. \qquad (2)$$

Conversion expressions are summarized in Table 18.2. Note that the conversion switches without warning from "per mole" to "per molecule". Moreover, the equations are dimensionally incorrect. The usefulness of the table is nevertheless clear - it permits changes from one value to another.

Table 18.2 Conversions.

1 kJ/mol = 0.239 kcal/mol = 10.36 meV = 2.50 GHz = 83.5 cm^{-1} = 120 K.

In Fig. 18.6, we compare energy, frequency, and wavelength scales, we label the various spectroscopic regions and indicate typical atomic or molecular transitions. As is evident from the diagram, the various types of

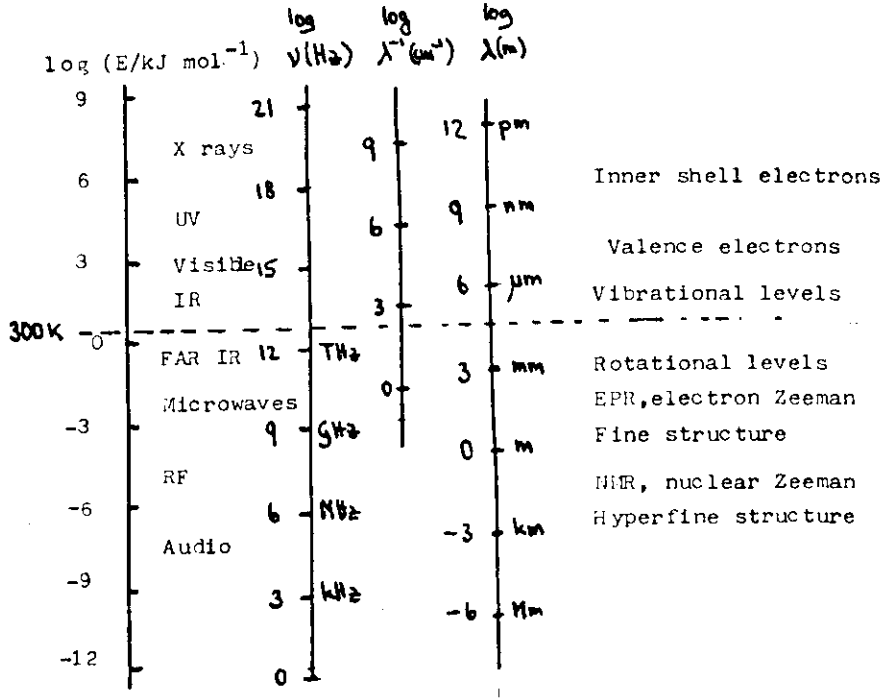

Fig. 18.6 Energies, frequencies, and wavelengths.

excitation are widely separated in frequency. In particular, there are many bands in which the molecule does not absorb any energy at all. If we tune in to a specific absorption band of a biomolecule, chances are that the absorption is due to a localized group only, a so-called chromophore. A typical example is the heme group in myoglobin which accounts for all the visible absorption and therefore the color of Mb.

The fact that the electronic, vibrational and rotational energies of a molecule are so far apart is due to the large ratio of the nuclear to the electronic mass

$$M/m \sim 10^4..10^5. \tag{3}$$

The zero-point motion of the nuclei is relatively small; nuclei have fairly well defined equilibrium positions about which they oscillate slowly compared to the electronic motion. The order of magnitude of the electronic, vibrational and rotational energies can easily be estimated. The uncertainty relation yields for an electron of mass m confined to a linear dimension a ~ 0.1 nm

$$E_e \sim \hbar^2/2ma^2 \sim \text{few eV}. \tag{4}$$

The ratio of vibrational to electronic energies is

$$\frac{E_{vib}}{E_e} \sim \left(\frac{m}{M}\right)^{1/2}, \text{ i.e. } E_{vib} \sim 0.01...0.1 \text{ eV}. \tag{5}$$

Rotational energy levels are the result of quantized rotation of the entire molecule about its center of mass; the energies are given by

$$E_{rot} \sim \frac{\hbar^2 \ell(\ell+1)}{2j} \sim 10^{-4}...10^{-5} \text{ eV}. \tag{6}$$

Here $j \sim Ma^2$ is the moment of inertia of the molecule. Eqs. (4) and (6) give

$$E_{rot}/E_e \sim m/M. \tag{7}$$

The energy of an excited state is thus given by

$$E = E_e + E_{vib} + E_{rot}. \tag{8}$$

If the E_{rot} levels are closely spaced, band spectra result.

23. THE CONFORMATIONAL ENERGY SURFACE

In Fig. 21.1 we showed vibrational and conformational levels. The existence of conformational substates implies that Eq.(18.8) must be generalized for a complex system to read

$$E = E_e + E_{vib} + E_{rot} + E_{conf}. \tag{23.1}$$

This equation expresses the fact that proteins with identical primary sequences but somewhat different structures also have different internal energies. We have treated the evidence for the existence of structurally different conformations in Chapter 17. In the present chapter, we treat the conformational energy landscape. In other words we ask for the energy of a protein as a function of position in the multidimensional space that describes a given conformation. While we can already give some insight into this problem, we should also realize that this discipline is at its very beginning. We can compare the present situation with that of atomic physics in 1910, when the Balmer series was known, but spectral lines were not understood.

23.1 States and Substates

Most proteins are machines and perform some function. They consequently must possess at least two different **states** like a switch which can be open or closed. Examples are Mb, which can have an bound dioxygen (MbO_2) or not (Mb), or cytochrome c which can be charged or neutral. In a given state, a protein can assume a large number of **conformational substates** (CS) as we discussed in Chapter 17. This situation is sketched in Fig. 23.1.

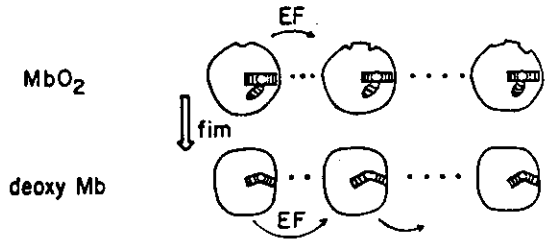

Fig. 23.1 Most proteins can exist in at least two different states, for instance MbO_2 and Mb. In each state, the protein can assume a large number of conformational substates.

Two types of motions are thus occurring: Equilibrium fluctuations (EF) lead from one substate to another. Nonequilibrium motions

accompany the transition from one state to another, for instance from Mb to MbO_2. We call these nonequilibrium transitions FIM, for functionally important motions.[1] [2] The following cartoon explains the equilibrium and nonequilibrium situation clearly.

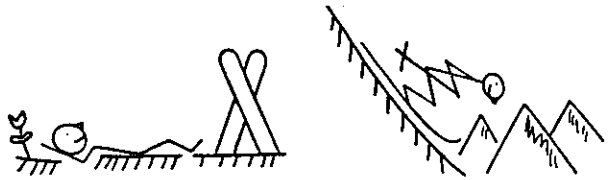

Fig. 23.2 A system at rest and in action.

EF and FIM are related through fluctuation-dissipation theorems. We have discussed the simplest case of this theorem in Section B.7. The connection is important for the studies of the energy landscape. It means that we can investigate a particular well in the conformational energy surface either by looking at fluctuations or by pushing the system into a non-equilibrium state and watching the return to equilibrium. Of course, there are limitations to this approach : The extreme fluctuations in equilibrium must reach the region that is involved in the non-equilibrium motion. limit of F-D theorem

We can summarize the most basic feature of the conformational energy surface of a protein by drawing a one dimensional cross section through the hypersurface and we expect that it will look as in Fig. 23.3. Schematically we can represent the highly degenerate groundstate by the drawing at right. In this picture, only the small circles at the bottom represent conformational substates. The apex is a transition state; a transition from one substate (1) to another substate (n) occurs by a passage through the apex.

Fig. 23.3 raises a number of questions. The first, of course, concerns the validity of the picture. Do substates indeed exist? What is the experimental evidence and what is the theoretical justification? If CS exist, what is the arrangement and the connection to structure and function?

---

[1] H. Frauenfelder, in **Structure and Motions, Nucleic Acids and Proteins.** Eds. E. Clementi, G. Corongiu, M.H. Sarma, & R.H. Sarma, Adenine Press, 1985. pp. 205-217.

[2] A. Ansari, J. Berendzen, S.F. Bowne, H. Frauenfelder, I.E.T. Iben, T.B. Sauke, E. Shyamsunder, and R.D. Young, Proc. Natl.Acad. Sci. USA **82**, 5000-5004 (1985).

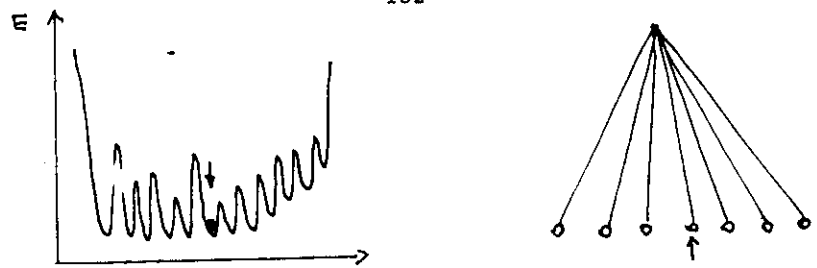

Fig. 23.3 a. One dimensional cross section through the conformational energy hypersurface in a particular state.
b. Tree diagram for the energy surface in a.

23.2 Experimental Evidence for Substates

In Chapter 18 we discussed the fact that both, theoretical arguments and experimental facts, lead to the conclusion that proteins cannot exist in just one unique structure. Here we discuss additional evidence for the existence of substates.[3] The strongest evidence comes from three observations : Reaction and relaxation processes at low temperatures are nonexponential in time, spectral lines are inhomogeneously broadened, above a certain temperature proteins show excess states (entropy), and the specific heat at very low temperatures is glass-like. We discuss some typical examples.

Nonexponential Time Courses. Dramatic evidence for the complexity of proteins appears in the rebinding kinetics of small molecules such as CO and O_2 to heme proteins at low temperatures.[4] We will discuss these experiments in more detail in Part IV and only describe the essential features here.

The "laboratory" for these experiments is the inside of a heme protein, for instance myoglobin. Fig. 23.4 shows a schematic cross section through the heme pocket, with a CO molecule covalently bound at the heme iron (state A). The bond between the iron and the CO can be broken by a light pulse. The CO then moves into the heme pocket (state B). At temperatures below 200 K, the CO cannot escape from the pocket into the solvent , but rebinds. The potential energy surface for photodissociation and rebinding is depicted in Fig. 23.4b. The barrier height for the binding process B→A is H_{BA}. Above about 40K, the rate coefficient, k_{BA}, can be described by an Arrhenius relation of the form

---

[3] H. Frauenfelder, F. Parak, and R.D. Young, Ann. Rev. Biophys. Biophys. Chem. **17**, 451-479 (1988).

[4] R.H. Austin, K.W. Beeson, L. Eisenstein, H. Frauenfelder, and I.C. Gunsalus, Biochemistry **14**, 1541-5373 (1975).

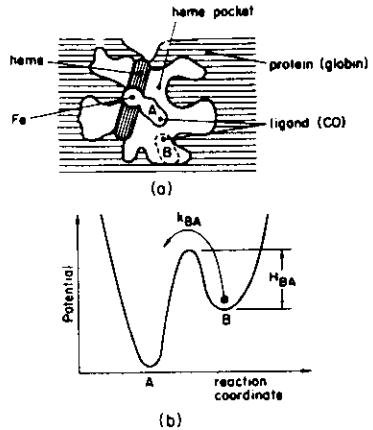

23.4.

Figure Schematic representation of the heme pocket in heme proteins. (*a*) Real-space cross section. (*b*) Potential diagram. *A* denotes the state where the ligand is bound to the heme iron, *B* the state where the ligand is in the heme pocket.

$$k_{BA}(T) = A_{BA}\ (T/T')\ \exp[-H_{BA}/RT]. \qquad (23.1)$$

T' is a reference temperature, usually set at 100K, H_{BA} is the barrier height (activation enthalpy),and R (= 8.31 J/mol) is the gas constant. If the preexponential A_{BA} and the barrier height H_{BA} have unique values, then the rate coefficient has a single value and rebinding is exponential in time,

$$N(t) = \exp(-k_{BA}(T)\ t)\ . \qquad (23.2)$$

Here N(t) is the survival probability, i.e. the fraction of Mb molecules that have not rebound a ligand at the time t after photodissociation.

The experimental results differ from the prediction of Eq.(23.2). A typical result is shown in Fig. 23.5 for the rebinding of CO to sperm whale myoglobin. Note that the plot does not display log N(t) versus t, but log N(t) versus log t. In a log-log plot, an exponential appears nearly like a step function and a power law gives a straight line. The nonexponential time course of N(t) in Fig. 23.5 can indeed be approximated by a power law,

$$N(t) \approx (1 + k_0 t)^{-n}\ , \qquad (23.3)$$

where k_0 and n are temperature-dependent parameters. The binding of CO to Mb is not an isolated case of nonexponential rebinding kinetics. Nearly every binding process studied at low T yields

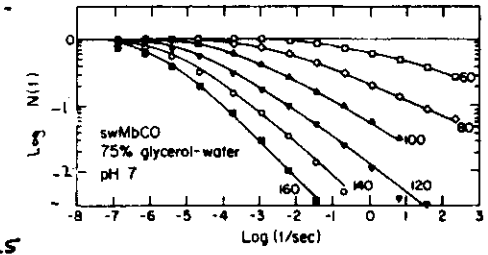

23.5

Figure Time dependence of the rebinding after photodissociation of CO to Mb. $N(t)$ is the survival probability, the fraction of Mb molecules that have not bound a CO at time t after the flash. The *solid lines* correspond to a theoretical fit, based on Equation 5, with the activation enthalpy distribution $g(H)$ as shown in Figure 6 below.

similar curves.3 Nonexponential kinetics has also been observed by time-resolved electron paramagnetic resonance (EPR) in the rebinding of nitric oxide (NO) to cytochrome c oxidase and Mb at low T.[5] The experimental data for a wide variety of heme protein-ligand combinations thus demonstrates that the binding from the heme pocket at temperatures below about 200 K is nonexponential in time.

Nonexponential rebinding can be explained in two very different ways, either by assuming inhomogeneous proteins with each protein having a simple pathway as shown in Fig. 23.4b[4], or by assuming homogeneous proteins with different pathways in each protein.[6] Experiments unambiguously show that the first alternative is correct.[3 4 7] This explanation is just what one expects from conformational substates as we now show.

Eq. (23.2) is valid if the preexponential A_{BA} and the barrier height H_{BA} have a unique value. We postulate that proteins in different conformational substates have different barrier heights and denote by $g(H_{BA})dH_{BA}$ the probability of a protein having a barrier height between H_{BA} and $H_{BA} + dH_{BA}$. Eq. (23.2) then is generalized to read

$$N(t) = \int dH_{BA}\ g(H_{BA})\ \exp\{-k_{BA}(H_{BA};T)\ t\}, \qquad (23.4)$$

where $k_{BA}(H_{BA};T)$ and H_{BA} are related by Eq. (23.1). If N(t) is measured over a wide temperature and time range, the preexponential A_{BA} and the activation enthalpy distribution

---

[5] LoBrutto,R., et.al. Biophys. J. **45**, 473 (1984).

[6] M. Marden, Eur. J. Biochem. **128**, 399 (1983).

[7] H. Frauenfelder, in **Structure and Dynamics of Nucleic Acids and Proteins.** Eds. E. Clementi and R.H. Sarma, Adenine Press, New York. pp. 369-376 (1983).

$g(H_{BA})$ can be found by Laplace inversion of Eq.(23.4). The preexponentials typically have values near 10^9 s^{-1} and some distributions are shown in Fig. 23.6.

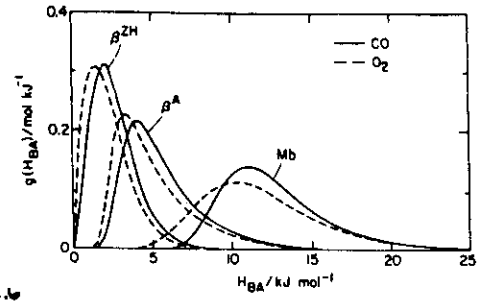

Figure 23.6 Activation energy distributions, $g(H_{BA})$, for rebinding of CO and O_2 to myoglobin and the separated beta chains of normal and mutant hemoglobin.

We repeat here the essential definitions and assumptions underlying the discussion. We have defined CS as having the same primary sequence, crudely the same structure, but differing in detail, and performing the same function, but with different rates. The observation of the nonexponential rebinding led to this definition : Eq. (23.4) implies that we can characterize a CS by the barrier height H_{BA}. In this particular substate, rebinding is exponential and given by the rate $k_{BA}(H_{BA};T)$. The different structures in the different CS result in different barrier heights and hence in different rates. At low T, each protein remains frozen in a particular CS and rebinding consequently is nonexponential in time. At temperatures well above 200K, a protein fluctuates rapidly from CS to CS and rebinding can become exponential in time.[4]

Inhomogeneous Spectral Lines. If proteins in different substates indeed possess somewhat different structures, we should expect that their electronic properties also to differ. Spectral lines consequently should not be homogeneous, but to consist of a superposition of homogeneous lines as sketched in Fig. 23.7.

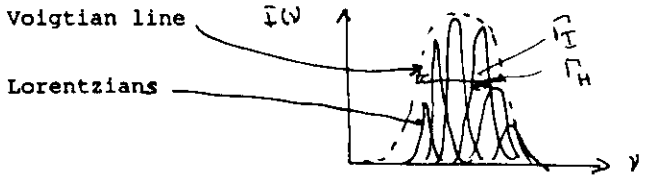

Fig. 23.7 Inhomogeneous spectral lines. The observed line is expected to have a Voigtian shape, namely a Gaussian superposition of Lorentzians.

A Gaussian superposition of Lorentzian lines is called a Voigtian. More general forms may also occur. A number of different approaches provides information about the line inhomogeneity. By analyzing the shape of the lines, the homogeneous and the inhomogeneous contributions can be separated.[8 9 10] A second approach uses the lifetime of fluorescing residues in proteins.[11] Fluorescence lifetimes are highly sensitive to the environment. If a protein contains only one of a given fluorescing residue, say tryptophan, and if the environment were identical in each protein molecule, the observed decay would have only a single lifetime. In reality, the observed decays can be fit better with a lifetime distribution, implying inhomogeneous sites.[11]

The most direct evidence for the inhomogeneity comes, however, from hole burning experiments. Because of the power of these experiments, we discuss two different types. Spectral hole burning was first introduced to NMR spectroscopy by Bloembergen et al..[12] We consider the optical version of hole burning here.[13,14] Consider first a single homogeneous component in Fig. 23.7. The line consists of a narrow zero-phonon line and a broad phonon sideband. The zero-phonon line represents transitions in which no phonon is emitted or absorbed. The photon sideband occurs because the environment starts vibrating as a result of the chromopho e excitation. The relative intensity of the zero-phonon line is given by the Debye-Waller factor (See Section 17.5) exp{-S}, where S characterizes the strength of the electron phonon coupling. Three different types of hole-burning processes are important. In transient hole burning, the incident laser line of wavenumber ν_0 excites just one homogeneous line (we neglect the phonon sideband) and the line after excitation shows a transient hole (Fig. 23.7b.) The hole will usually be refilled quickly by the deexcitation. In photochemical hole burning (PHB), the

---

[8] A. Cooper, Chem. Phys. Lett. **99**, 305 (1983).

[9] K.T. Schomacker and P.M. Champion, J. Chem. Phys. **84**, 5314-5325 (1986).

[10] V. Srajer, K.T. Schomaker, and P.M. Champion, Phys. Rev. Letters **57**, 1267-1270 (1986).

[11] J.R. Alcala, E. Gratton, and F.G. Prendergast, Biophys. J. **51**, 925-936 (1987).

[12] N. Bloembergen, E.M. Purcell, and R.V. Pound, Phys. Rev. **71**, 679 (1948).

[13] J. Friedrich and D. Haarer, Angewandte Chemie, Int. Ed. **23**, 113-140 (1984).

[14] R. Jankowiak and G.J. Small, Science **237**, 618-625 (1987).

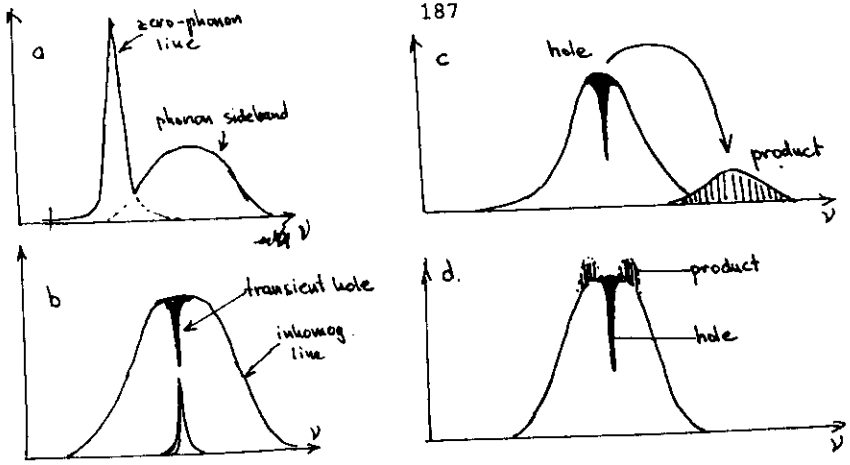

Fig. 23.7 a. Line shape of a chromophore in a perfect lattice. b. Transient hole burning. The phonon sideband is not shown. c. Photochemical hole burning d. Nonphotochemical hole burning.

incident laser beam induces a photochemical reaction. The spectrum of the photoproduct is usually well separated from that of the chromophore and the hole consequently remains until the reaction has been reversed. In a nonphotochemical hole burning (NPHB) process, the incident light modifies the chromophore-protein interaction. . The wavenumber of the absorption of the photoproduct is close to that of the photolyzing light. In other words, the incident light transfers the protein from one conformational substate to another. PHB and NPHB are well known and studied in chromophores included in glasses. Holeburning experiments with proteins have also been performed and photochemical and non-photochemical hole burning has been observed.[15] [16] [17] [18] These experiments show unambiguously that the spectral lines of the chromophores are inhomogeneously broadened and add to the evidence for conformational substates.

---

[15] S.G. Boxer, D.J. Lockhart, and T.R. Middendorf, Chem. Phys. Lett. **123**, 476 (1986).

[16] S.R. Meech, A.J. Hoff, and D.A. Wiersma, Chem. Phys. Lett. **121**, 287 (1985).

[17] W. Köhler, J. Friedrich, R. Fischer, H. Scheer. J. Chem. Phys. **89**, 871 (1988).

[18] S.G. Boxer, D.S. Gottfried, D.J. Lockhart, and T.R. Middendorf, J. Chem. Phys. **86**, 2439-2441 (1987).

23.3 Glasses (Amorphous Solids).

At this point it is useful to discuss some characteristic properties of glasses. (We use the terms "glass" and "amorphous solids" nterchangeably.) The physics of glasses was somewhat neglected by physicist for a considerable time. Within the past one or two decades, however, interest has been increasing and it has been realized that glasses share a number of fundamental properties with other complex systems. We sketch here some of these properties and refer to the literature for details.[19] [20] [21] [22] We note here that many properties of glasses can be intuitively understood if we consider a glass a **frozen liquid.**

Glass Formation. A liquid may solidify in two ways, either discontinuously to a crystal or continuously to a glass. The two pathways are shown in Fig. 23.8.

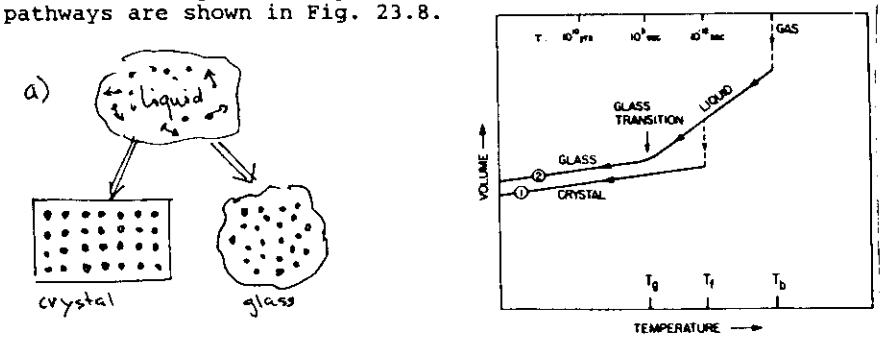

Fig. 23.8 Crystallization and glass formation. a. General picture. b. Route 1 is the path to the crystal, route 2 to the glass. (After Zalle, ref. 20.)

The fundamental difference between a glass and a crystal is in the atomic-scale structure. Crystals are periodic and possess long-range order. Glasses are aperiodic or random and have no long-range order. In a crystal, every atom knows where it should be and has no competition for its equilibrium position. Glasses

---

[19] J.M. Ziman, **Models of Disorder.** Cambridge U. Press, 1979.

[20] R. Zalle, **The Physics of Amorphous Solids.** Wiley, New York (1983).

[21] **Amorphous Solids.** Topics in Current Physics, Vol. 24. Ed. W.A. Phillips. Springer, Berlin, 1981.

[22] **Structure and Mobility in Molecular and Atomic Glasses.** Annals N.Y. Acad. Sci. 371. Eds. J.M. O'Reilly and M. Goldstein (1981).

are **frustrated**[23] : many atoms may compete for the same position and a given atom may have more two or more quasi-equilibrium positions. In principle, essentially every liquid can be brought to the glassy state by cooling so rapidly that the atoms have no time to reach their periodic equilibrium position. For many substances the cooling rate,however, must be so rapid that only a computer situation can reach the glassy state. The structure in the glassy state has been studied by many different techniques[20], but we are not interested in this aspect here apart from the fact that the arrangement is aperiodic. Finally we note that crystals are in equilibrium at all temperatures, whereas a glass is usually in a nonequilibrium (metastable) state.

The Glass Transition.[24] [25] [26] Fig. 23.8 shows that the liquid ⇔ crystal transition is sharp and a melting or freezing temperature can consequently be defined unambiguously. The liquid⇔glass transition, however, is wide and the **glass temperature**, T_g, therefore is not clearly defined. To get some better feeling for the behavior of a glass-forming system near the glass temperature we show in Fig. 23.9 the temperature dependence of the specific heat and the excess entropy of some glasses. In Fig. 23.10, we

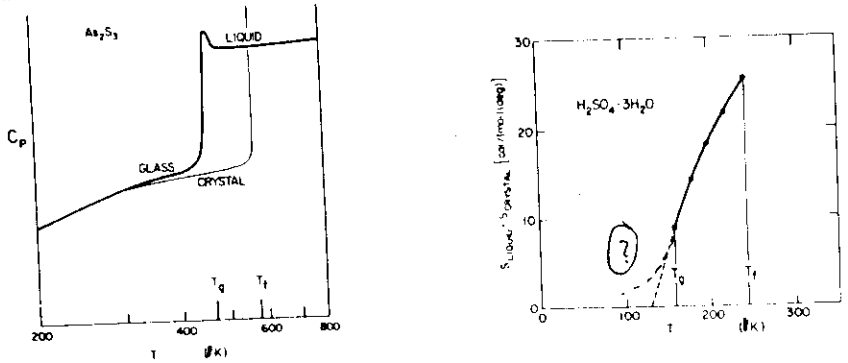

Fig. 23.9 Typical temperature dependencies of a. the specific heat, b. the excess entropy. (After Zalle, ref.20.)

[23] G. Toulouse, Comm. Physics 2, 115 (1977).

[24] J. Jäckle, Rep. Prog. Phys. **49**, 171-231 (1986).

[25] S. Brawer, **Relaxation in Viscous Liquids and Glasses.** American Ceramic Soc. Columbus, Ohio,1985.

[26] P.G. Wolynes, **AIP Conference Proceedings 180.** Eds. S.S. Chan and P.G. Debrunner, pp. 39-65. Am. Inst. Phys. New York (1988).

display the temperature dependence of the specific volume and the viscosity.

The curves demonstrate that it is difficult to define T_g unambiguously. It is customary to denote by T_g the temperature where the viscosity reaches 10^{13} poise . Alternatively one can

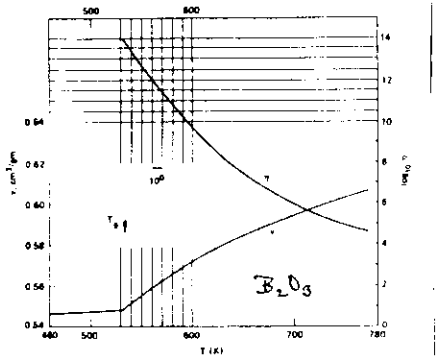

Fig. 23.10 The temperature dependence of the viscosity and the specific volume of a glass. (After Brawer, ref. 25.)

call T_g the midpoint of the step in the specific heat , Fig. 23.9a. However, the specific heat curve is largely determined by the speed with which the calorimeter measures! If a faster calorimeter is used, the curve shifts to lower temperatures and this definition of T_g consequently is technique dependent.
We will return to the behavior of the data shown in Figs. 23.9 and 23.10 later when we compare proteins and glasses.

The energy landscape. The energy landscape of a crystal is simple (Fig. 3.1a), that of a glass complex and it shows a highly degenerate ground state (Fig.3.1b).[27]

[27] M. Goldstein , J. Chem. Phys. 51, 3728 (1969).

One way to understand the appearance of a highly degenerate groundstate as in Fig.3.1b follows from a simple gedankenexperiment, sketched in Fig. 23.11. We consider a large number of identical glass-forming liquid drops. We cool the entire ensemble at the same time and each liquid drop will form a small glass droplet. While the composition of all droplets will be identical, their structures will be different because they froze when the atoms in the liquid had different positions. Moreover, they will have slightly different energies and will be separated by energy barriers : In order to move from one conformation to another, a droplet must partially or completely melt. We therefore find an energy landscape as also sketched in Fig, 23.11, with a large number of energy valleys separated by high barriers.

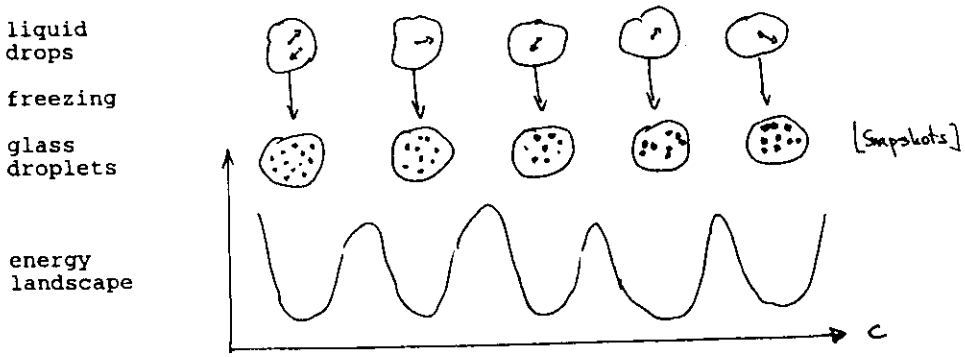

Fig. 23.11 An ensemble of liquid drops will form, on cooling, an ensemble of glassy drop. Each glassy drop will have a different conformation and a somewhat different energy. To change the conformation, an energy barrier must be surmounted.

While this gedanken experiment makes the appearance of a complex energy landscape plausible, it gives no information about the structure of the landscape. In fact, it is difficult to explore the landscape in glasses in detail and we will see later that the corresponding problem is less difficult for proteins.

Tunnel States. At low temperatures, glasses show characteristic phenomena that distinguishes them clearly from crystals.[4,28] We describe here only one, the behavior of the specific heat or heat capacity, Eq. (B.26). In crystals, the Debye theory predicts that the specific heat at low temperatures

---

28 W.A. Phillips, Rep. Progr. Phys. **50**, 1657-1708 (1987).

is proportional to T^3. [29] It is therefore customary to plot the experimental data in the form of C/T^3. Crystals, as expected, possess a constant C/T^3 as is shown in Fig. 23.12. Glasses,

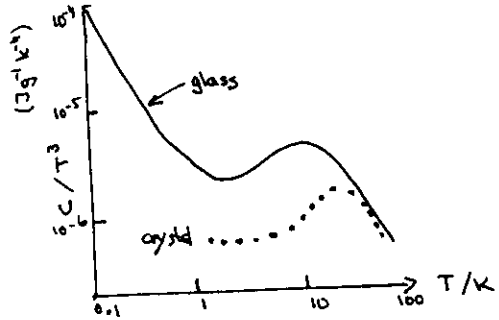

Fig. 23.12 The heat capacity C(T) for a crystal (quartz) and a glass (vitreous silica) , plotted as $\log(C(T)/T^3)$ vs. log T.

however, show a very different behavior[30] : Deviations from the crystalline behavior start around 5 K and below 1 K, C can be approximated by

$$C(T) = A\,T + B\,T^3. \qquad (23.5)$$

The coefficient A describes the amount of excess specific heat. Glasses thus display additional specific heat. Since the specific heat describes the amount of energy that the system can take up, the observation means that glasses possess additional degrees of freedom that are not present in crystals.

The presently accepted model was introduced by Phillips[31] and by Anderson et al..[32] The model is sketched in Fig. 23.13. It is well known that energy levels in a double-well potential are split. The splitting is caused by tunneling and this tunneling has been observed in many phenomena. The two most

---

29 See any texts on condensed matter physics, for instance C. Kittel, **Introduction to Solid State Physics**. John Wiley, New York. Any edition.

30 R.C. Zeller and R.O. Pohl, Phys. Rev. **B4**, 2029 (1971).

31 W.A. Phillips, J. Low Temp. Phys. 7, 351-360 (1972).

32 P.W. Anderson, B.I. Halperin, and C.M. Varma, Phil. Mag. **25**, 1-9 (1972).

spectacular ones are the ammonia maser and the K mesons.[33]

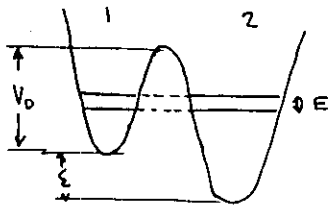

Fig. 23.13 Two-level system.

It is straightforward to calculate the energy splitting[28] , with the result

$$E = \sqrt{(\varepsilon^2 + \delta^2)} \ , \qquad (23.6)$$

where δ is the matrix element between the two wells,

$$\delta = 2 \langle 2|H|1\rangle \ . \qquad (23.7)$$

Here 1 and 2 denotes the unperturbed eigenfunctions in the two wells and H is the Hamiltonian of the system.

At T=0, only the lower of the two levels is occupied. As the temperature is increased, the higher level will also become occupied according to the Boltzmann factor. This process , of course, leads to a contribution to the specific heat that is not present in a crystal without two-level states (TLS). In order to obtain the term linear in T in Eq.(23.5), one TLS is not enough. However, if a distribution of levels in introduced, the excess specific heat can be explained.

The properties of glasses enter the arguments in two ways : The structure has to be such that TLS are possible, and the disorder (randomness) makes the appearance of a distribution of TLS plausible. The model hence is nearly universally accepted. There are, however, some problems : Where are the TLS ? Every glass, regardless of the structure and composition, shows a specific heat of the form Eq.(23.5). Why is the distribution such that Eq. (23.5) results ? Yu and Leggett have recently looked at this problem and they suggest an alternative approach.[34] We do not discuss their approach here, but mention it because it may become important also for proteins.

---

[33] R.P. Feynman, R.B. Leighton, and M. Sands, **The Feynman Lectures on Physics.** Vol. III, 9.1 .Addison -Wesley, Reading,1965.

[34] C.C. Yu and A.J. Leggett, Comments Cond. Mat. Phys. **14**, 231-251 (1988).

We have sketched some of the important properties of glasses here because the similarity between proteins and glasses may be important for an understanding of both systems, as already stated briefly in Chapter 3. The most profound similarity is expressed in Figs. 23.3 and 23.11 : Proteins and glasses both possess a rugged energy landscape. The energy as a function of the conformational coordinates possesses a very large number of minima or conformational substates. Both figures represent a one-dimensional cross section through the energy hypersurface and in both cases we have just one type of substates. The actual situation is more complicated as is suggested by the data in Figs. 23.10 and 23.12: The glass transition occurs typically near 300K, but the tunnel states become apparent near 1 K. The two phenomena consequently must involve barriers different in height by about two to three orders of magnitude. How can we incorporate such vastly different barriers in the energy landscape? It turns out that proteins may actually be better systems than glasses to explore this question and we therefore return to substates in proteins.

23.4 The Hierarchy of Substates.

In Figs. 23.3 we have shown the energy landscape to be arranged in the form of an inverted bush. All substates are connected through one vertex; while the barriers between substates are not all equal, it is possible to go from any one CS to any other in one step. We will show here that it is more likely that substates are arranged in a hierarchy as shown in Fig. 23.14.[2]

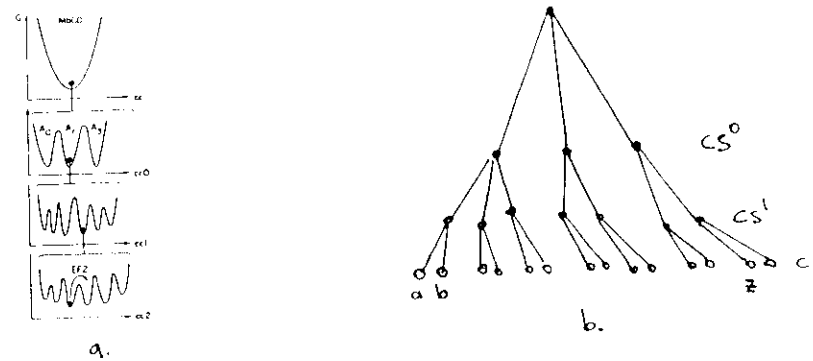

Fig. 23.14 Hierarchical organization of substates.

In Fig. 23.14a, we show one-dimensional cross sections through the energy landscape. A protein, say MbCO, is in the crudest

approximation described by the single potential well at the top. Closer inspection then shows that it can exist in a small number of substates of tier 0, CS^0, which are described as deep wells along the conformational coordinate cc0. Each of these CS^0 is again furcated into a large number of substates of tier 1, CS^1. These are described along a different coordinate, cc1. Each of these is again split into substates of tier 2, CS^2, described along coordinate cc2. The branching may continue to tiers with increasingly smaller barriers. In Fig. 23.14b, the arrangement is shown in the form of an inverted tree. The barriers between substates decrease in height with increasing tier. The barriers even within one tier do not all have the same height, but are distributed.

The difference to the bush-like arrangement shown in Fig. 23.3 and the hierarchical arrangement in Fig. 23.14 involves energy barriers and conformational changes. In a bush, only one structural change is needed to go from any one CS to any other. In the hierarchical arrangement, however, a number of structural arrangement must occur. To go from a to b, only a minor structural change must occur and the corresponding barrier is small. To go from a to z, however, small and large changes must take place. (Note that only the circles at the bottom represent actual protein states; the higher vertices simply indicate in which well of the higher tiers the protein is.)

The Fig. 23.14 makes the experimental and theoretical goals clear. Experimentally, the arrangement in tiers must be verified and the properties of the different substates must be determined. Theoretically, the organization should be understood in terms of the protein structure.

23.5 Substates of Tier 0.

MbCO Stretch Bands. In heme proteins, nature has provided a superb tool for the study of some substates, namely the stretch vibration of the CO bound to the heme iron (Fig.23.4). CO as a gas or in a liquid shows a stretch band centered at about 2140 cm^{-1}.[35] A CO molecule bound covalently to the heme iron is expected to have a somewhat lower frequency, because the Fe-CO bond will weaken the C-O bond. Indeed, the wavenumber of CO bound to the iron atom in myoglobin has a value of about 1950 cm^{-1}. However, instead of just one stretch band, MbCO shows at least three as has been known for a considerable time.[36] An example of the transmission spectrum of MbCO, obtained by FTIR spectroscopy, is given in Fig. 23.15. To prove that the prominent lines are indeed caused by CO, a mixture of $C^{12}O^{16}/C^{12}O^{18}$ was used. Indeed,

[35] G.E. Ewing, J. Chem. Phys. 37, 2250-2256 (1992).

[36] J.O. Alben, in **The Porphyrins, Vol. III.** Academic Press,pp.323-345 (1978).

two characteristic spectra are obtained that are shifted by the expected amount.

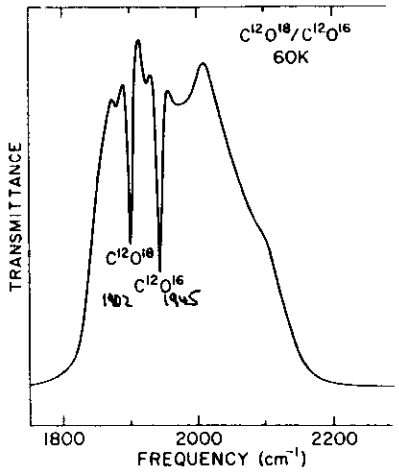

(already shown Fig. 21.7

Fig. 23.15 The infrared transmission spectrum of MbCO. Two different isotopes of dioxygen are used.

While the transmission spectrum in Fig.23.15 clearly shows CO lines, a detailed study is difficult, because it is difficult to determine an exact baseline (the spectrum of Mb without CO) . Improved spectra are obtained with a **difference technique:** The spectrum of MbCO is first measured at low temperature. The CO-Fe bond then is broken by an intense light and the spectrum of the resulting photoproduct Mb* is determined. The difference spectrum MbCO-Mb* yields the spectrum of the CO lines both in the bound and the photolyzed state, as shown in Fig. 23.16.

The data in Fig. 23.16, taken at 5.5 K, clearly show three IR bands in the bound and three in the photodissociated state. We label the bands as indicated in the figure. A weak line may be present between A_1 and A_3. We tentatively assume that each IR band characterizes a particular substate of tier 0 and denote these substates also with A_0, A_1, and A_3. In the following we prove that this assumption is strongly supported by all experimental data.

Properties of the CS0. The three substates of tier 0 in MbCO show a number of remarkable properties. While their wavenumbers are largely independent of external conditions, their relative intensities depend strongly on temperature, pressure, pH, and solvent. As an example, Fig. 23.17 shows the ratio A_0/A_1 as a function of temperature for three different pressures. (Note that 100 MPa = 1 kbar).

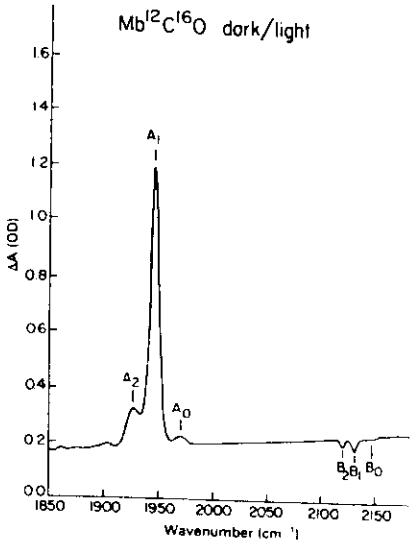

Fig. 23.16. Difference spectrum for MbCO. The difference in absorbance between MbCO and Mb* is shown as a function of wavenumber. The bound states appear near 1950 cm^{-1}, the weak lines of the photodissociated CO are near 2150 cm^{-1}.

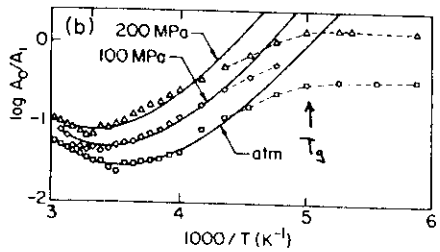

Fig. 23.17 Temperature dependence of the ratio A_0/A_1 at pH 6.6 for three pressures.[39]

The ratio A_0/A_1 shows four regions : Below about 200 K, it is constant. Between 200 and 220 K, a gentle bend occurs. Above 200 K, it first decreases, reaches a minimum near 300 K, and then increases again.[37] [38] [39]

---

[37] I.E.T. Iben et al., Phys. Rev. Letters 62, 1916-1919 (1989).

38. M.K. Hong et al., Biophys. J., 58, 429-436 (1990).
39. H. Frauenfelder et al., J. Phys. Chem. 94, 1024-1038 (1990).

With decreasing pH (See Appendix D) the ratio A_0/A_1 increases strongly.[40]

Interpretation. The behavior in Fig. 23.17 can be interpreted by assuming that the three bands represent three CS^0. For simplicity, consider only A_0 and A_1 and assume that the two substates have slightly different entropies, energies, and volumes, and that the transitions between the two substates are characterized by rates k_{01} and k_{10} (Fig. 23.18). Above a certain

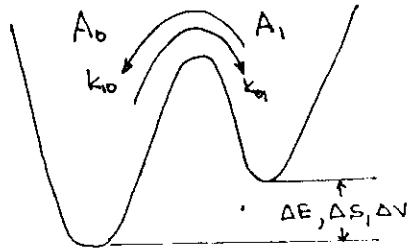

Fig. 23.18 Substates of tier 0

temperature, T_g, transition between the CS^0 will be so fast that the two states are in equilibrium so that the ratio of their populations is given by

$$A_0/A_1 = \exp[-\Delta G/RT] = \exp[-(\Delta E + P\Delta V - T\Delta S)/RT], \qquad (23.8)$$

where for instance $\Delta E = E_0 - E_1$. Well below T_g, the exchange is so slow that the populations no longer change and the ratio becomes constant; the protein has become glassy. To verify this scenario, we consider the two regions well below T_g and well above T_g in more detail.

The Glass Phase. One of the characteristics of a glass is metastability; a glass is a non-equilibrium system and its properties depend on its history. Metastability implies that the state of a system below its glass temperature depends on its history. History dependence can be proven by a general approach.[39] The properties of the system are measured at a given temperature and pressure below T_g after reaching the point (T,P) by two different pathways, as shown in Fig. 23.19. On the solid pathway, the system is first frozen (F) and then pressurized (FP); on the dashed pathway, pressurization (P) is followed by freezing(PF). Fig. 23.20 shows the result of such an experiment, where the IR spectrum of MbCO is measured at the four points F, FP, PF, and PFR in the TP plane, with T_i=225 K, T_f=100K, P_i=0.1 MPa, P_f=200 MPa. The infrared spectra obtained on the two pathways differ; metastability is proven.

---

[40] A. Ansari et al., Biophys. Chem. 26, 337-355 (1987).

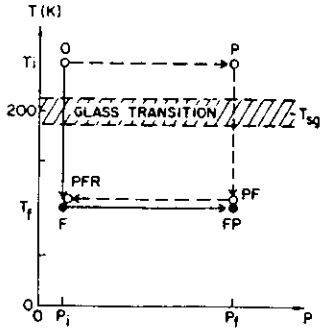

Fig.23.19 The system is taken from an initial state (T_i,P_i) to a final state (T_f,P_f) on different pathways, e.g. 0→F→FP (solid path) and 0→P→PF (dashed path).

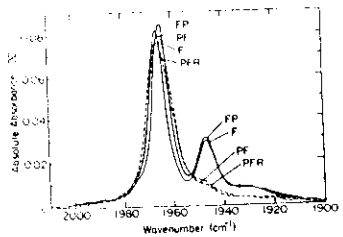

Fig. 23.20 The MbCO stretch spectrum determined at the four points F, FP, PF, and PFR in Fig. 23.19. (Ref. 41).

The Equilibrium Region. Consider now the behavior of A_0/A_1 well above T_g in Fig. 23.17. Eq.(23.8), with constant values of S, E, and V, predicts a straight line in a plot of $\log(A_0/A_1)$ versus 1/T and does not explain the observed change in slope near 300K. A phase transition near 300K, with a change from ,e.g., substate A_0 to a new substate A_0' can fit the data. However, no pronounced change in the position or width of either stretch band is observed and this explanation therefore is not attractive. The solution comes from Fig. 23.9b which indicates that the entropy of a glass or of the liquid above the glass temperature is not constant, but increases nearly linearly with T. A similar behavior has been observed for proteins.[41] We therefore assume as simplest possibility that the entropy depends on T and P as

$$S(T,P) = S(0) + sT + vP. \qquad (23.9)$$

The term linear in T is justified by experiment; the term linear

[41] G.M. Mrevlishvili, Sov. Phys. Usp. 22, 433 (1979).

in P is justified by noting that the Maxwell relation $(\partial S/\partial P)_T = -(\partial V/\partial T)_P$ (Table B.1) yields

$$V(T,P) = V(0) - vT. \qquad (23.10)$$

The standard relation describing thermal expansion is usually written as

$$V(T) = V(0)[1 + \beta T], \qquad (23.11)$$

where β is the coefficient of thermal expansion and where the compressibility has been neglected. Eqs.(23.10) and (23.11) show that

$$v = -\beta V(0). \qquad (23.12)$$

At constant pressure, $dG = -S\,dT$. With Eq.(23.9) we therefore get[42]

$$G(T) = G(0) - \int_0^T [S(0)+sT+vP]dT = G(0) - S(0)T - vPT - \tfrac{1}{2}sT^2. \qquad (23.13)$$

The difference in Gibbs free energy between two substates becomes with $\Delta G(0) = \Delta E(0)$

$$\Delta G(T,P) = \Delta E(0) + P\,\Delta V(0) - T\,\Delta S(0) - \Delta v\,PT - \tfrac{1}{2}\,\Delta s\,T^2 \qquad (23.14).$$

Fits with Eqs.(23.8) and (23.14) yield the solid lines in Fig. 23.17. A similar procedure can also be used for the ratio A_3/A_1. We therefore know the relative thermodynamic parameters of the three substates of tier 0 as a function of T and P and therefore have made a first step toward the exploration of the energy landscape of MbCO.

The Structure of the CS^0. A first step toward the exploration of the spatial structure of the CS^0 is done by determining the angle of the CO dipole with respect to the heme normal by using a photoselection technique.[43] [44] [45] The basic idea of the technique is simple : Small fractions of MbCO are photolyzed at low temperatures with linearly polarized light. The absorption is most efficient when the electric vector of the incident light is parallel to the transient dipole moment of the

[42] H.B. Callen, **Thermodynamics**, Wiley, New York, 1985. See in particular Chapter 7.

[43] A.C. Albrecht, J. Mol. Spectrosc. **6**, 84-108 (1961).

[44] P. Ormos et al., Proc.Natl. Acad. Sci. USA **85**, 8492-8496 (1988).

[45] J.N. Moore P.A. Hansen, and P.M. Hochstrasser, Proc. Natl. Acad. Sci. USA **85**, 5062-5066 (1988).

heme-CO system. Partial photolysis hence produces a polarized sample which shows a linear dichroism. By measuring the linear dichroism of the different CO stretch bands , the angle α between the CO dipole and the heme normal is determined. The result, plotted versus the center wavenumber of the bands, is shown in Fig. 23.21.

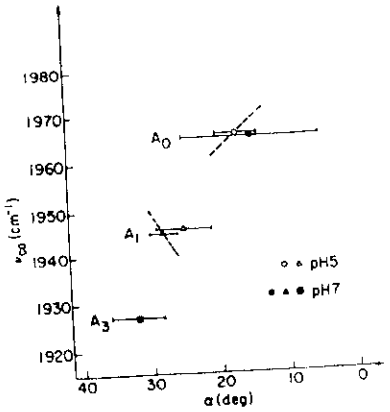

Fig. 23.21. Correlation of the angle α between CO and the heme normal in MbCO with the stretch wavenumber in the CS^0 substates. The dashed lines represent the wavenumber dependence of the CO orientation within the A^0 and the A_1 substate.(Ref.45)

The results in Fig.23.21 demonstrate that the structures of the three substates of tier 0 are different. Fig. 23.22 shows possible conformations near the heme group.[38]

Fig. 23.22 Substates of tier 0 in MbCO.

X-ray diffraction on MbCO also show the presence of more than one CO orientation.[46] The data are not yet sufficient to decide if the different angles α agree with the ones determined by the photoselection technique and if the different CS^0 also have different overall structures. What is needed are experiments on single crystals with different pH.

Functional Properties of CS0. Do the different CS^0 bind CO with different rates? Do answer this question, experiments similar to the ones discussed in Subsection 23.2 were performed, but the rebinding of the photodissociated CO_0 was monitored separately in the three substates A_0, A_1, and A_3.[40] The result at one particular temperature, shown in Fig.23.23, demonstrates two important features: The different substates indeed bind CO with different rates, and rebinding to each individual CS^0 is nonexponential in time. A_0 is fastest and A_3 slowest.

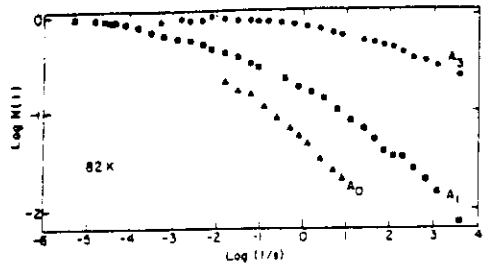

Fig.23.23. Rebinding of CO to Mb after photodissociation in the three substates of tier 0.

The information gathered so far indeed shows that A_0, A_1, and A_3 are substates : They have similar overall structure; otherwise they would not have essentially the same optical spectra and the X-ray diffraction data would show evidence for vastly different structures. They differ in detail; the angles α are different in each substate. They all have the same function, binding of CO, but perform it with different rates.

The Biological Importance of the CS^0. At this point we can speculate at the biological importance of the substates of tier 0. First it is tempting to assume that similar substates occur in other proteins. Secondly we note that many external agents, such as temperature, pressure, pH, and solvent, can change the population ratio of the three CS^0 in Mb. Thirdly we know that the CS^0 in Mb perform the same function, but with considerably different rates. The CS^0 can consequently be a means for the control of protein reactions : Rather than change the rate in one

---

46 J. Kuriyan, S. Wilz, M. Karplus, and G. A. Petsko, J. Mol. Biol. **192**, 133-154 (1986).

g. Phillips

An idea of the richness of substates of tier 0 comes from the figure below (Reinhard Scholl, Thesis University of Illinois, 1991). The figure shows that substates occur in all heme proteins studied, and that their relative intensities depend critically on many parameters.

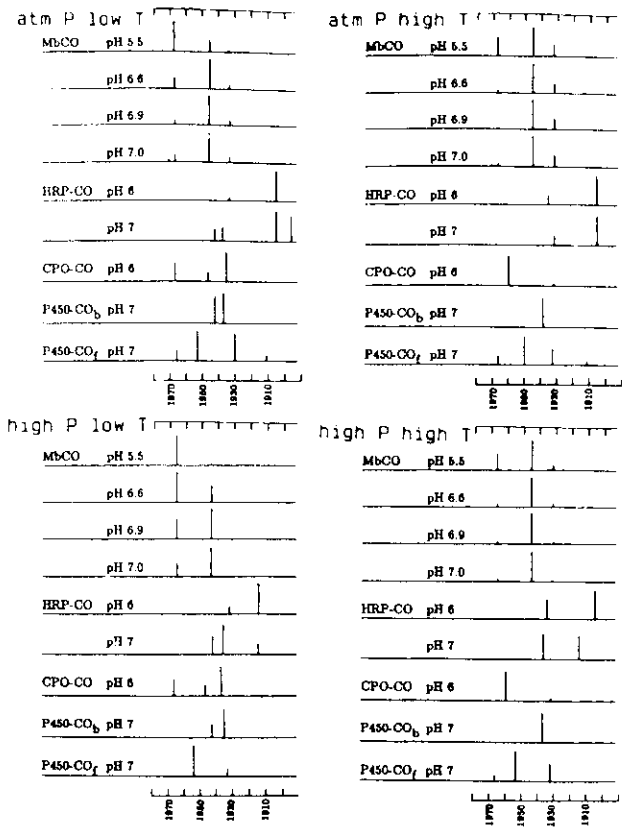

Fig. 23.13 The A substates of carbonmonoxy heme proteins (schematics). Top left: atmospheric pressure and ≃ 150 K. Top right: atmospheric pressure and room temperature. Bottom left: 200 MPa and ≃ 150 K. Bottom right: 200 MPa and ≃ room temperature.

given structure, control is achieved by switching the protein from one C^0 to another.

23.6 Substates of Tier 1.

Fig.23.14 shows each CS^0 to be furcated into a large number of substates of tier 1. The strongest evidence for this tier comes from nonexponential rebinding observed in the IR. In Subsection 23.2 we explained nonexponential rebinding in a straightforward way by postulating that different proteins are in different substates, with corresponding barrier heights for rebinding. Fig. 23.23 shows that rebinding of CO to Mb is nonexponential in time in each CS^0. This fact implies that each CS^0 is branched into a large number of substates of tier 1, just as shown in Fig.23.14.

A more detailed study of the characteristics of tier 1 is based on relaxation experiments and will be treated in Part IV. One crucial property of the CS^1, however, does not need a detailed examination and is evident from the rebinding experiments . These experiments[40] demonstrate that rebinding to individual CS^0 is nonexponential in time up to about 160 K. Relaxation in this tier therefore does not begin below 160 K and this observation places a lower limit on the height of the barriers between CS^1.

23.7 Substates of Tier 2.

Evidence for substates of tier 2 comes from the Mössbauer effect and from rebinding experiments. Here we only describe the Mössbauer data, using a very simple theory to extract the essential information.

The Mössbauer Effect. The iron atom in Mb is an excellent object for Mössbauer studies, as sketched in Subsection 22.2. In the experiments discussed here[47,48], the iron in Mb is enriched with ^{57}Fe. The transmission of a beam of ^{57}Fe gamma rays from a Mössbauer source through the Mb sample is studied and the fraction, f(T), of the gamma rays absorbed without recoil is determined. It is customary to plot instead f(T) the mean square deviation of the Mössbauer nucleus, defined by Eq.(17.7) as $\langle x^2 \rangle = -\lambda^2 \ln f(T)$. In Fig.23.24, $\langle x^2 \rangle$ is plotted versus T for a number of myoglobin systems.[49] Except for the "dry" MbCO, all systems show the same behavior. Up to about 200 K, $\langle x^2 \rangle$ increases linearly with T. Near 200 K, a pronounced change in slope occurs

---

[47] F. Parak, E.N. Frolov, R.L. Mössbauer, and V.I. Goldanskii, J. Mol. Biol. **145**, 825 - 833 (1981).

[48] H. Keller and P.G. Debrunner, Phys. Rev. Letters **45**, 68-71 (1980).

[49] P.G. Debrunner, unpublished results.

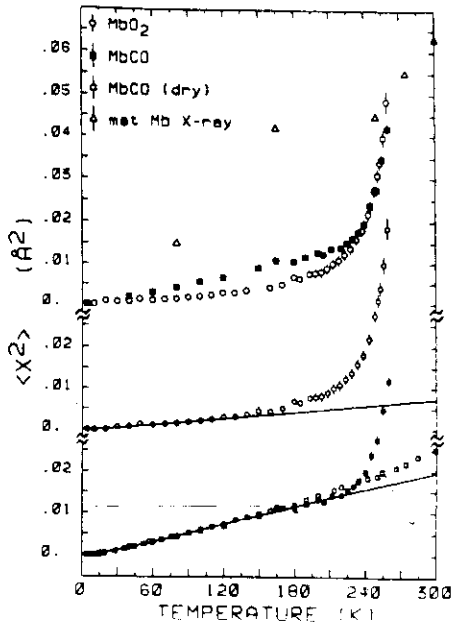

Fig.23.24 The temperature dependence of the mean-square deviation, $\langle x^2 \rangle$, of the ^{57}Fe atom in a number of systems.

and $\langle x^2 \rangle$ becomes rapidly larger. The behavior up to about 200 K is like that in any crystalline solid and is explained by an increased vibrational contribution. The rapid increase above 200 K implies that new degrees of freedom become available. In other words, the ^{57}Fe nucleus experiences new motions. The same behavior is observed in glasses near and above the glass temperature.[50] At first sight, the behavior appears to be just as expected: above the glass temperature, new motions set in. A closer look, however, shows that the situation is more complicated. As we pointed out earlier, nothing important happens at T_g; it is simply the point where the relaxation time is about 10^5 s. The Mössbauer effect, however, has a characteristic time of about 10^{-7} s and should not be sensitive to motions as slow as 10^5 s. Indeed, a more detailed analysis shows that the characteristic energies involved in the Mössbauer effect are typical for substates of tier 2, not tier 1. The essential feature of the analysis can be expressed simply.

[50] F.J. Litterst, Nuclear Instr. Methods **199**, 87 (1982).

Below about 160 K, $\langle x^2 \rangle$ is determined by vibrations and we call this contribution $\langle x^2 \rangle_v$ and assume that it is linear in T up to at least 300K. Above about 160 K, the conformational motion sets in and we denote its mean-square deviation by $\langle x^2 \rangle_c$. For random motions we can write

$$\langle x^2 \rangle = \langle x^2 \rangle_v + \langle x^2 \rangle_c . \qquad (23.15)$$

For the corresponding contributions to the recoilless fraction we consequently can write

$$f(T) = f_v(T)\, f_c(T), \qquad f_c(T) = e^{-\langle x^2 \rangle_c / \lambda^2} . \qquad (23.16)$$

It is straightforward to extract the $\langle x^2 \rangle_c$ or $f_c(T)$ from Fig. 23.24. For the further evaluation we note that $\langle x^2 \rangle$ in Fig. 23.24 refers to the intensity of the sharp Mössbauer line. We now assume that the Fe nucleus experiences conformational motions with an average rate coefficient $\langle k_r \rangle$. The decay rate of the Mössbauer state is given by $k_N = 1/\tau$, where τ is the mean life of the emitting nuclear level. (For ^{57}Fe, $k_N = 7.08 \times 10^6\ s^{-1}$). The fraction $f_c(T)$ of nuclei that remain unaffected by the conformational motion is given by

$$f_c(T) = \exp\{-\langle k_r \rangle / k_N\} . \qquad (23.17)$$

The average rate coefficient for the conformational motions hence is given by

$$\langle k_r \rangle = k_N \langle x^2 \rangle_c / \lambda^2 . \qquad (23.18)$$

Fig.23.25 gives log $\langle k_r \rangle$ versus inverse temperature for single crystal deoxy Mb and for MbO_2 in aqueous solution. The data show Arrhenius behavior between about 200 and 250 K. Above 250 K in aqueous solution, a new motion appears to set in. Values of the preexponential factor and the activation energy are given in Fig. 23.25. These values also imply that the motion sensed by the Fe nucleus is much faster than motions involved in tier 0 and 1. We will discuss these relaxation phenomena in more detail in PART IV. The essential conclusion to remember here is that motions occur even at temperaturers below T_g.

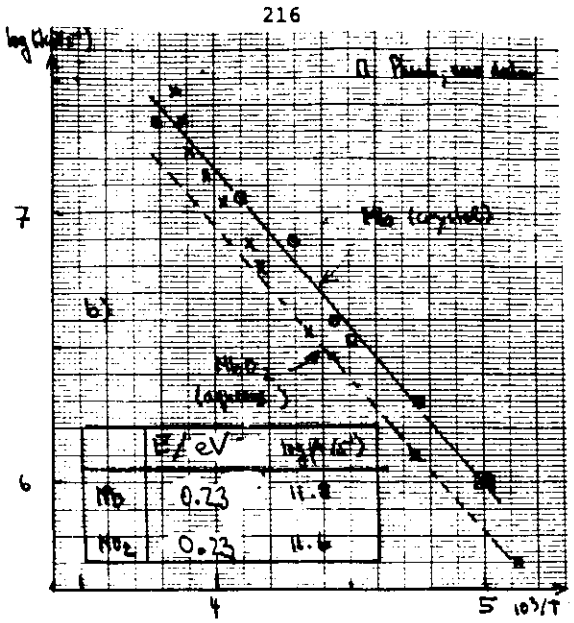

Fig.23.25 The average relaxation rate for the Mössbauer effect versus 1000/T.

23.8 Lower Tier Substates

So far, we have explored the substates shown in Fig. 23.14 down to tier 2. No additional tiers are shown in that figure. There is good evidence, however, of substates with even lower activation energies. The biological importance of these tiers and motions is not clear. It is likely, however, that they will be important for a full understanding of complex systems. Nevertheless we only make a few short remarks here and treat one example in more detail.

Evidence for substates of the lower tiers comes from the excess low-temperature specific heat[51] [52] [53], inelastic neutron scattering[54], hole burning[15-18] [55], dielectric relaxation,[56] [57], and NMR.[58] [59] [60] It is not clear yet if one tier can explain all observed relaxations occuring between 0.1 and,say, 100 K. Morover, it is also not clear if different proteins behave similarly or not. We describe here only one beautiful hole-burning experiment.

Hole burning has already been discussed in section 23.3. Köhler and Friedrich[61] used this technique to study the relaxation taking place at very low temperatures. They used a large protein assembly, phycobilisome, which serves as a molecular light pipe in cyanobacteria and red algae.[62] The phycobilisomes contain a chromophore, allophycocyanin (APC) at the core. APC has a broad absorption band around 650 nm. Laser irradiation (wavelength 657.3 nm) at 4K yields the deep hole shown in the insert of Fig. 23.26. This hole proves that the absorption band in the APC chromophore is inhomogeneously broadened and consequently implies the existence of conformational substates. At the burning temperature T_b = 4 K, the width of the hole is nearly time independent. To study the relaxation of the CS, Köhler and Friedrich used a temperature cycling technique. After measuring the hole at 4 K, they increased the temperature by 1 K, stayed at five K for a set time, rewturned to T_b, and measured the area, the shape and the width of the hole. The cycling is then repeated by going to a higher T. The experiment yields interesting results : The line stays Lorentzian if it was Lorentzian before the burning, the area changes little, but the width increases with the cycling temperature T as shown in Fig. 23.26.

---

51 V.I. Goldanskii, Yu.F. Krupyanski, and V.N. Flerov, Dokl. Akad. Nauk SSSR **272**, 978-981 (1983).

52 G.P. Singh, H.J. Schink, H.V. Lohneysen, F. Parak, and S. Hunklinger, Z. Phys. B **55**, 23 (1984).

53 I.-S. Yang and A.C. Anderson, Phys. Rev. B **34**, 2942-2944 (1986).

54 W. Doster, S. Cusack, and W. Petry, Nature **337**, 754-756 (1989).

55 T. Kushida, A. Kurita, Y. Kanematsu, and Y. Touyama, Can. J. Physics, in press.

56 R. Pethig

57 L. Genzel, F. Kremer, A. Poglitsch, and G. Bechtold, Biopolymers 22, 1715-1729 (1983).

58 E.R. Andrew, D.J. Bryant, and E.M. Cashell, Chem. Phys. Letters **69**, 551-554 (1980).

59 M.A. Keniry. T.M. Rothgeb, R.L. Smith, H.S. Gutowsky, and E. Oldfield, Biochemistry **22**, 1917-1926 (1983).

60. H.C. Lee and E. Oldfield, J.Am.Chem. Soc.**111**,1584-1590(1989).

61 W. Köhler and J. Friedrich, J. Chem. Phys. **90**, 1270-1273 (1989).

62 L. Stryer, **Biochemistry**, 3rd ed. p. 531 (1988).

Explain much more clearly!

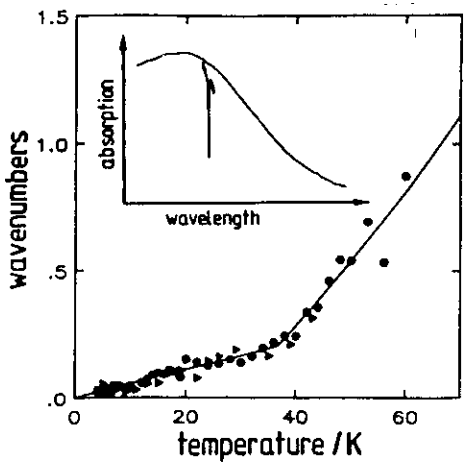

Fig. 23.26 Insert : Hole burned into the absorption spectrum of the chromophore allophycocyanin (ACP) embedded in the protein supramolecular aggregate phycobilisome of the algae mastigogladus laminosus. Main curve: Broadening of the hole as a function of the cycling temperature T. (From Köhler and Friedrich, ref. 61).

The results in Fig. 23.26 can be explained in terms of substates. In the hole-burning process, a photon-induced process changes the substate and the CS corresponding to the wavelength of the hole are rearranged and moved over the entire absorption band. Since this process is photon induced, it is not thermally reversible at low temperatures and the area of the hole remains essentially constant. Equilibrium fluctuations among the substates change the width of the hole. Fig.23.26 shows two distinct regions for the substate rearrangement. Below about 37 K, the broadening is proportional to $T^{\frac{1}{2}}$ and the transitions among substates in this temperature range occur by quantum-mechanical tunneling. (We will discuss this process in more detail in Part IV). Above 37 K, broadening is proportional to $T^{3/2}$ and it can be explained as being due to thermally activated transitions.

23.8 Summary and Open Problems

As pointed out at the beginning, the exploration of the conformational-energy landscape of proteins is at a beginning. We dimly see the basic features, but most of the important data are still lacking. Much experimental and theoretical work remains to be done before we will have a complete picture.

PART IV

FUNCTION AND DYNAMICS

In the first three parts, we discussed the " primitive" aspects of proteins, namely their structure and energy landscape. The object of the discussions could just as well have been glasses instead of proteins. We did not use the fact that proteins are parts of living systems and have well-defined functions. In the present part we turn to the function of proteins and the connection between structure, dynamics, and function. While we already had to be selective in the first three parts, here we have to select even more. An enormous amou..t is already known about the function of proteins and in many cases, the essential features of protein reactions are well known and well characterized. We are interested here in a more fundamental approach : Can we connect structure, dynamics, and function ? Even in very simple cases, these relations are not fully understood and certainly not yet described quantitatively. We will therefore take some well known protein reactions, namely the binding of small ligands such as dioxygen or carbon monoxide, to heme proteins. The biological reaction here appears to be extremely simple, namely the association and dissociation of, for instance, O_2, to myoglobin (Mb) or hemoglobin (Hb). Nevertheless, the detailed study of such a biological reaction demonstrates that it is exceedingly complex and can already teach us a great deal about biological reactions and biological control. In fact, even now the details of the reactions are not known and many problems remain to be solved. We consequently take these binding reactions as prototypes that will teach us the underlying principles.

The approach taken here involves a number of areas:

a. The phenomenological description of the function.
b. The molecular description of the same function, assuming essentially rigid proteins ("single particle model".
c. The exploration of the motions of the protein (dynamics).
d. The dynamic picture of the function : connect motions and function.

In order to treat even a, we require a knowledge of

e. Reaction theory. Because reaction theory is involved in all aspects, we treat it already after a.

24. THE FUNCTIONS OF MYOGLOBIN AND HEMOGLOBIN[1-5]

Hemoglobin is the vital protein that conveys oxygen from the lungs to the tissues and facilitates the return of carbon dioxide from the tissues back to the lungs. Myoglobin accepts and stores the oxygen released by hemoglobin and transports it to the mitochondria. The pathways are shown in Fig. 24.1.

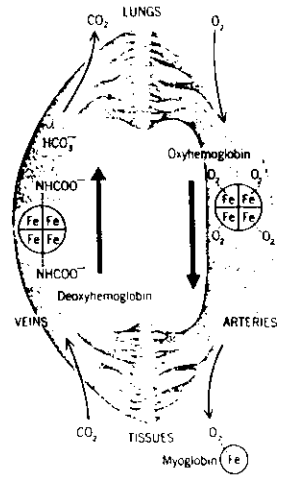

Fig. 24.1 Oxygen is carried from the lungs to the tissues by hemoglobin, and carbon dioxide is carried back to the lungs. Part of the CO_2 transport occurs because the amino termini of the four chains in hemoglobin can bind CO_2 directly to form carbamino compounds: $R\text{-}NH_2+CO_2 \rightarrow R\text{-}NH\text{-}COO^-+H^+$. (After Dickerson & Geis)

1. M. Weissbluth, Hemoglobin, Springer, New York, 1974.
2. M. F. Perutz, Sci. American 239(6), 92-125 (1978).
3. L. Stryer, Biochemistry, Freeman, San Francisco, 1988. 3rd ed.
4. M. F. Perutz, Mol. Biol. Evol. 1, 1-28 (1983). Q. Rev. Biophys. 22, 139-236 (1989)
5. R. E. Dickerson and I. Geis, Hemoglobin, Benjamin/Cummings, Menlo Park, 1983.

Myoglobin is about as simple a protein as can be found and we use it as prototype for studying many of the aspects of protein physics. Hemoglobin is already more complex. While Mb is a monomer, Hb is a tetramer. ~~Mb is very little affected by outside agents,~~ Hb is the prototype of an allosteric protein which is regulated by specific molecules in the environment. Moreover, Hb shows cooperative behavior: It can bind four oxygen molecules. The first binds much more slowly than the last. Mb from different species are similar, Hb shows pronounced and fascinating species adaptation.[4,6]

In the present chapter we give some of the basic features and numbers concerning the binding of small ligands, O_2 and CO, to Mb and Hb.

24.1 Ligand Binding to Myoglobin

We use Mb as prototype of a monomeric protein and write for the reaction of deoxyMb with a ligand, for instance O_2

$$Mb + O_2 \underset{\lambda_{off}}{\overset{\lambda'_{on}}{\rightleftharpoons}} MbO_2. \qquad (1)$$

Here λ'_{on} is the rate coefficient for association and λ_{off} the corresponding coefficient for dissociation. Since these coefficients can change over many orders of magnitude, we refuse to call them constants. Moreover, for reasons that will become clear later, we denote them with λ and not with k. We keep k for elementary steps. The prime on λ'_{on} denotes that it is a second-order coefficient, with units different from the first-order coefficient λ_{off}; λ'_{on} depends on the concentration of the reactants, λ_{off} does not. Denoting concentrations (mol/liter) by [ ], we write the rate equation for the reaction (1) as

$$-\frac{d[Mb]}{dt} = +\frac{d[MbO_2]}{dt} = \lambda'_{on}[Mb][O_2] - \lambda_{off}[MbO_2]. \qquad (2)$$

6. A. C. T. North and J. E. Lydon, Contemp. Phys. 25, 381-393 (1984).

In equilibrium, d[Mb]/dt = 0, and

$$A_a = \frac{\lambda'_{on}}{\lambda_{off}} = \frac{[MbO_2]}{[Mb][O_2]}. \qquad (3)$$

Here A_a is the equilibrium coefficient for association, connected to the equilibrium coefficient for dissociation by

$$A_a = 1/A_d. \qquad (4)$$

If the system is not in equilibrium, the general solution of Eq. (2) depends on the initial conditions and is usually found by computer. We return to this problem later and continue here with the equilibrium case.

Assume that Mb is in a solution in equilibrium. The partial oxygen pressure above the solution, given by P, is also assumed to be in equilibrium with the solvent. Some Mb molecules will be in the deoxy form, some will have an O_2 bound. The degree of fractional saturation is given by

$$y = \frac{[MbO_2]}{[MbO_2]+[Mb]} \qquad (5)$$

or with Eq. (3)

$$y = \frac{A_a[O_2]}{1+A_a[O_2]} = \frac{[O_2]}{[O_2]+A_a}. \qquad (6)$$

The O_2 concentration is proportional to the partial pressure P of the dioxygen and hence

$$y = \frac{P}{P+P_{1/2}}. \qquad (7)$$

Here $P_{1/2}$ is the partial oxygen pressure at which half of the Mb molecules are in the deoxy state. The pressure is usually given in torr, where 1 torr = 1 mm Hg = 133.32 Pa (pascal) and 10^5 Pa = 1 bar.

In Fig. 24.2, the experimental curves for the fractional saturation y are given as function of P for Mb and for Hb. The curve for Mb follows the theoretical expression Eq. (7) well. The curve for Hb, however, does not follow the hyperbolic behavior predicted by Eq. (7) but shows a sigmoidal shape.

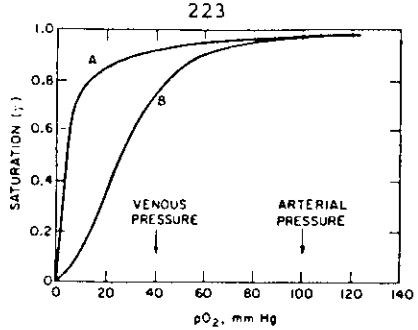

Fig. 24.2 Oxygen equilibrium curves of A. myoglobin and B. hemoglobin.

The difference between Mb and Hb becomes even clearer in the **Hill plot**, Fig. 24.3. To introduce the Hill plot, we use the ratio of oxy to deoxy protein (y/[1-y]) and write with Eqs.(24.6) and (24.7)

$$\frac{\text{oxy}}{\text{deoxy}} = \frac{y}{1-y} = \frac{O_2}{\Lambda_a} = \frac{P}{P_{1/2}} . \qquad (24.8)$$

A plot of y/[1-y] as a function of oxygen pressure P should yield a straight line, if Λ_a is constant. As shown in Fig. 24.3, Mb yields a straight line, but Hb does not.

24.2 Ligand Binding to Hemoglobin

Fig., 24.2 demonstrates that Hb does not satisfy the simple hyperbolic relation Eq. (24.7). To fit the data, Hill introduced in 1913 a hypothetical equilibrium[1]

$$Hb + n\ O_2 \leftrightarrow Hb(O_2)_n . \qquad (24.9)$$

The fractional saturation for this hypothetical reaction is given by

$$y = \frac{[Hb(O_2)_n]}{[Hb(O_2)_n]+[Hb]} = \frac{P^n}{P^n + P_{1/2}^n} \qquad (24.10)$$

where we have again used the fact that the concentration of O_2 is proportional to the partial dioxygen pressure. With Eq.(24.10) we get

$$\frac{y}{1-y} = \left(\frac{P}{P_{1/2}}\right)^n . \qquad (24.11)$$

In a Hill plot, log (y/(1-y)) versus log ($P/P_{1/2}$), Eq. (24.11) gives a straight line with slope n. For Mb, n = 1. Fig. 24.3 shows a Hill plot for Hb. At small and large values of P, n = 1. This result is reasonable: At very low P, only a small fraction of Hb molecules are occupied and they have only one of the four sites occupied. The molecule acts like a monomer and the relation deduced for Mb applies. At very large P, nearly all states will be occupied and again Hb acts like Mb, but with smaller value of $P_{1/2}$. In the transition region, Eq. (24.11) is a good approximation, with a Hill coefficient n = 2.8.

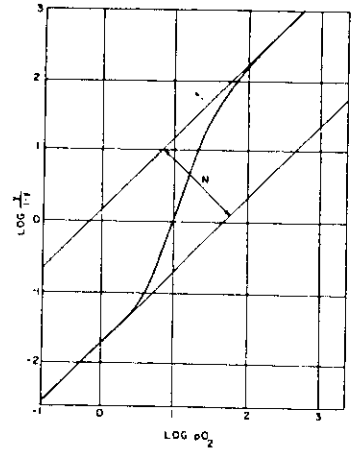

Fig. 24.3 Hill plot. Hb at pH 7.

NOTE:

Do not confuse association rates and equilibrium coefficients. Mb binds oxygen more tightly than Hb, but the binding of O_2 to Mb is slower than to Hb.

24.3 The Bohr Effect

Christian Bohr, 1855-1911, the father of Niels, discovered that the affinity of hemoglobin for O_2 depends on acidity. The relevant curves are shown in Figs. 24.4 and 24.5. The cooperative characteristics are not affected by pH. Removal of protons increases the affinity for ~~protons~~ dioxygen. The importance is clear. In the lung, uptake of O_2 is facilitated; in the tissues, O_2 is more easily given off.

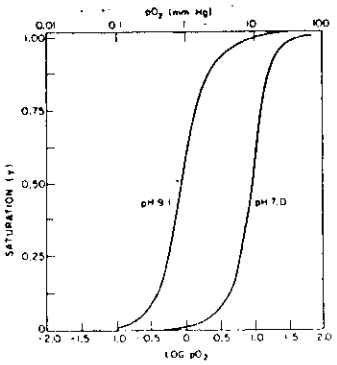

Fig. 24.4 The effect of pH on oxygen equilibrium curves.

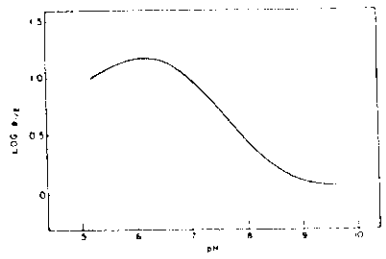

Fig. 24.5 Effect of pH on the affinity of hemoglobin for oxygen.

For a long time, it was stated that the binding of ligands to Mb is independent of pH. Careful measurements show, however, a small pH dependence for the binding of CO to Mb. (W. Doster et al., Biochemistry 21, 4831-4839 (1982). This effect can be explained in terms of substates of tier 0.

25. REACTION THEORY

Chemical reactions govern all aspects of biological processes, from enzyme catalysis to transfer of charge, matter, and information. Any deep understanding of biological reactions must be based on a sound theory of chemical reaction dynamics. Most of the knowledge of reaction dynamics, however, has been deduced from two-body interactions of small molecules in the gas phase.[1] In contrast biomolecules provide a complex but highly organized environment which can affect the course of the reaction. Fortunately, the complexity implies a richness of phenomena that allows the examination of fundamental aspects of reaction dynamics. Biomolecules, in particular heme proteins, form an excellent laboratory.

In this chapter we describe some of the main features of reaction theory and stress aspects where experiments with proteins have yielded new insight into reaction theory or call for a reevaluation and extension of the theory. These topics include tunneling, friction, gating, adiabaticity versus nonadiabaticity, pressure, and the role of intermediate states. The results indicate that the field is rich. One word concerns the terms kinetics and dynamics. With kinetics we mean the description of the time dependence of a reaction in terms of rate coefficients, ~~as for instance in Subsection 25.1~~. Dynamics is concerned with the explanation of the reaction parameters in terms of the structure of the protein.

---

1. S. Glasstone, K.J. Laidler, and H. Eyring, The Theory of Rate Processes, McGraw-Hill, 1941 (the standard work).

If one looks through a standard text treating chemical reactions [1], it appears as if the problem had been solved and only minor questions remained to be answered. The actual situation is very different and reactions in complex systems are still being investigated. In an incomplete and probably misleading way, we can explain some of the problems in the following diagram.

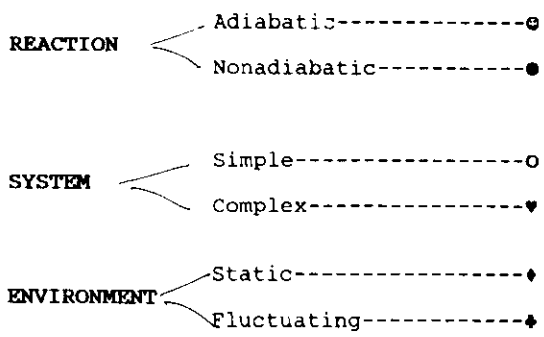

Any combination of these cases can occur. A reaction can, for instance, occur in a complex, static (frozen) system and involve a non-adiabatic transition. And, to make matters worse, the cases shown above are limits and most real situations are mixed. A complete discussion of all cases is far beyond this course. The treatment should, however, provide some insight into the various areas.

The standard treatment in biochemistry and chemistry is based on two equations: The time course of a reaction is usually fitted to one or possibly two exponentials,

$$N(t) = N(0)\ \exp\{-k(T)t\},$$

and the temperature dependence of the rate coefficient k(T) is usually fitted to an Arrhenius (transition state) expression

$$k(T) = A\ \exp\{-E/RT\}.$$

The two expressions fit almost any data well. Why do we reject them? Because the fits are usually done over small ranges in N(t), t, and T. Since there is no fundamental benchmark by which the results can be gauged, even totally inappropriate values of A and E are accepted. The discussions that follow should indicate where theoretically better founded equations can be found and used.

25.0 Chemical Kinetics

Chemical kinetics is like sleep: it is essential, but boring. It contains no information about the physics or chemistry of a eaction, but is necessary for its description and for the evaluation of the important parameters. We consequently present the minimum of equations and refer to the literature for all details [1 a].

First-order reactions.

The simplest reaction is of the form A → B. We assume that the rate of the reaction is independent of the number of species present so that

$$dA(t) = -\,dB(t) = -\,k\,A(t)\,dt.$$

Here k is the time-independent reaction rate coefficient. A(t) and B(t) are the concentrations of the species A and B at the time t. The equation yields

$$A(t) = A(0)\ \exp\{-kt\},$$

the relation that is most often used, even if inappropriate. The reaction rate is defined as

$$R = dA(t)/dt = -\,kA(t).$$

While the reaction rate coefficient is independent of the time t and the concentration of the reacting species, the rate depends on time and on A(t).

Slightly more general is the reaction

$$A \underset{k_{BA}}{\overset{k_{AB}}{\rightleftharpoons}} B.$$

The differential equation is easily written down. With the normalization A(t) + B(t) = 1, and the definition of the equilibrium coefficient K ,

$$K = k_{AB}/k_{BA}$$

we get for the case A(0) = 1, B(0) = 0

$$A(t) = \left(\frac{1}{1+K}\right) + \left(\frac{K}{1+K}\right) \exp\{-(k_{AB} + k_{BA})t\}.$$

---

[1] a . S.W. Benson, **The Foundations of Chemical Kinetics**, McGraw-Hill,NY, 1960; K.J. Laidler, Reaction Kinetics, Mc Graw-Hill, NY,1965; R.E. Weston,Jr. and H/.A. Schwarz, **Chemical Kinetics**, Prentice Hall 1972; H. Eyring, S.H. Lin, and S.M. Lin, **Basic Chemical Kinetics**, Wiley, 1980. See also textbooks on Physical Chemistry.

Note that the reaction proceeds with the rate $k_{AB}+k_{BC}$, even though some of the ones that have gone from A to B return to A.

The meaning of the equilibrium coefficient K is easy to see. In equilibrium, the concentration rate in the two states A and B is given by $A\ k_{AB} = B\ k_{BA}$, or

$$B/A = K\ .$$

First order reaction.
Consider now the reaction

$$A + B \rightarrow P,$$

where P denotes the product. The equation govern this process is

$$dA/dt = dB/dt = -\ k\ A\ B.$$

Since A and B disappear at the same rate, we can write

$$B - A = \alpha$$

where α is the excess (or deficiency) of B compared to A. Then

$$dA/dt = -\ k\ A\ [A + \alpha].$$

Define

$$\beta = A + P, \qquad L = \alpha/\beta.$$

The normalized fraction of A(t) [A(0) = 1] that has not reacted at time A is given by $N(t) = A(t)/\beta$.

If A and B are present in equal concentrations ($\alpha = L = 0$), N(t) is a power law with slope -1 at long times:

$$N(t) = [1/f + \beta kt]^{-1}.$$

Here f is the fraction of A that participates in the reaction,

$$f = A(0)/\beta.$$

The general solution becomes

$$N(t) = \frac{L}{(1+L/f)\,e^{L\beta kt} - 1}\ .$$

If B»A, B remains essentially constant in time and the reaction becomes pseudo-first order, with

$$N(t) = \exp\{-Bkt\}.$$

Note that the coefficients k ina first and a second order reaction have different dimensions; k(first order) is given in s^{-1} , k(second-order) in $s^{-1}\ mol^{-1}$.

The time dependence of a second-order reaction for various values of L is given in the figure below.

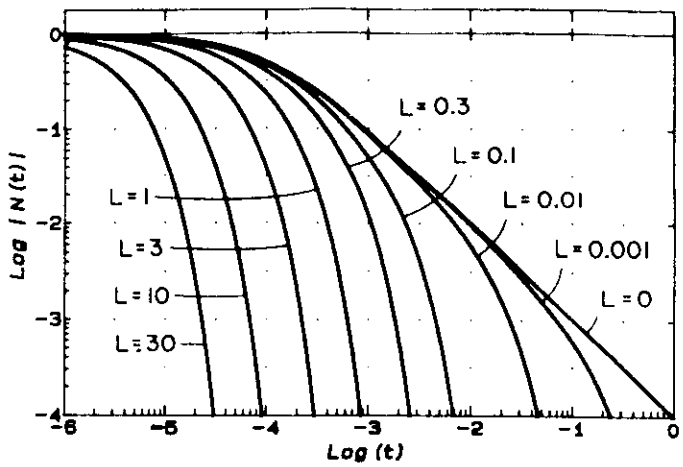

Figure A.1: **Bimolecular Reaction** Bimolecular reaction for various values of L ($L = \frac{[B]-[A]}{[A]+[AB]} = \frac{\gamma}{\alpha}$) where $f = 1$, $\alpha k = 10^4/s$.

25.1 Arrhenius Transitions and Tunneling

The reaction rates depend on many parameters, the most important one of which is temperature. Empirically most reaction rate coefficients depend exponentially on temperature,

$$k(T) = A\, E^{-E/k_B T}. \qquad (25.1)$$

The preexponential or frequency factor A is essentially temperature independent. The activation energy E controls the temperature dependence. Eq. (1) was first given by Hood in 1878, then by Arrhenius in 1887;[2] it is called the Arrhenius equation. From the measured reaction rates, A and E are found by plotting log k versus 1/T. (Arrhenius Plot).

Let us consider a binding process in more detail by using a simplified case. Assume that the potential between two reacting particles depends only on their distance. We represent the situation by the potential energy map in Fig. 25.1. The map shows two wells, separated by a saddle. Well A is much deeper than B. Two cross sections as indicated in Fig. 25.1 are given in Fig. 25.2. A particle placed in one well, say B, has a certain probability of

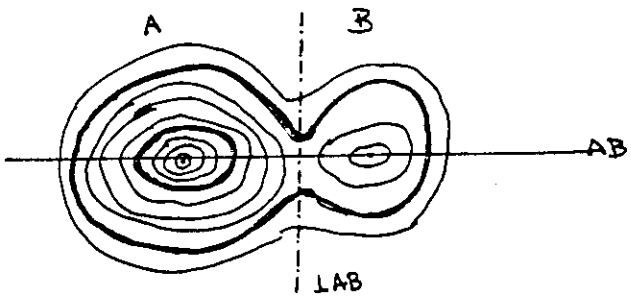

Fig. 25.1 Extremely simplified potential energy map for a transition B → A.

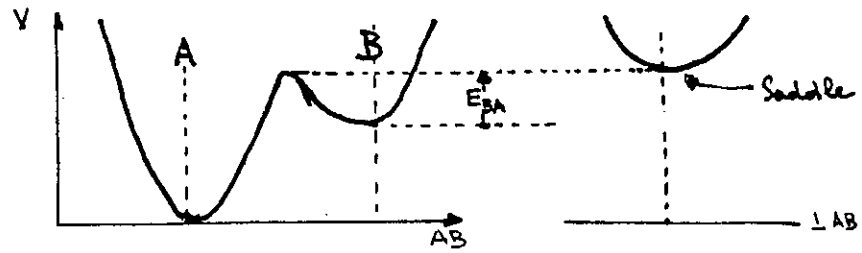

Fig. 25.2 Two cross sections through the energy map of Fig. 25.1.

moving to the other well. What are the essential aspects of such a process? If well A is much deeper than B, say by about 1 eV (100 kJ/mol), the transition corresponds to a chemical binding.

The energy levels in the two wells are quantized. An enormous amount of energy has been spent by many people to calculate energy levels in detail.[3] We sketch in Fig. 25.3 the energy levels in a two-well system as obtained in

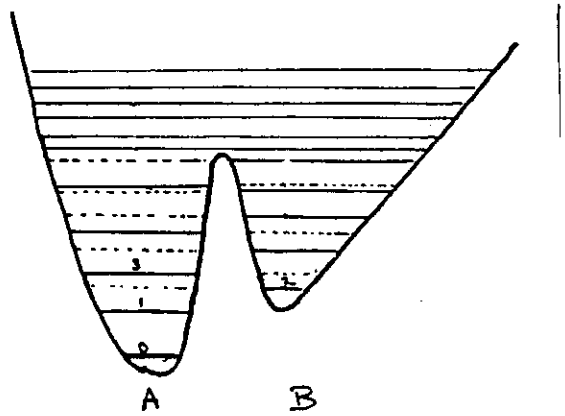

Fig. 25.3 Vibrational eigenvalues in a double well.[3] Levels below the separating barrier are predominantly localized in one or the other well.

2. S. Arrhenius, Z. Phys. Chem. 4, 226 (1889).

3. B. G. Wicke and D. O. Harris, J. Chem. Phys. 64, 5236-5242 (1976).

in ref. 4. Since the two wells form one system, energy levels are always common to both wells, even below the barrier. However, the wave function depends drastically on level, as sketched in Fig. 25.4.

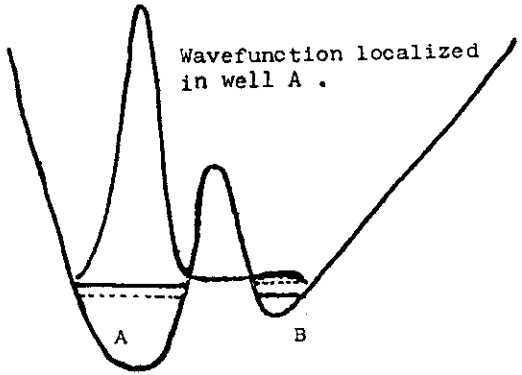

Fig. 27.4 Localized wave function.

Assume now that a particle is initially placed in well B and that there are very many identical systems so that we can consider averages. At a temperture T, the levels in well B will be occupied according to a Boltzmann distribution and two situations must be considered as indicated in Fig. 25.5. At very low temperatures, only the lowest levels in B will be occupied. To move to A, particles have to tunnel through the barrier. At high temperatures, some levels above the saddle point will be occupied and particles can move over the barrier classically, by the standard Arrhenius motion. We will treat the two cases in more detail in the next sections.

The discussion given so far is extremely simplified and corresponds to a single particle potential model. The complex many-body system of a protein is replaced by a potential and the particle (CO, for instance) moves in a fixed potential. Clearly, such an oversimplified approach misses many of the essential aspecs of protein dynamics. Equally clearly, as we know from nearly

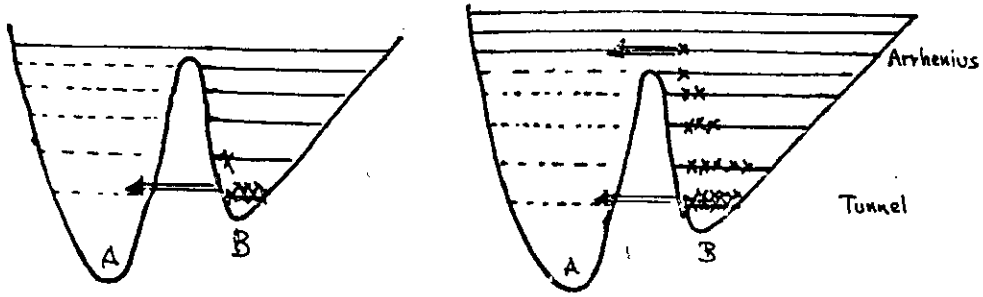

Low T. Only levels below barrier occupied. Only tunneling.

High T. Some levels above barrier occupied. Arrhenius and tunneling occur.

Fig. 25.5 Temperature dependence of transition B → A.

every field of physics, the single-particle approach is a necessary first step. Improvements come when the most primitive approximation is understood.

Fig. 25.5 demonstrates that tunneling and classical motion are not two different phenomena, but two aspects of the same process.

25.2 Transition State Theory (TST)

A "derivation" of the Arrhenius relation is given by the transition state theory.[1] Here we give a simple "derivation" of the corresponding rate coefficient k_{TST} for the transition over a barrier of height E. This leads essentially to the Eyring relation. This relation has been used extensively in chemistry in the past 50 years. We will later show that its use is not justified in reactions in the condensed phase, in particular in protein reactions. Nevertheless, it forms the starting point for many discussions and we therefore need to understand its basic features. ~~A somewhat different derivation is found in ref. 2.~~

Consider the situation shown in Fig. 25.6, where $E^{\ddagger}_{BA}$ denotes the height of the barier between the well B and the transition state between B and A. Assume the system to be in equilibrium at temperature T. The fraction of molecules having an energy E greater than E_{BA} is then given by

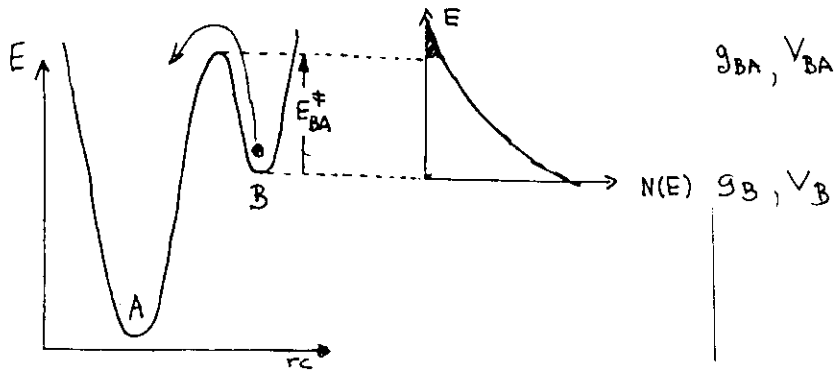

Fig. 25.6 Thermal transitions over the barrier between B and A. The Boltzmann distribution N(E) vs E for the particles in well B are shown at right.

$$\frac{\int_{E^{\ddagger}_{BA}}^{\infty} \exp[-E/RT]dE}{\int_{0}^{\infty} \exp[-E/RT]dE} = \exp[-E^{\ddagger}_{BA}/RT]. \qquad (25.2)$$

The molecules vibrate in well B with a frequency given by $\hbar\omega = k_B T$, or

$$\nu = \frac{k_B T}{h}, \qquad (25.3)$$

about 10^{13} s^{-1} at 300 K. We further denote the number of states (degeneracy) in well B by g_B, on top of the barrier by g_{BA}. The rate coefficient with which a molecule passes from well B to A by overcoming the barrier is given by the product of attack frequency ν, ratio of states g_{BA}/g_B, and probability of having an energy larger than $E^{\ddagger}_{BA}$:

$$k_{TST} = \nu\,(g_{BA}/g_B)\, e^{-E^{\ddagger}_{BA}/k_B T}.$$

But

$$g_{BA}/g_B = e^{S^{\ddagger}_{BA}/k_B}, \qquad (25.4)$$

where $S^{\ddagger}_{BA}$ is the entropy difference between the bottom of well B and the top of the barrier B → A. The rate thus finally can be written as

$$k_{TST} = \nu\, e^{-F^{\ddagger}_{BA}/k_B T}, \qquad (25.5)$$

where $F^{\ddagger}_{BA} = E^{\ddagger}_{BA} - T\,S^{\ddagger}_{BA}$ is the difference in Helmholtz energy between well B and the top of the barrier (activation Helmholtz energy).

Assume now in addition that the system is placed under a pressure P and that the volume of the system is V_B in state B and V_{BA} at the transition state on top of the barier. The particle moving from B to A then has to have an energy $E_{BA} + P\,V^{\ddagger}_{BA}$, with

$$V^{\ddagger}_{BA} = V_{BA} - V_B, \qquad (25.6)$$

in order to reach the top of the barrier. Here $V^{\ddagger}_{BA}$ is called the <u>activation volume</u>. The limit of integration E_{BA} in Eq. (2) is replaced by $H^{\ddagger}_{BA} = E^{\ddagger}_{BA} + P\,V^{\ddagger}_{BA}$, the activation enthalpy. $H^{\ddagger}_{BA}$ then appears instead of $E^{\ddagger}_{BA}$ in all subsequent equations and the final expression can be written as

$$k_{TST} = \nu \exp(-G^{\ddagger}_{BA}/RT), \qquad (25.7)$$

with

$$G^{\ddagger}_{BA} = H^{\ddagger}_{BA} - T\,S^{\ddagger}_{BA}, \qquad (25.8)$$

and

$$H^{\ddagger}_{BA} = E^{\ddagger}_{BA} + P\,V^{\ddagger}_{BA}. \qquad (25.9)$$

Note that if $V^{\ddagger}_{BA}$ is negative, the reaction becomes faster with increasing pressure.

Comparison of Eqs. (25.7)-(25.9) and Eq. (25.1) shows that

$$A = \nu \exp(S^{\ddagger}_{BA}/k_B T), \qquad (25.10)$$

$$E = H^{\ddagger}_{BA}. \qquad (25.11)$$

With Eq.(25.3), Eq.(25.7) becomes the standard Eyring expression

$$k_{TST} = (k_B T/h) \exp(-G^{\ddagger}/RT). \qquad (25.12)$$

This relation, in some form or other, is found in most texts.[4] While it may be justified for gas-phase reactions, its application to biomolecular reactions ~~can lead to serious problems~~ is inappropriate. To discuss improved relations we note that Eq.(25.12) is based on a number of assumptions. The most essential assumptions are :

(i) The system is in thermal equilibrium.
(ii) A trajectory crosses the barrier only once and the system does not return from B to A.
(iii) The system can be treated classically.
(iv) The reaction proceeds adiabatically.
(v) The reaction surface is static.

All of these assumptions are questionable for biomolecular reactions and must be removed and the treatment must be generalized.

25.3 The Kramers Equation.

In 1940, H.A. Kramers[5] treated a simple model of a chemical reaction, namely the escape of a particle from a potential well, by using the Fokker-Planck equation.[6] For a long time, Kramers' work was appreciated only by a few theoreticians[7] and not at all by the experimentalists. Within the last two decades, Kramers' work has become the central point of an improved approach to reaction theory and reactions in solids and it has also been discovered by the experimentalists. The number of papers has become extremely large so that we refer to reviews for a complete discussion.[2 8 9] No really simple discussion of the approach of Kramers exists and his original paper is not easy to read. We therefore follow an earlier, somewhat handwaving, introduction to

---

[4] See for instance R.S. Berry, S.A. Rice, and J. Ross, **Physical Chemistry**, Wiley, New York, 1980. Eq.(30.68).

[5] M. Dresden, **H.A. Kramers**, Springer New York, 1987.

[6] H.A. Kramers, Physica **7**, 284 (1940).

[7] H.C. Brinkman, Physics **22**, 149 (1956). R. Landauer and J.A. Swanson, Phys. Rev. **121**, 1668 (1961).

[8] P. Hanggi, J. Stat. Phys. **42**, 105-148 (1986).

[9]. P. Hänggi, P. Talkner, and M. Borkovec, Rev. Mod. Phys. **62**, 251-341 (1990).
9a. See also the issue "Rate Processes in Dissipative Systems: 50 Years after Kramers." Ber. Bunsenges. Phys. Chem. **95**,#3 (1991).
6# Reprinted in H.A. Kramers, **Collected Scientific Papers.** North-Holland, Amsterdam, 1956.

the Kramers theory.[10] Before doing so, we describe briefly why the approach of Kramers is important for biomolecules.

Biomolecular Reactions. We have pointed out a few times that proteins are dynamic systems and that we expect protein fluctuations to influence protein reactions. If a protein is embedded in a solvent, the solvent will influence the fluctuations . In particular, we can expect that some protein reactions will decrease with increasing viscosity.[11 12] Indeed, experiments show that viscosity affects for instance enzyme reactions[13] and the binding of ligands to heme proteins.[14] To evaluate such experiments, the following general approach can be used.

Assume that we have measured an observable F as a function of temperature T and viscosity η, keeping other parameters constant. F consequently is a function of the two variables T and η, $F(T,\eta)$, and represents a surface in a T-η plot. For a given solvent, η depends approximately exponentially on temperature. If we plot F vs η, η spans too large a range. Thus we take log η as second variable. The plot of $F(T,\eta)$ in a T-log η plot is sketched in Fig. 25.~~4~~7. If the surface is smooth it can be assumed that the various solvents do not change the protein in an unacceptable manner. Isothermal cuts through the $F(T,\eta)$ surface show how the viscosity affects F. ~~one example is given in Fig. 25.4~~. Isoviscosity cuts provide the temperature dependence of $F(T,\eta)$ at fixed viscosity.

---

[10] H. Frauenfelder and P.G. Wolynes, Science **229**, 337-345 (1985).

[11] B. Somogyi and S. Damjanovich, J. Theor. Biol. 48, 393 (1975).

[12] B. Gavish, Biophys. Struct. Mech. 4, 37 (1978).
B. Gavish and M. M. Werber, Biochemistry 18, 1269 (1979).

[13] ~~B. Gavish and~~

[14] D. Beece, L. Eisenstein, H. Frauenfelder, D. Good, M. C. Marden, L. Reinisch, A. H. Reynolds, L. B. Sorensen, and K. T. Yue, Biochemistry 19, 5147-5157 (1980).

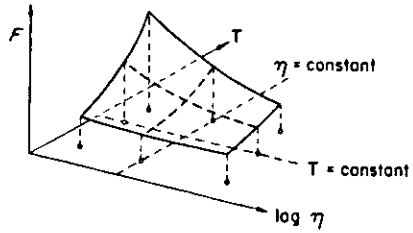

Fig. 25.7 Idealized plot of an observable F as a function of the two independent variables T and log η, where T is temperature and η the viscosity. Isothermal (T = constant) and isoviscosity (η = constant) sections are indicated.

The conclusion of experiments over a wide range of viscosity[14 15] is clear : Protein reactions are strongly influenced by viscosity. This result implies that protein motions are indeed important for protein function and it also suggests that the standard TST relation is not sufficient for the data evaluation.

Reaction Coordinate and Friction. In Fig. 25.6, we show a reaction from state B to state A as a transition along a reaction coordinate rc. Reality is, of course, far more complex. In the actual reaction, the entire protein and its surrounding takes part. If we could treat the entire system without approximations, all dynamical effects would be incorporated and there would be no need to introduce viscosity or friction. Indeed, in molecular dynamics calculations such an approach is used. Usually, however, the reaction is treated by separating the coordinates into a reaction coordinate and invisible coordinates. The invisible coordinates exchange energy and momentum with the reaction coordinate. Energy and momentum of the reaction coordinate alone are not conserved; the reaction coordinate can gain or lose energy and momentum. The effect of this exchange on the reaction coordinate is called friction. Friction is essential for the trapping of the system in the product state A. The fluctuation-dissipation theorem (Subsection B.7) tells us that the friction (dissipation) is necessarily accompanied by fluctuating forces, arising also from the neglected coordinates. When friction is large the motion along the reaction coordinate looks like a Brownian motion or a random walk, and not the smooth ballistic motion required for the derivation of the TST equation. Friction can be roughly characterized by a velocity autocorrelation time τ_v which is given by

$$\tau_v = m/\zeta \quad . \tag{25.13}$$

Here m is an effective mass and ζ is the friction coefficient.

15 D. Beece, S.F. Bowne, J. Czégé, L. Eisenstein, H. Frauenfelder, D. Good, M.C. Marden, J. Marque, P. Ormos, L. Reinisch and K.T. Yue. The effect of Viscosity on the Photocycle of Bacteriorhodopsin. Photochem. Photobiol. 33, 517-522 (1981).

In a liquid, ζ is approximately related to the viscosity η by Stokes law,

$$\zeta = 6\pi\eta a \tag{25.14}$$

where a is a characteristic linear distance.

The Transmission Coefficient. Friction will clearly affect the reaction rate coefficient k. The effect of friction (or the invisible coordinates) can be characterized by a transmission coefficient, κ , by writing

$$k = \kappa \; k_{TST} \; , \tag{25.15}$$

where k_{TST} is given by Eq.(25.7). Kramers' theory shows that κ has the form sketched in Fig. 25.8 : At low friction, is proportional, and at high friction inversely proportional to the friction coefficient. In the intermediate regime, the value 1 predicted by TST is an upper limit and can be significantly in error.[16]

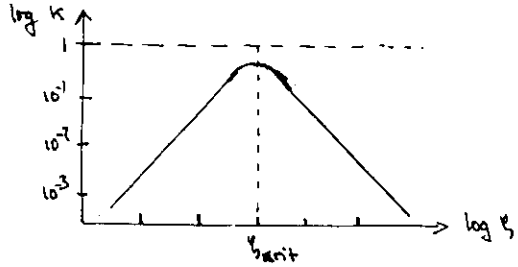

Fig. 25.8 General behavior of the transmission coefficient as predicted by the Kramers theory.

The general behavior can be easily understood. At low friction, the systems above the barrier in Fig. 25.6 quickly react, but then equilibrium has to be reestablished: Systems with lower energy have to acquire sufficient energy to move over the barrier and this process is proportional to viscosity. At high viscosity, the system must diffuse over the barrier and this process is inversely proportional to viscosity.

The rate coefficient k reaches a maximum at a value

$$\zeta_{crit} = d\,m\,\omega \tag{25.16}$$

16 D.G. Truhlar, W.L. Hase, and J.T. Hynes, J. Phys. Chem. 87, 2664 (1983).

where $\omega = 2\pi\nu$ and where d is a numerical coefficient that depends on the reaction energy surface and the damping mechanism but is smaller than 1. With the Stokes relation, Eq.(25.14), and d = 1, Eq. (25.16) becomes

$$\eta_{crit} = (1/3)(m/a)(\omega/2\pi). \qquad (25.17)$$

The typical values of $m/a = 2 \times 10^{-15}$ g cm^{-1} and $\omega/2\pi = 10^{13}$ sec^{-1} yield η_{crit} = 7 millipoise (mP). Water at 300 K has a viscosity of 8.5 mP, so we expect most protein reactions to be overdamped.

Whereas the calculation of the reaction rate over the entire range of friction is difficult [8,9], the limiting cases $\zeta \ll \zeta_{crit}$ and $\zeta \gg \zeta_{crit}$ can be treaed by using simple physical arguments based on the two characteristic lengths in the problem. The first length is the mean free path, λ, the average distance before the coordinate reverses its direction of motion. From Eq. (25.13), λ is related to the velocity autocorrelation time τ_v or the friction ζ by

$$\lambda = v_{rms}\,\tau_v = (2mk_BT)^{1/2}/\zeta \qquad (25.18)$$

where v_{rms} is the root-mean-square velocity. The second relevant length is the size of the transition region, ℓ_{TS}, defined by the condition that the energy in this region is within k_BT of the transition state energy. For a parabolic Gibbs energy barrier with curvature $m(\omega^*)^2$ at the col, as drawn in Fig. 25.9, ℓ_{TS} is given by

$$\ell_{TS} = 2\{2k_BT/m(\omega^*)^2\}^{1/2} \qquad (25.19)$$

where ω^* is the undamped frequency of motion in the top of the transition barrier.

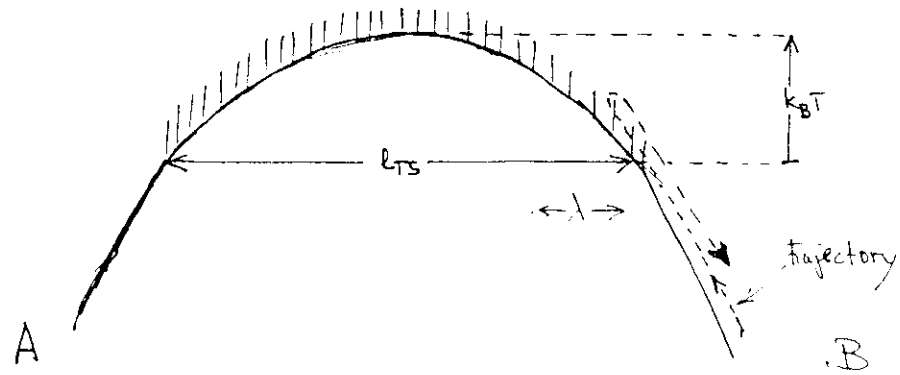

Fig. 25.9 Parabolic barrier, with characteristic lengths. Only the top of the barrier is shown. The transition region is shaded. A typical trajectory in the overdamped regime is shown at the right.

The character of the transition is determined by the ratio λ/ℓ_{TS}, given by Eqs. (25.18) and (25.19) as

$$\lambda/\ell_{TS} = m\omega^*/2\zeta. \qquad (25.20)$$

The system is critically damped if only one collision occurs during the passage so that $\lambda \approx \ell_{TS}$ or $m\omega^* \approx 2\zeta$. This criterion agrees with the general criterion Eq. (15.16). If $\lambda >> \ell_{TS}$, the system moves ballistically, without collisions, through the transition region; it is underdamped. If $\lambda << \ell_{TS}$, the system undergoes many collisions in the transition state and it is overdamped. Both situations can be discussed in simple terms.[10] We first treat the high-friction case, ~~with a slightly different approach than used in reference 2.~~

High friction. When the friction is high, the reacting system is always in equilibrium with the surrounding heat bath, but the particle cannot traverse the transition region in a single attempt. Rather, as sketched in Fig. 25.9, a particle that attempts the crossing will make a random walk over the transition region. Most of the time, it will only penetrate a small distance into the transition region and will then return to the bottom of well B before trying again. The number of tries required for a successful crossing is given by the ratio $\ell_{TS}/2\lambda$. The transmission coefficient is the inverse of the ratio of tries and thus given by Eq. (15.20). Introducing this transmission coefficient into Eq. (15.7) gives with $\nu = \omega_B/2\pi$

$$k(T,\zeta) = \frac{m\omega^*\omega_B}{2\pi\,\zeta}\, e^{-G^*/RT} . \qquad (15.21)$$

Eq. (15.21) is the relation Kramers found at the high-damping limit.[6] (This limit is sometimes called the "diffusion limit". Diffusion here refers to the Brownian passage over the col and not to the ordinary diffusion that governs "diffusion-controlled" ~~biomolecular~~ reactions.)

Low Friction. If the friction is low, the system, on leaving the transition state, will not lose sufficient energy to drop into well A (Fig. 25.6) but will bounce off the other side and recross the barrier. If τ_r is the time to traverse the well and τ_E the time to lose approximately the energy k_BT, the system will go back and forth across the barrier roughly $N_c = \tau_E/\tau_r$ times before reacting. In general, τ_E is proportional to the velocity autocorrelation time τ, Eq. (15.13), and consequently proportional to $1/\zeta$. The transmission factor thus is proportional to the friction coefficient ζ, as shown in the left branch of Fig. 25.8. The same result is obtained by considering the time it takes to activate the system.

The result of these considerations can be summarized simply. At low friction, the reaction coefficient is proportional, and at high friction inversely proportional, to the friction coefficient. In the intermediate regime, the reaction coefficient depends somewhat on the potential surface topography and the frictional mechanism, but the value predicted by TST is an upper limit that can be significantly in error.

Experimental Verification of the Kramers Equation. Experiments, in particular by Fleming and collaborators[17], has confirmed the essential aspects of the Kramers theory. Fig. 25.10 gives the reaction rate for the photoisomerization of stilbene as a function of the inverse of the diffusion coefficient in gaseous and liquid alkanes. The pattern predicted in Fig. 25.8 is confirmed. The maximum rate coefficient occurs, however, at a viscosity lower than predicted by Eq.(25.17).

---

[17] G.R. Fleming, S.H. Courtney, and M.W. Balk, J. Stat. Phys. **42**, 83-104 (1986).

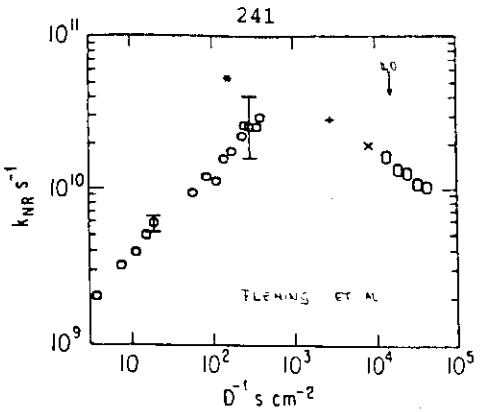

Fig. 25.10 Experimental verification of the Kramers relation. From Fleming et al., ref. 17.

Biological Importance. The behavior of the Kramers relation, as shown in Figs. 25.8 and 25.10, can be crucial for the control of biomolecular reactions. If the TST relation were correct, a reaction could be controlled only by changing the activation Gibbs energy, by either changing the activation energy, activation volume, or activation entropy. Such changes would usually involve a change within the biomolecule. The Kramers relation shows that control can also be exerted from the outside by changing the friction through changing the viscosity. Such changes can occur for instances in membranes where cholesterol is very efficient in affecting the viscosity.

Additional Remarks. Experimental data are usually fitted with an Arrhenius relation, $k = A \exp[-E/RT]$, and activation enthalpy and entropy are obtained with Eqs.(25.10) and (25.11). These approximations are based on the assumption of a temperature- independent transmission coefficient. Fig.25.10 shows, however, that κ depends on friction. Friction is strongly temperature dependent. With

$$\zeta = \zeta_o \exp(E_\zeta/RT) \qquad (25.22)$$

the connections between activation enthalpies and entropies corresponding to the high-damping result Eq. (21) are

$$H^\ddagger - H^* = E_\zeta, \quad S^\ddagger - S^* = E_\zeta/T_o \qquad (25.23)$$

where T_o is the average tempetature where the data were taken. As before ‡ denotes data taken in a given solvent and * indicates isoviscosity data.

Some Preliminary Remarks Concerning the Tunnel Effect

The tunnel effect is one of the first simple applications that a physics student learns in QM. The problem is as sketched in the next figure.

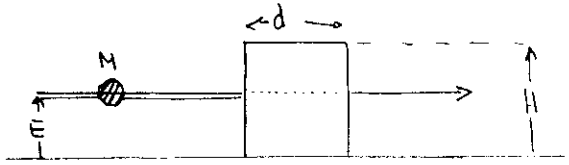

Fig. 25... Tunneling through a potential barrier.

A particle with energy E impinges on a barrier. If the energy E is less than the barrier height H, the particle is reflected in classical physics. In QM, the particle is described by a wave and transmission occurs even for $E \ll H$. A simple calculation shows that the transmission coefficient is given by

$$T = \left[1 + \frac{\sinh^2 kq}{4(E/H)(1-E/H)}\right]^{-1}$$

with

$$\hbar k = \sqrt{2M(H-E)}\ .$$

If the transmission is small, the rate coefficient k_t for tunneling can be written as

$$k_t = A_t\ (T)\ \exp\{-\alpha\ [2M(H-E)]^{1/2}\ d/\hbar\}.$$

The preexponential factor A_t contains a number of factors that we do not treat here. The coefficient α depends on the shape of the barrier and it is given by $\alpha = 4/3$ for a triangular barrier, $= \pi/2$ for a parabolic barrier, and $\alpha = 2$ for a square one.

$\left(\sinh x = \frac{1}{2}\left(e^x - e^{-x}\right)\right)$

25.4 The Tunnel Effect

Quantum-mechanical tunneling is important in nearly every part of physics, from cosmology to condensed matter. We discuss tunneling here from a restricted point of view, namely the binding of ligands to heme proteins. The concepts are, however, valid for many other processes in biological physics and chemistry and additional information is given in a number of excellent books.[18 19 20 21]

The Tunneling Temperature. In Section 23.2 we briefly discussed the binding of CO to heme proteins at low temperatures and used the Arrhenius equation, Eq.(23.1), to evaluate the data. At first sight it appears that this approach could be used even at very low temperatures, because quantum-mechanical tunneling depends exponentially on the mass. However, the activation barriers, shown in Fig.23.6, are very small. Intuition obtained from work with standard chemical reactions can therefore fail. To obtain an estimate of the temperature where tunneling should set in, we follow an argument by Goldanskii.[22] The parameters involved are sketched in Fig. 25.11. We first assume that tunneling is given by the well- known Gamow factor, calculated in most texts.[23] Lumping attempt and entropy factors into one coefficient A_t, we write

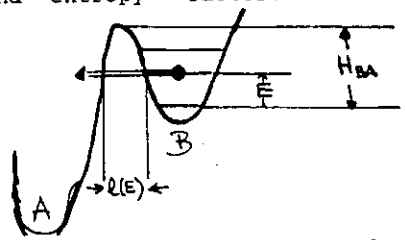

Fig.25.11 Parameters determining tunneling : height H_{BA}, energy E, and barrier width $\ell(E)$.

18 **Tunneling in Biological Systems.** B. Chance et al., Eds. Acad. Press, New York, 1979.

19 R.P. Bell, **The Tunnel Effect in Chemistry,** Chapman and Hall, London, 1980.

20 D. DeVault, **Quantum-Mechanical Tunneling in Biological Systems.** Cambridge University Press, Cambridge, 1984.

21 V.I. Goldanskii, L.I. Trakhtenberg, and V.N. Fleurov, **Tunneling Phenomena in Chemical Physics.** Gordon and Breach, New York, 1989.

22 V. I. Goldanskii, Dokl. Akad. Nauk. SSSR 124, 1261 (1959). See also P Hänggi et al., Phys. Rev. Lett. 55, 761-764 (1985).

23 See for instance L.D. Landau and E.M. Lifshitz, **Quantum Mechanics**, Pergamon Press, 1958.

$$k_t = A_t \exp\{-\gamma[(2M(H_{BA}-E)]^{1/2}\ell(E)/\hbar\}. \qquad (25.24)$$

Here, M is the mass of the tunneling system, H_{BA} the barrier height, E the excitation energy in well B, $\ell(E)$ the barrier width at the energy E. The value of the numerical factor γ depends on the shape of the barrier: for a triangular barrier, $\gamma = 4/3$, for a parabolic one $\gamma = \pi/2$, and for a square one $\gamma = 2$.

Eqs. (1) and (24) together imply that Arrhenius transitions will dominate at high, tunneling at low temperatures, just as we have explained earlier. To find the temperature T_t at which both have similar rates, we assume equal preexponentials and $H_{BA} >> E$ (Note that E in Eq. (1) has the meaning of H_{BA}); we then get

$$T_t = (\hbar/k_B\gamma)(H_{BA}/2M)^{1/2}\ell^{-1}, \qquad (25.25)$$

For a parabolic barrier, with mass M corresponding to a molecule with A = 30, the numerical value of T_t is

$$T_t = 0.9\,[H_{BA}(\text{kJ/mol})]^{1/2}/\ell(\text{nm}). \qquad (25.26)$$

For a barrier of 0.1 nm width and 5 kJ/mol height, $T_t \approx 20$ K.

Experimental Results. The values of T_t implied by Eq. (26) suggest that it should be easy to observe the molecular tunnel effect in heme proteins. Indeed, the experiments are straightforward and the result is clear.[24-26] The rebinding curves for CO to β^A at temperatures below 50 K

24. N. Alberding, R. Austin, K. Beeson, S. Chan, L. Eisenstein, H. Frauenfelder, and T. Nordlund, Science 192, 1002-1004 (1976).
25. N. Alberding, S. S. Chan, L. Eisenstein, H. Frauenfelder, D. Good, I. C. Gunsalus, T. M. Nordlund, M. F. Perutz, A. H. Reynolds, and L. B. Sorensen, Biochemistry 17, 43-51 (1978).
26. H. Frauenfelder, in Tunneling in Biological Systems, B. Chance et al., Eds., Acad. Press, New York, 1979, pp. 627-649.

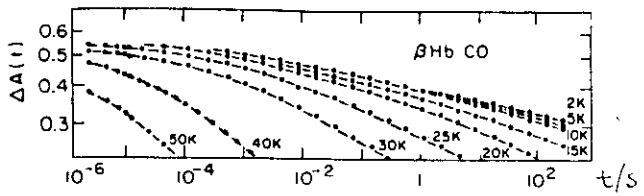

Fig. 25.12 Rebinding of CO to the separated beta chain of human hemoglobin at low temperatures.

are given in Fig. 25.12. Rebinding does not slow down as predicted by an Arrhenius behavior; below about 20 K, it becomes essentially temperature independent. To characterize the rate, we define the coefficient $k_{0.75} = 1/t_{0.75}$, where $t_{0.75}$ is the time at which N(t) drops from 1 to 0.75. The coefficient $k_{0.75}$ is shown in Fig. 25.13 as function of log T.

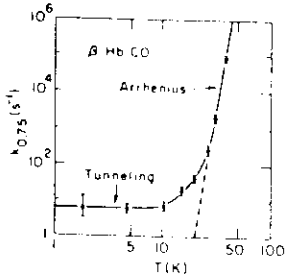

Fig. 25.13 *The rate $k_{0.75} = 1/t_{0.75}$ plotted as a function of log T for binding of CO to βHb. The steeply dropping part corresponds to the classical Arrhenius motion over the barrier. The approximately temperature-independent rate below about 10 K is interpreted as quantum mechanical tunneling through the barrier.*

Fig. 25.13 demonstrates that tunneling sets in at about 20 K in β^A.

The Isotope Effect. Tunneling is characterized by two properties, temperature independence in the limit T->0 and a pronounced dependence on the mass of the tunneling system. The first of these characteristics is clearly shown in Figs. 25.12 and 25.13. Nevertheless, skeptics remain unconvinced; the temperature independence could be caused by some other phenomenon such as a purely entropic barrier at low temperature. The isotope effect can provide a second independent proof for tunneling. There exists a small mass dependence even in a classical Arrhenius rate. The frequency ω_B in Eq. (25.2) depends, of course, on the mass of the system. The dependence is, however, weak and usually neglected. Eq. (25.24), in contrast, shows an exponential mass dependence. With Eq. (25.24) and $\Delta M \ll M$ the mass dependence can be expressed as

$$\ln(k_\ell/k_h) \approx (\Delta M/2M)\ \ln(A_\ell/k_\ell), \qquad (25.27)$$

where the subscripts ℓ and h refer to the light and the heavy isotope, $\Delta M = M_h - M_\ell$, and $M = (M_h + M_\ell)/2$. Eq. (25.27) tells us that the isotope effect can be observed best at small values of k, hence at long times. If binding were exponential in time, we would have little choice: k would be single valued at a given temperature and k_ℓ/k_h would be time independent. As Fig. 25.12 shows however, binding is not exponential in time and the binding rates vary over an enormous range. It is consequently most efficient to measure the rate of rebinding at long times.

While the nonexponential character of rebinding permits us to select a suitably long time, it also causes a problem. Fig. 25.13 demonstrates that the curves of N(t) are "flat" at low temperatures. If we have to compare two different samples with two different isotopes of ~~key~~ CO it would be exceedingly difficult to measure a small effect of about a factor of 2 or less. Such an experiment would not be believable. Fortunately there exists a method that permits a simultaneous observation of the rebinding rates for two isotopes.[27]

Optically, by observation in the Soret region, different isotopes cannot be distinguished. Different CO or dioxygen isotopes have, however, very different infrared spectra as is shown in Fig. 23.15.[28] This fact allows the

27. J. O. Alben et al., Phys. Rev. Letters 44, 1157-1160 (1980).
28. J. O. Alben et al., Proc. Natl. Acad. Sci. USA 79, 3744-3748 (1982).

simultaneous observation of the rebinding of two different isotopes in the same sample. The stretching frequences of the three isotopes of interest in MbCO are 1945 cm for $^{12}C^{16}O$, 1901 cm for $^{13}C^{16}O$, and 1902 cm for $^{12}C^{18}O$. CO rebinding after photodissociation is monitored by measuring the growth of the absorption spectra at the Mb-bound stretching frequencies. Typical curves are shown in Fig. 25.14.

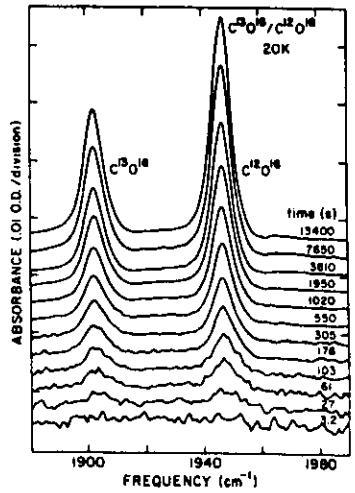

Fig. 25.14. The growth of the CO stretching frequency for two isotopes after photodissociation.

The result is unambiguous: The lighter isotope rebinds faster, as is shown in Fig. 25.15[27].

Fig. 25.15

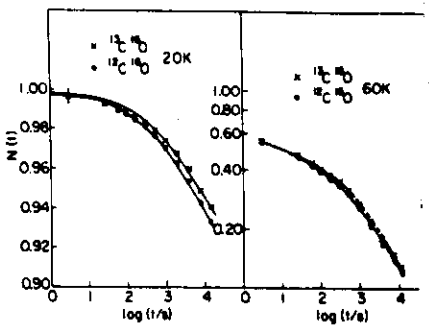

Rebinding of $^{12}C^{16}O$ and $^{13}C^{16}O$ to Mb after photodissociation at 20 and 60 K. $N(t)$ denotes the fraction of Mb molecules that have not rebound CO at time t after the end of the steady-state illumination. The solid curves at 20 K are fits to the data as described in the text. The dashed curves at 60 K are drawn to guide the eye. For 20 K, errors at the earliest times are shown; by 10^3 s, the errors are smaller than the size of the data points. For 60 K the errors are smaller than the size of the data points.

Values of k_l/k_h at the time 1 ks are given in Table I. With some additional assumptions, values of ΔM/M can be extracted.[27]

TABLE I. Values of k_l/k_h at ≈ 1 ks and values of $\Delta M/M$, the relative mass change, in the binding of carbon monoxide to myoglobin. The model calculations refer to point particles moving in fixed potentials.

Quantity		$^{12}C^{16}O$ vs $^{13}C^{16}O$	$^{12}C^{16}O$ vs $^{12}C^{18}O$
Experimental: k_l/k_h	60 K	1.26 ± 0.05	1.15 ± 0.05
	20 K	1.53 ± 0.05	1.20 ± 0.05
$\Delta M/M$	(20 K)	0.040 ± 0.015	0.019 ± 0.007
Model: $\Delta M/M$			
M is the mass of	CO	0.035	0.069
	C	0.080	0
	O	0	0.118
M is the reduced mass of	CO-Fe	0.023	0.045
	C-Fe	0.066	0
	O-Fe	0	0.090

The data lead to three main conclusions:

(1) The rate coefficient k for binding of CO to Mb shows a mass dependence at 60 K and below.

(2) The most natural explanation for the isotope effect is quantum-mechanical tunneling. The effect at 60 K is about one-half as big as at 20 K, in agreement with an independent estimate that at 60K the ratio of tunneling to Arrhenius transitions can be of the order of 0.5.

(3) The structure of CO affects tunneling. If CO moved as a point particle, the value of ΔM/M would be about twice as large for the replacement $^{16}O \rightarrow {}^{18}O$ than for $^{12}C \rightarrow {}^{13}C$. The data in Table I show the opposite behavior. Predictions for some simple models are also given in Table I. It is amusing to note that the value of ΔM/M obtained in the experiment on $^{12}C\,^{16}O$ vs $^{13}C\,^{16}O$ is close to that predicted for a point CO molecule tunneling through a fixed potential. If only one isotope pair would have been studied, excellent agreement with the simplest model would have been noted. Both pairs together exclude any explanation not involving the structure of the CO molecule and the details of the binding process. A quantitative

explanation of the tunneling rates may require features such as rotational motion around an axis perpendicular to the C-O vector, excitation of the CO molecule, and participation of other protein-constituents near the heme.

Theory.* The longer one looks at tunneling in biomolecules, the more complex the theory becomes. We only state the ~~various~~ problems here.

(i) Phonons. Unless the tunneling system can interact with the surrounding heat bath, tunneling may be slow. Two different influences of phonons can be distinguished. As shown in Fig. 25.4, in unequal wells, the wavefunctions in a given level are ~~usually~~ highly localized in one well. If the transition occurs with energy conservation, the probability of remaining in the other well will be ~~slow~~ small. Phonon transition can lead to a level with larger wavefunction and from there to the bottom of the well. Vibrations can also reduce the distance d(H). Since k_t depends exponentially on d(H), these vibrations can change the tunneling rate.[29] The general behavior expected then is as shown in Fig. 25.16. The various contributions can be understood as follows. Quantum theory tells us that the probability of emission of a boson into a state x is proportional to

$$P(x) = \text{const}(1 + n_x) \qquad (25.28)$$

---

29. J. A. Sussman, Ann. Phys. Paris 6, 135-156 (1971).

*) P. Hänggi et al RMP 62, 251-342 (1990).

where n_x is the number of phonons present in state x. (Phonons like each other). Assume that the energy of state x is E_x. The number of bosons in

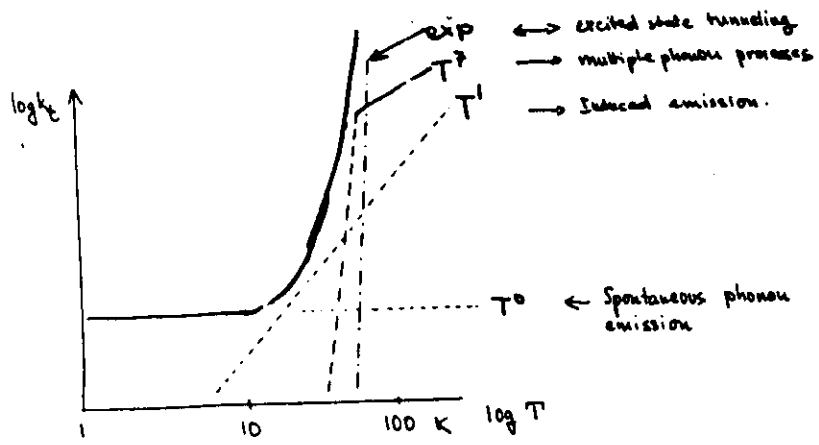

Fig. 25.16, Schematic representation of the temperature dependence of tunneling.

state x is given by the Planck distribution law,

$$n_x = (\exp(E_x/k_BT)-1)^{-1} \qquad (25.28)$$

For low temperatures, where $E_x >> k_BT$, Eq. (25.28) gives

$$n_x = e^{-E_x/k_BT}. \qquad (25.30)$$

We can identify a protein with a small solid, E_x with the energy of a phonon or lattice vibration, and the boson with this phonon. Eqs. (25.28) and (25.30) then explain the linear and quadratic terms in Fig. 25.16. At very low temperatures, only the term "1" in Eq. (25.28) contributes and tunneling becomes T independent. This term corresponds to spontaneous emission of a phonon: the energy is removed by single phonon emission. At somewhat higher energy, the second term becomes important and tunneling becomes proportional to T.

This process is called induced single phonon emission or absorption. At still higher temperatures, multiphonon processes set in and the tunneling rate becomes proportional to a higher power of T, for instance T^7. Such a process corresponds to phonon Raman scattering.

(ii) Friction. In the discussion of the Kramers approach to classical reactions we found that friction plays an essential role. Will friction also be important in tunneling? If we think of friction as a classical effect, the answer to the question is not so clear. We have pointed out, however, that friction is the "fudge factor" that takes the motion of the neglected reaction coordinates into account. Obviously, these coordinates are also neglected even at very low temperatures and friction must play an important role. Friction corresponds to energy dissipation and thus energy is not conserved. In the ordinary treatment of quantum mechanics, energy is always assumed to be a constant of the motion. It consequently took a considerable time before the correct approach was found. The work of Leggett and coworkers[30,31], Wolynes[32], and Hanggi and collaborators[8,9] has solved many aspects of this difficult problem and it is now clear that friction is important and in general reduces the tunneling rate.

---

30. A. O. Caldeira and A. J. Leggett, Phys. Rev. Lett. 46, 211-214 (1981)
31. A. J. Leggett, S. Chakravarty, A. T. Dorsey, M. P. A. Fisher, A. Garg, and W. Zwerger, Rev. Mod. Phys. 59, 1-86 (1987).
32. P. G. Wolynes, Phys. Rev. Lett. 47, 968-971 (1981).

(iii) Adiabatic and nonadiabatic tunneling. Tunneling in heme proteins has been treated by Jortner and Ulstrup by using a nonadiabatic approach[33,34]. We return to the question of adiabaticity later and only note here that it is likely that the tunneling phenomena discussed so far in heme proteins proceed on an adiabatic surface.

(iv) Structure effects. We have already encountered one structure effect when we discussed the isotope effect. A second one is also apparent in Fig. 25.13: tunneling becomes temperature independent at about 10 K. In paraelastic relaxation in solids, the tunneling rate is proportional to T down to at least 1 K.[35] Why does tunneling become T independent at such a high temperature in heme proteins? One possible explanation can be discussed with Fig. 25.17.

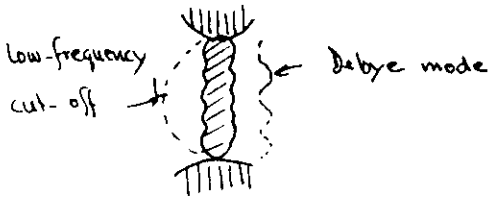

25.17
Fig. 27.24 If the heme behaves like a two-dimensional system embedded in a protein, the lowest-frequency mode is, as shown, determined by the size of the heme group. The high-frequency cut-off is given by the Debye mode.

In the figure we show the heme embedded in the globin, making contact essentially only at the periphery. The longest wavelength, corresponding to the smallest frequency, then is given by the diameter L of the heme.

---

33. J. Jortner and J. Ulstrup, J. Am. Chem. soc. 101-14, 3744 (1979).
34. J. Ulstrup, Charge Transfer Processes in Condensed Media, Lecture Notes in Chemistry, Springer, New York, 1979.
35. G. Pfister and W. Känzig, Phys. Kondens. Materie 10, 231-264 (1969).

The shortest wavelength is given by the distance between two atoms. The ratio L/d is about 5. Assuming a Debye temperature of about 100 K would thus predict a lower cut-off temperature of about 20 K, in approximate agreement with experiment.

We can summarize the situation by stating that tunneling in heme proteins still offers many possibilities for further research.

25.5 Barriers and Gates.

In the reactions described so far we have assumed that the reaction surface, shown for instance in Fig. 25.1 or 25.2, is fixed and time-independent. At the same time we have stated many times that proteins are moving and flexible systems. These two statements clearly are contradictory. How can be retain much of the reaction theory described so far while treating the proteins as dynamic systems? One way to take the dynamic aspects into account is by introducing the concept of a gated reaction.[24,25,26] The concept of gating is illustrated in Fig. 25.18.

Fig. 25.18

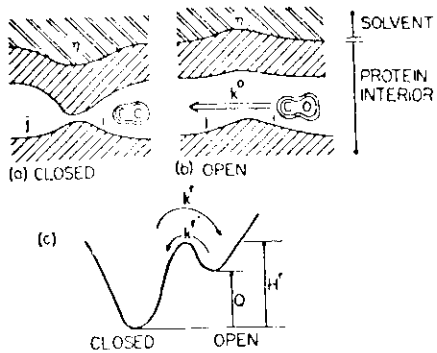

A CO molecule inside Mb moves from state i to j. In (a) Mb is in a conformational substate where the channel from i to j is closed, and in (b) the gate is open. (c) gives the potential for conformational transitions between the open and the closed substates.

---

24 J.A. Mc Cammon and S.H. Northrup, Nature 293,318 (1981).

25 A. Szabo et al., J. Chem. Phys. 77, 4484-4493 (1982).

26 J.A.McCammon and S.C. Harvey, **Dynamics of Proteins and Nucleic Acids.** Cambridge Univ. Press, 1987.

In Fig. 25.18 we consider a specific case, the motion of a CO molecule in the interior of a protein. Case and Karplus have shown that interior groups must move in order to let a small ligand escape or enter the heme pocket.[27] We describe this situation by postulating two conformational substates, "closed" and "open". In the open substate, the transition from well i to j occurs with a rate coefficient k_{ij}, in the closed substate the transition cannot occur. With k^r, we denote the relaxation rate coefficient for the transition from the closed to the open substate; $k^{r'}$ is the coefficient for the reverse step. Parts a and b of Fig. 25.18 represent the real states a and b inside the protein, Fig. 25.18c depicts the open and closed conformational substates. In the simplest case, we assume $k_{ij} = k_{ji}$, $k^r \ll k^{r'}$, and $k_{ij} \gg k^r$. The first assumption implies that the entropies of the states i and j are the same, the second that the probability of finding the system open is small, and the third that the transition i⇔j is fast compared to the closing of the passage. With these assumptions, the transitions between i and j are given by $k_{ij} \approx k^r$.

Such a gating model connects the reaction coordinate (Figs. 25.18a and b) with a conformational coordinate (c). Since the motion of the residue or protein, described by c, can be influenced easily by viscosity, the dependence of a motion inside the protein on external viscosity can be understood.[14] More general treatments of gating can be found in references 24-26.

25.6 Electronically Controlled Reactions.

Most reactions involve motion of the nuclei of the reacting species and changes in their electronic structure. For many reactions the electronic structure adiabatically follows the nuclear motions. The reaction then is controlled by the nuclear motion and is termed adiabatic or sometimes steric or even "nuclear". The treatment given so far then is appropriate and no explicit attention need to be paid to the dynamics of the changing electronic structure . When the spins of the reactants change or when long-range electron transfer is involved, however, the changes in the electronic structure may be slower than the nuclear motion.The characteristics of the electronic motion then become important and a theory of nonadiabatic transitions from one state to another is needed. In this section, we will first describe our "standard problem", the binding of small ligands to heme proteins, then assess then relative importance of nuclear and electronic motions, and finally sketch the adiabatic approach.[10]

---

[27] D.A. Case and M. Karplus, J. Mol. Biol. 132, 343- 368 (1979).

The Binding of CO and O_2 to the Heme Iron. The inside of the heme pocket in a typical hemoprotein is sketched in Fig.23.4. The molecular arrangement is shown in Fig.25.19. At low temperatures, two states are involved in the binding process, as indicated in Fig.23.4b. In the initial (deoxy) state B, the ligand is somewhere in the pocket,the heme iron has spin 2 and lies about 40 pm out of the mean heme plane, and the heme is domed. In the bound state A, the spin is zero, the iron has moved closer to the

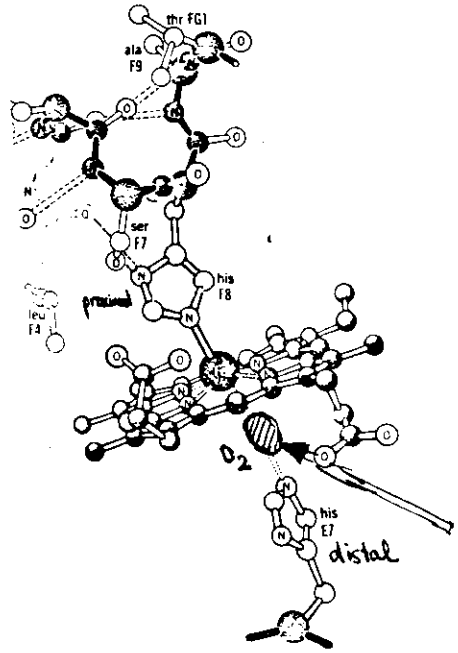

Fig.25.19 Atomic arrangement at the heme binding site.

mean heme plane, and the heme is nearly planar. The free CO molecule in state B has closed shells and is in the singlet configuration $^1\Sigma$. Binding hence starts in state B with total spin 2 (quintuplet state). As the CO approaches the iron, it may first encounter a repulsive potential caused by the four nitrogen atoms that surround the iron. A concerted motion then occurs, with the iron atom and the proximal histidine moving closer, the F helix shifting, the heme becoming planar and the spin-0 state moving lower in energy. Finally, upon binding, the spin 0 (singlet) state becomes the ground state. The binding process as described entails both nuclear and electronic motions. The nuclear motions involve changes in the coordinates of most of the atoms shown in

Fig.25.19. The electronic rearrangement consists in the change of the total spin of the system from 2 to 0. We can no longer describe the binding process as an adiabatic motion over a steric barrier, but now must also consider the rate with which the spin change 2→0 occurs.

Adiabatic and Nonadiabatic Reaction Surfaces. In chemical reactions, both electrons and nuclei move. Because of their mass difference, we can consider the nuclei at any moment to be fixed and obtain the energy levels for the electronic motion in the fixed field of the nuclei as a function of the distance between the nuclei (the Born-Oppenheimer approximation).[28] As an example we show in Fig. 29.20 the energy surfaces for the reaction of CO with the heme group in a one-dimensional model in two different approximations. We assume that only two electronic states exist, the bound state s (for singlet, S=0) and the unbound state q (for quintuplet, S=2). If the matrix element V_{sq}

25.20

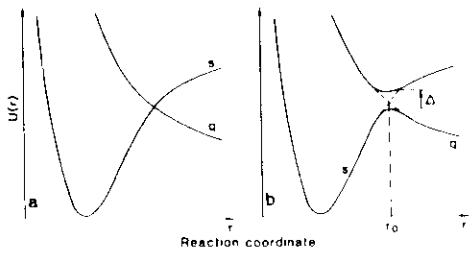

Fig. Schematic representation of the potential energy curves for the reaction of CO with the heme iron: (a) diabatic energy levels; (b) adiabatic energy levels. Here s denotes the singlet state, and q the quintuplet state; transitions s ↔ q are forbidden in (a).

connecting the two states is zero, the resulting diabatic energy curves (Fig. 25.20a) cross each other. If the interaction is not zero, the two curves "repel" each other, as shown in Fig. 25.20b.[29] The splitting between the two curves is given by

$$\Delta = 2|V_{sq}| \ . \qquad (25.31)$$

The lower curve starts out as q at large values of r, changes character in the mixing region, and becomes s at small values of r. In the mixing region, both curves are superpositions of s and q. Note that the curves in Fig. 25.20 do not represent potentials to be used in the Schroedinger equation to determine energy levels; they **are** the energy levels (or energy surfaces) as a function of the distance r.

---

[28] G. Baym, **Lectures on Quantum Mechanics**, Benjamin, New York, 1969.

[29] L.D. Landau and E.M. Lifshitz, **Quantum Mechanics**, pp. 269, § 76 W. Kauzmann, **Quantum Chemistry**, Academic Press, New York, 1957.

If the energy splitting Δ is very large compared to k_BT, the upper electronic state is inaccessible and the entire reaction takes place on the lower adiabatic curve. The electronic dynamics can be ignored, except in so far as it determines the adiabatic curve. The reaction is then determined by the nuclear motion and can be described by the Kramers equation. If, however, the splitting is small, the situation becomes more complex as will be discussed in the following subsection.

Curve Hopping (The LZS Relation). We now consider the dynamics of the association process Fig.25.20 by using a semiclassical model in which the nuclei move classically and the electronic state adjusts to the changing nuclear coordinates. Assume that the system starts out in state B. If $V_{sq} = 0$, the system will remain in state B because the electronic state cannot change even if the nuclear coordinates thermally move to the A configuration. To bind, the system must hop from the q to the s level. Hopping outside of the mixing region can be neglected.[30] The transition q → s must occur during the passage of the nuclei through the crossing region. If $\Delta \gg k_BT$, the upper state will be inaccessible and the nuclei will move on the adiabatic curve as pointed out above. If $\Delta \leq k_BT$, thermodynamic considerations alone do not determine whether the electronic state can change. Depending on the relative time scale of the electronic and nuclear motions, the system can either remain in state q, move along the dashed diabatic curve in Fig. 25.20b, and reach the upper surface, or it can move along the solid adiabatic curve and undergo the transition q → s.

To obtain a criterion characterizing adiabaticity we use the uncertainty relation : If the energy uncertainty of the system in the mixing region is small compared to the splitting Δ , the system will remain on the adiabatic lower surface. The energy uncertainty is given by $\hbar/\tau_{LZ}$, where τ_{LZ} is the time spent in the mixing region, called the Landau-Zener region. If the system moves through the mixing region with a velocity v and if the length of the Landau-Zener region is ℓ_{LZ}, τ_{LZ} is given by

$$\tau_{LZ} = \ell_{LZ}/v \ . \qquad (25.32)$$

Fig.25.20b shows that ℓ_{LZ} is approximately given by

$$\ell_{LZ} \cong \Delta/|F_2 - F_1| \ , \qquad (25.33)$$

where the forces F_1 and F_2 are the slopes of the diabatic curves at the avoided crossing r_0. The adiabaticity parameter γ_{LZ} is defined as the ratio of the splitting to the energy uncertainty,

$$\gamma_{LZ} = \frac{\Delta}{\hbar/\tau_{LZ}} = \frac{\Delta\,\ell_{LZ}}{\hbar v} = \frac{\Delta^2}{\hbar v|F_2 - F_1|} \ . \qquad (25.34)$$

---

[30] E.J. Heller and R.C. Brown, J. Chem. Phys. **79**, 3336 (1983).

If $\gamma_{LZ} \gg 1$, the transition is adiabatic. If $\gamma_{LZ} \lesssim 1$, the system can remain on one surface. Not every crossing through the mixing region then results in a reaction B ↔ A. The probability P for staying on the adiabatic surface in a single crossing has been calculated by Landau[31], Zener[32], and Stueckelberg[33] [34] as

$$P = 1 - \exp\{-\pi \gamma_{LZ}/2\}. \qquad (25.35)$$

This expression verifies the hand-waving arguments given above; if $\gamma_{LZ} \gg 1$, P = 1 and the transition is adiabatic. If $\gamma_{LZ} \ll 1$, P is given by

$$P = \pi \gamma_{LZ}/2 = \frac{\pi}{2} \frac{\Delta^2}{\hbar v |\dot{F}_2 - \dot{F}_1|} \qquad (25.36)$$

and it is proportional to Δ^2. The dependence on Δ^2 is the hallmark of a fully nonadiabatic reaction. The dependence on Δ^2 is also obtained by deriving the rate coefficient with nonadiabatic perturbation theory (the golden rule) in which Δ is treated as a small perturbation that causes the electronic transition.

Friction and the LZS Theory. The treatment of nonadiabatic transitions sketched in the previous subsection assumes ballistic motion through the Landau-Zener region. Friction, however, is also present in this process and it is intuitively obvious that it must play a role. The longer the system stays in the mixing region, the more we should expect hopping from one electronic surface to the other to occur. The effect of friction on nonadiabatic transitions has been treated in a number of publications.[35] [36] [37] The central results can be obtained again by a hand-waving approach, using the three characteristic lengths of the problem, the mean free path λ, the length ℓ_{TS} of the transition region, and the length ℓ_{LZ} of the mixing region.[30]

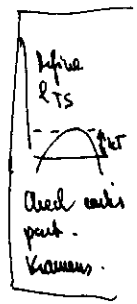

---

[31] L. Landau, Sov. Phys. 1, 89 (1932). Z. Phys. Sov. 2, 46 (1932).

[32] C. Zener, Proc. Roy. Soc. **A 137**, 696 (1932).

[33] E.C.G. Stueckelberg, Helv. Phys. Acta 5, 369 (1932).

[34] J. Ulstrup, **Charge Transfer Processes in Condensed Media**, Springer Berlin, 1979.

[35] L.D. Zusman, Chem. Phys.**49**, 295 (1980).

[36] R.E. Cline,Jr., and P.G. Wolynes, J. Chem. Phys. **86**, 3836-3844 (1987).

[37] I.V. Aleksandrov and V.I. Goldanskii, Sov. Sci. Rev. B. Chem. **11**, 1-67 (1988).

We state only one result here, for $\ell_{TS} \gg \lambda \gg \ell_{LZ}$. On each passage through the transition region, multiple crossings through the Landau-Zener region occur. The number of crossings is approximately given by $N_c = (\ell_{TS}/\lambda)$ and the probability P becomes

$$P = \tfrac{1}{2} [1 - \exp\{-\pi N_c \gamma_{LZ}\}]. \qquad (25.37)$$

Even if the Landau-Zener factor, Eq.(25.34), is small, the reaction may appear adiabatic since the parameter $N_c \gamma_{LZ}$ can be large. The effective transmission coefficient κ is shown in Fig. 25.21 as a function of the friction coefficient (in units of $m \omega^*$) for three different values of the Landau-Zener coefficient γ_{LZ}. The curves show that the reaction may appear adiabatic for large or small friction coefficients even if it is in reality largely controlled by curve hopping, i.e. electronic factors.

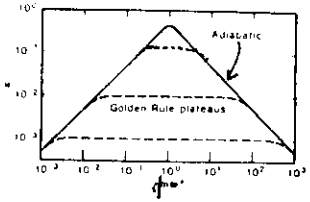

Fig. 25.21. The transmission factor κ as a function of the friction coefficient $\wp$ (in units of $m \omega^*$) for three different values of the Landau-Zener parameter. The solid curve gives the adiabatic Kramers curve. The dashed lines correspond to nonadiabatic transitions for three different values of the Landau-Zener parameter.

How To Recognize Non-Adiabaticity. As shown in the previous sections, entropy, friction, and electronic structure can all affect the preexponential factor in an Arrhenius relation. Friction and nonadiabaticity reduce A, whereas entropy can either decrease or increase A. Some of the effects can be separated if the preexponentials A_{AB} and A_{BA} for both reactions A → B and B → A (Fig.25.6) can be measured. Friction and nonadiabaticity reduce both coefficients by the same factor; the entropy contribution yields

$$\frac{A_{BA}}{A_{AB}} = \frac{\exp(S^*_{BA}/R)}{\exp(S^*_{AB}/R)} = \exp(S_A - S_B)/R. \qquad (25.37)$$

The ratio Eq.(25.37) thus provides some information on the role of entropy. A second clue can come from the effect of viscosity on the reaction rate. If the rate coefficients depend strongly on viscosity at constant temperature, the data must be evaluated with the Kramers relation and friction may be responsible for the

reduction of a preexponential factor below the TST value. If the rate depends on viscosity, and if the preexponential factor is reduced below the TST value, the adiabaticity factor ζ_{LZ} is increased by the amount that the rate coefficient k is decreased. A transition that without friction is nonadiabatic can have been made adiabatic by the friction.

25.7 Collective Effects.

All reactions discussed so far have been described in terms of fixed and temperature-independent potential energy surfaces. It is easy to see, however, that biomolecular reactions may not always satisfy this assumption. Consider as an example a rotation of an internal group. At high temperature, the group may be nearly free to rotate; at low temperatures, the protein has contracted and rotation may now be hindered. If the energy surface depends on temperature, we can now longer expect that the reaction rate coefficient obeys a simple Arrhenius behavior. Indeed, departures from a standard Arrhenius behavior are found frequently in glasses. The literature is enormous, but the underlying physics is still not fully understood. We therefore quote only some results and a small selection of relevant references.[38] [39] [40] [41] To describe the ideas, we return to glasses (Section 23.3).

The α Relaxation in Glasses. Near and above the glass temperature T_g the response of a glass to a mechanical, thermal, or electrical perturbation is dominated by the α relaxation. The time dependence of the relaxation is usually nonexponential and can often be described by a stretched exponential (Kohlrausch-Williams-Watts) :

$$\Phi(t) = \Phi(0)\ \exp\{-(k(T)t)^{\beta}\} \ . \qquad (25.38)$$

The exponent β usually lies in the range from 0.3 to 1. The rate coefficient k(T) usually does not follow an Arrhenius relation. Fig. 25.22 shows a beautiful example for the temperature

[38] S. Brawer, J. Chem. Phys. **81**, 954-975 (1984). **Relaxation in Viscous Liquids and Glasses.** American Ceramic Soc. Columbus, Ohio, 1985.

[39] F.H. Stillinger, Phys. Rev. B. **32**, 3134-3141 (1985).

[40] J. Jäckle, Rep. Prog. Phys. **49**, 171-231 (1986).

[41] J.D. Bryngelson and P.G. Wolynes, J. Phys. Chem. **93**, 6902-6915 (1989).

dependence of a relaxation rate in glycerol.[42]

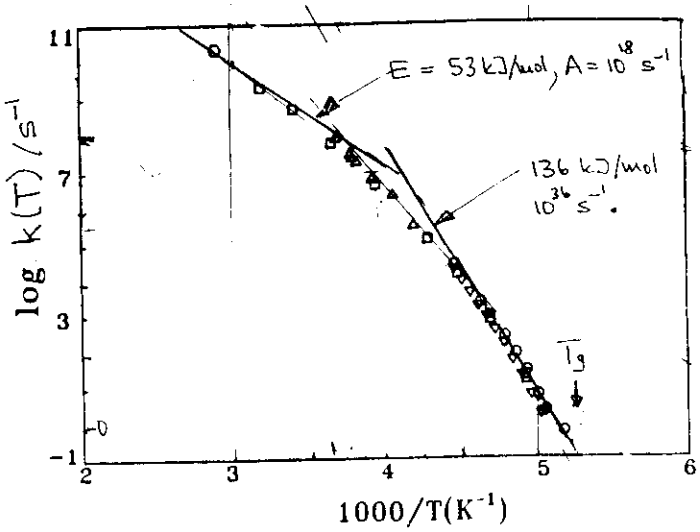

Fig. 25.22. Relaxation rates in glycerol. After Jeong et al. Ref. 42.

The data in Fig. 25.22 show that the relaxation rate k(T) does not satisfy an Arrhenius relation. At each T, we can define "local " activation energies and preexponential factors by drawing tangents. Two such tangents are shown. At high T, the preexponential factor is not much larger than the expected 10^{13} s^{-1}. Near the glass temperature, however, the preexponential factor is about 10^{36} s^{-1}, much larger than any physically reasonable value. This value implies that the observed relaxation phenomenon is cooperative in nature and that the Arrhenius relation is not appropriate for its description.

As stated above, no universally accepted theory exists at present for collective phenomena like the glass transitions. Often, the empirical Vogel-Fulcher-Tammann relation[43]

[42] Y.H. Jeong, S.R. Nagel, and S. Bhattacharya, Phys. Rev. A **34**, 602-608 (1986).

[43] H. Vogel, Physik. Z. 22, 645 (1921). G.S. Fulcher, J. Am. Ceram. Soc. **77**, 3701 (1925). G. Tammann and W. Hesse, Z. Anorg. Allg. Chem. **156**, (1926).

$$k(T) = A_{VF} \exp\{-E_{VF}/R(T-T_0)\} \qquad (25.39)$$

is used. A second relation

$$k(T) = A_F \exp\{-[E/RT]^2\} \qquad (25.40)$$

also fits data over at least ten orders of magnitude in k(T).[44] [44] [45] The first Eq. uses three parameters, the second only two. It is therefore often to be preferred.

When do we know that a transition state expression is not correct? If data over an extended range in k(T) are available, a deviation for a straight Arrhenius plot is a clear indication. If only a small range is available, or if the data are not accurate, this method does not work. However, if the preexponential factor A in an Arrhenius fit becomes unphysically large , say $A > 10^{15}$ s^{-1}, we can assume that the reaction is not simple.

While no complete theoretical underpinning of the Eqs. (25.39) and (25.40) exists, some justification emerges from the treatment of complex systems.[41]

---

[44] J.D. Ferry, L.D. Grandine,Jr., and Fitzgerald, E.R. J. Appl. Phys. **24**, 911 (1953).

[44] H. Bässler, Phys. Rev. Letters **58**, 767-770 (1987).

[45] R. Richert and H. Bässler, J. Phys. :Condens. Matter **2**, 2273 (1990).

26. PROTEIN MOTIONS

26.1 Equilibrium and Nonequilibrium Motions.

In Section 23.1, we pointed out that the existence of states and substates in biomolecules leads to two different types of motions, equilibrium fluctuations (EF) and nonequilibrium motions (functionally important motions or FIM). To discuss the observation and characterization of these motions, we consider first the simplest case of a double well as shown in Fig.23.18. In equilibrium, the ratio of the populations in the two wells are given by Eq.(23.8) as

$$N_B/N_A = \exp(-\Delta G/RT) \qquad (26.1)$$

and the number of transitions either way are equal ,

$$N_A\, k_{AB} = N_B\, k_{BA} \,. \qquad (26.2)$$

The two relations together give

$$k_{AB}/k_{BA} = \exp(-\Delta G/RT). \qquad (26.3)$$

Experimentally, one desires to find the rate coefficients over a wide range c temperature. Two cases must be distinguished:

(1) ΔG small, $N_A/N_B \simeq 1$. When the populations of the two wells are not too different, two methods can be used to find the rate coefficients - relaxation and fluctuation. In the relaxation methods[1-3] we apply a sudden (or periodic) perturbatio to the system, for instance by changing the temperature from T_o to $T_o + \Delta T$.

---

1. M. Eigen, Q. Rev. Biophys. 1, 3-33 (1968).
2. M. Eigen and L. DeMayer, in Techniques of Chemistry, Vol. VI, Part II, Chapter III, Wiley, 1973.
3. G. Schwarz, Rev. Mod. Phys. 40, 206 (1968).

The system adjust to the new temperature by transitions A⇔ B. The rate at which the new equilibrium is established gives information about the rate coefficients k_{AB} and k_{BA} as will be shown below. The second method is based on fluctuations.[4-6] Fluctuations are discussed in Section B.7 where the connection between fluctuations and relaxation (dissipation) is shown in Fig. B.5. The fluctuations, for instance in state A, can be Fourier analyzed to give $\delta N_A(f)$, the fluctuations in state A with frequency f.

Relaxations and fluctuations can be described quantitatively. Assume that the number of particles in state A at the temperature T_0 is given by $N_A(T_0)$. If the temperature is suddenly raised to $T_0 + \delta T$, the new equilibrium is $N_A(T_0+\delta T)$; it will be reached with a time dependence as shown in Fig.26.1.

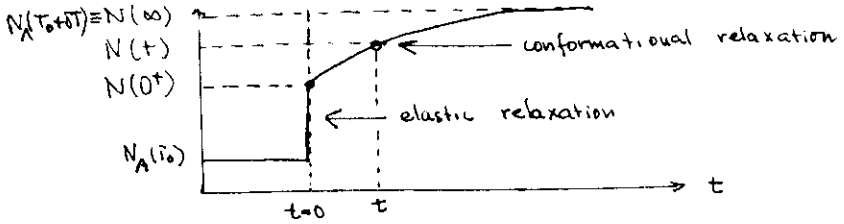

Fig. 26.1. Approach to the new equilibrium after a temperature jump.

The time dependence will in general show two parts, a very fast elastic component and a slower conformational component. Both components can be understood in terms of what we know about proteins (and glasses). The elastic component is caused for instance by the thermal expansion of the system, without concomitant change in the structure or rearrangement of atoms. The conformational component is due for instance to a structural rearrangement of the protein.

If the barrier in Fig. 23.18 has a unique height, the rate coefficient for relaxation is given by

$$k_r = k_{AB} + k_{BA}. \qquad (26.4)$$

To characterize the relaxation, we only consider the conformational part and define a relaxation function $\Phi(t)$,

4. G. Feher and M. Weissman, PNAS 70, 870-875 (1973).
5. M. Weissman, H. Schindler, and G. Feher, PNAS 73, 2776-2780 (1976).
6. M. B. Weissman, Ann. Rev. Phys. Chem. 32, 205-232 (1981).

$$\Phi(t) = \frac{N(t) - N(\infty)}{N(0^+) - N(\infty)} \quad . \qquad (26.4)$$

For a barrier of unique height, $\Phi(t)$ is exponential in time,

$$\Phi(t) = \exp\{-k_r t\} \quad . \qquad (26.5)$$

The observation of the relaxation function thus yields $k_{AB} + k_{BA}$. With Eqs.(26.1) and (26.3), the equilibrium coefficient yields k_{AB}/k_{BA} and consequently the individual coefficients are determined. In general, however, the relaxation function will not be exponential in time and it cannot be characterized by a unique rate coefficient.

The relaxation rate $k_r = 1/\tau$ can also be determined from the fluctuations (Fig.B.5a) by a Fourier analysis; the fluctuation of frequency f in the number of particles in one well is given by

$$|\delta N_A(f)|^2 = \frac{4\tau \bar{N}_A[1-\bar{N}_A]}{1+(2\pi f\tau)^2} \quad . \qquad (26.6)$$

The autocorrelation gives another approach to τ:

$$\langle \delta N_A(t)\, \delta N_A(t+t')\rangle \propto e^{-t'/\tau}. \qquad (26.7)$$

(2) ΔG large, $N_B \ll N_A$. If, for all practical purposes, only the ground state is populated, both methods discussed so far fail. A small perturbation cannot lift a sufficient number of systems to the higher state B and relaxation therefore cannot be seen. The fluctuations in state A then are also so small that they cannot be observed. To study reactions under such circumstances, the system has to be brought into a state very different from the ground state. Three approaches are flash photolysis, stopped-flow, and pulse radiolysis. Consider the system MbO_2. In a stopped flow experiment, two solutions, one containing free Mb, the other O_2, are mechanically mixed. After mixing, the change in optical spectrum is observed. This method can be applied to many problems, but it is slow (the lower limit is about 1 ms) and works only in a limited temperature range. Flash photolysis can be used if

the initial state (MbO_2) can be photodissociated:

$$\text{photon} + MbO_2 \rightarrow Mb + O_2.$$

An intense short pulse of light photodissociates MbO_2 or MbCO. Subsequent rebinding is followed optically or through some other means. In pulse radiolysis, the initial state of a reaction is reached by irradiating the sample with electrons of, say, 15 MeV.

To connect this brief discussion of techniques to EF and FIM, we note that the fluctuation experiments indeed explore equilibrium fluctuations; the system remains in equilibrium throughout the experiment. Relaxation techniques, however, look at nonequilibrium motions. Here again two different extreme cases exist, as sketched above. In (1), the system always stays close to equilibrium and only small excursion are studied. In this case it is likely that the fluctuation-dissipation theorem is valid and that fluctuation and relaxation techniques give the same information. In (2), where the system starts very far from equilibrium, the nonequilibrium state may never be reached by fluctuations and the F-D theorem may be useless. This case may occur often in the investigations of biological reactions, where the observed FIM can involve major changes in the protein structure .

26.2 Experimental Techniques.

Many techniques exist to study motions and we describe here just a small selection to describe some of the key ideas. Nevertheless, the exploration of protein motions calls for even more sophisticated approaches than are available today and room for improvements in techniques and data evaluation.

Line Shape Measurements. (To be written).

T and P Jump Techniques. As an example of a relaxation technique that works close to equilibrium, we sketch in Fig. 26.2 a simple T-jump set-up. C is a capacitor, S a spark gap. The charged capacitor is discharged through the cell by triggering the spark gap. The cell is heated with a characteristic time RC, where R is the

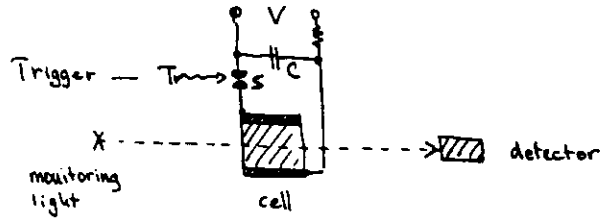

Fig. 26.2 Principle of T-jump technique.

cell resistance. The change in absorbance is observed. As a rule, the measurement is performed as a difference between two cells, one with the substance to be studied plus a proper conducting solvent, the second the solvent only. Heating through capacitor discharge limits the time range to about μs. For faster T jumps, laser heating is used.

In the example discussed here the small perturbation is induced by a temperature jump. Jumps in pressure or electric fields can also provide the perturbation.

Dispersion Techniques.

The small perturbation (electric fields or pressure) that changes the equilibrium concentration can also be applied periodically, as sketched in Fig. 26.3. Assume that the relaxation time of the system under study is τ, the frequency of the applied perturbation ω. The equilibrium concentration then will vary periodically, with amplitude

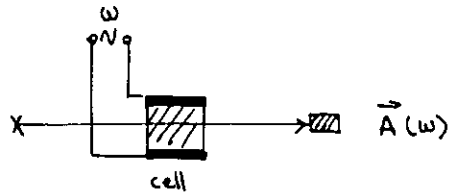

Fig. 26.3 Periodic perturbation (relaxation technique).

$$\Delta C = \Delta C^{o} \exp(i \omega t). \qquad (26.8)$$

The observed signal will also vary periodically, with amplitude and phase

$$A(\omega) = \Delta C^{o}/(1 + \omega^2\tau^2)^{1/2}. \qquad (26.9)$$

$$\phi(\omega) = -\tan^{-1}\omega\tau.$$

The relaxation time can thus be determined from the frequency dependence of the amplitude or the phase shift. This approach is similar to the phase fluorometry sketched in Section 20.6.

Flash Photolysis- Principle. The basic principle of flash photolysis is simple and dates back a long time.[7,8] Flash photolysis experiments work if the system can be photodissociated and if the ground state and the photodissociated state can be distinguished, for example by their optical or infrared absorption spectrum. Both criteria are satisfied for heme proteins. The general features of a of flash photolysis are sketched in Fig. 25.4.

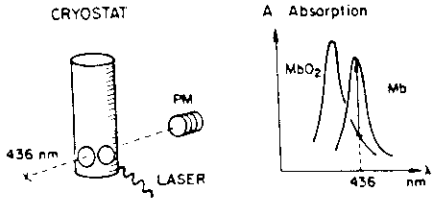

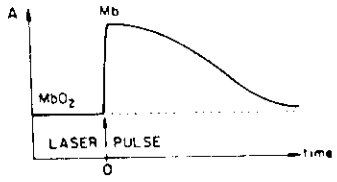

Fig. 26.4 Flash photolysis. The protein sample (MbO_2) is placed in a cryostat, the absorbance is monitored at a suitable wavelength, and the MbO_2 is photodissociated by a laser flash. Because MbO_2 and Mb differ in the optical absorbance, photodissociation and rebinding can be monitored.

[7] H. Hartridge and F.J.W. Roughton, Proc. Roy. Soc. B 94, 336-367 (1923).

[8] R.G.W. Norrish and G. Porter, Disc. Farad. Soc. 17, 40-46 (1954).

The bound system, for instance MbO_2 or MbCO, is placed into a cryostat. DeoxyMb and MbO_2 have a different absorption spectrum (venous and arterial blood have different color). Observation at a suitably chosen wavelength indicates the degree of oxygenation. The sample is photodissociated with a laser pulse. Photodissociation and rebinding are then followed in time.

The times involved in rebinding range from about 100 fs to ks or longer. Ideally, all times should be observed after each laser pulse. At present, no equipment covers the entire range. We discuss here approaches that together are capable to span the entire range.

Logarithmic Transient Digitizer[9,10] The story is told of the wise man who, when asked for the payment he was to receive for a particularly important job, told the king: One rice corn on the first square of a chess board, two on the second, four on the third and so on. "Not more?" said the king. We encounter this story here when we try to build an efficient recording system that works over an extended range in time. We will describe a solution here.[9,10]

The schematic outline of a "slow" flash photolysis system is shown in Fig. 26.5. Customarily the photomultiplier output is fed into a storage oscilloscope, and the data are taken from the scope tracing. Since the time bases of oscilloscopes are linear, only a limited range in time is observed after a single flash and data from several flashes must be pieced together for complete coverage. Such an approach is time consuming and open to misinterpretation. As an example, we show in Fig. 26.6 two curves. On top, they are plotted in a log N versus log t diagram; at the bottom the same curves are

[9] R. H. Austin, K. W. Beeson, L. Eisenstein, H. Frauenfelder, and I. C. Gunsalus, Biochemistry 14, 5355 (1975).

[10] R. H. Austin, K. W. Beeson, S. S. chan, P. G. Debrunner, R. Downing, L. Eisenstein, H. Frauenfelder, and T. M. Nordlund, Rev. Sci. Instrum. 47, 445 (1976).

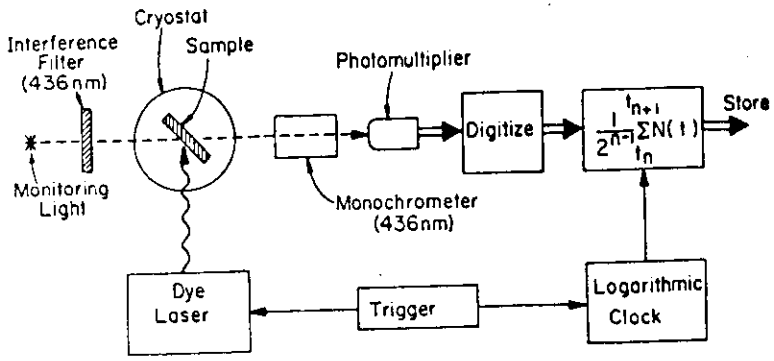

Fig. 26.5 "Slow" flash photolysis system.

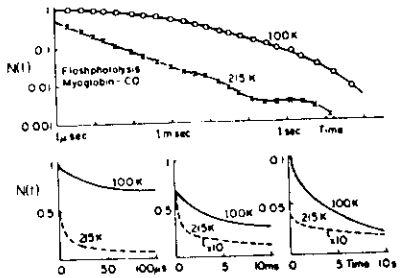

Rebinding of carbon monoxide to myoglobin after photodissociation by a laser flash (Ref. 1). $N(t)$ denotes the fraction of myoglobin molecules that have not rebound a carbon monoxide molecule at the time t after the flash. The upper curves are each obtained in one sweep with the digital analyzer with logarithmic time base TRANSLOG described in the present paper. The lower figures show how a voltage $N(t)$ would appear on an oscilloscope. To get the same information as with the TRANSLOG, at least four different measurements have to be taken.

Fig. 26.6

shown in the customary log N versus linear t diagrams. The upper curves suggest that the process shown must be described by a power law. The lower curves mislead the observer into decomposing N(t) in each time range into two exponentials.

A logarithmic transient digitizer overcomes the problem.[10]

The approach and components are explained with Fig. 26.6. A trigger simultaneously fires the laser and starts a "logarithmic clock". The flash illuminates the sample in the cryostat and photodissociates, say, MbCO. Rebinding is followed by detecting the transmitted 436 nm beam with a photomultiplier. After triggering, the crystal-controlled logarithmic clock emits signals in exponentially increasing intervals. The first m intervals have a length Δ, the second m intervals 2Δ, the third $2^2\Delta$, and the n-th set of m intervals $2^{n-1}\Delta$. Here m is an integer adjustable from 1-10. The photomultiplier output is integrated over time Δ, digitized, and summed over a given interval of length $2^{n-1}\Delta$. The sum is divided by 2^{n-1} and the result stored. Thus, even though the interval length increases exponentially with time, a constant input signal results in a constant output. In the present system, the maximum $n = 24$ and the minimum $\Delta = 2$ μs. If the first interval is 2 μs, the longest interval is $2^{24-1} \times 2$ μs = 16.8 s, and the entire measurement extends over $m(2^n-1)\Delta$ or 336 s when $m = 10$. Kinetics at longer times can be observed by increasing the length Δ of the basic interval. From the observed intensity as a function of time, the optical density is computed. The result is expressed in terms of N(t), the fraction of Mb molecules that have not rebound a ligand molecule at time t after the flash.

The system is capable of measuring the changes in absorbance over more than four orders of magnitude, because no information is lost. As time increases, signals usually become smaller. However, the ever increasing length of the time interval over which an average is taken compensates for the decrease.

Fast Flashphotolysis Systems.[10-12] The fastest lasers today have pulse lengths of only a few fs. The difficulties arise not with the production of such short pulses, but with the reliable observation of the signals. Ordinary detectors are too slow. The fastest oscilloscope, for instance, has a resolution of about 300 ps. It is therefore necessary to use indirect methods. Two important ones are the streak camera and a delayed probe pulse.

An arrangement used with a streak camera is shown in Fig. 26.7[9]

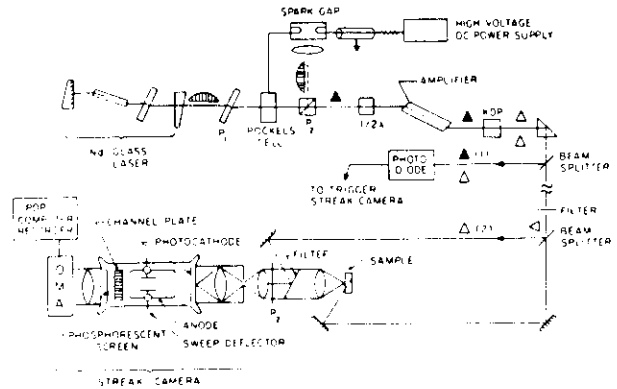

Schematic diagram of the apparatus used to measure fluorescence kinetics by a streak camera. A single pulse is selected, amplified, and passed through a KDP crystal to produce the second harmonic. A beam splitter provides two side beams. Beam 1 triggers the streak camera. Beam 2 arrives at the streak camera at an earlier time to provide a calibration pulse. The main 530-nm pulse excites the fluorescence from the sample. The streak produced at the phosphorescent screen is recorded by an optical multichannel analyzer (OMA).

Fig. 26.7

---

10. Biological Events Probed by Ultrafast Laser Spectroscopy, R. R. Alfano, Ed., Academic Press, New York, 1982.
12. Ultrafast Phenomena, IV, D. H. Auston and K. B. Eisenthal, Eds., Springer, Berlin, 1984.

In a streak camera, photoelectrons are emitted by the photocathode when struck by the incoming photons. A ramping voltage, applied to the anode, is triggered oy a part of the laser pulse. Photoelectrons emitted at different times are deflected to different parts of the phorsporescent screen. The time of arrival is thus mapped onto a spatial position on the screen. The intensity at a given spatial position is proportional to the intensity at a given time. The intensity can be read by an optical multichannel analyzer (OMA). The entire system is $$$$.

The method of delayed probe pulses uses the fact that light travels 0.3 mm in 1 ps in air. The arrangement is sketched in Fig. 26.8. The laser pulse is first split into the photolyzing and the probe pulse, in an intensity ratio of about 20:1. The photolyzing pulse hits the sample first. The probe pulse is delayed by a time 2L/c and then traverses the sample. Its intensity is recorded as a function of L. If necessary, the wavelength of the probe pulse can be changed by wavelength-shifters.

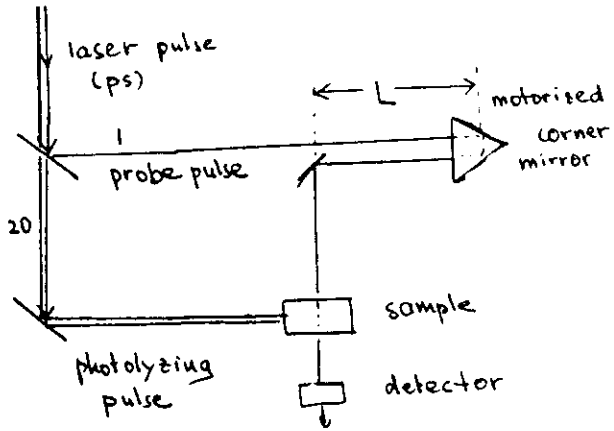

Fig. 25.8 Principle of the probe-pulse method.

How to Read Log-Log Plots.

When data extend over more than two orders of magnitude in time (and this case is very likely the normal one) plotting log N(t) vesus t distorts the information; either the slow components are left out or the fast ones are compressed so as to be unrecognizable. ~~It is better to give~~ ~~In the following, essentially~~ all data ~~will be given~~ by plotting log N versus log t. At first, such a log-log plot is unfamiliar; once one becomes familiar with it, t is the most informative way to look at complex processes. The examples in Figs. 26.9 and 25.10 give the most important shapes. The exponential drops extremely fast in a log-log plot. It only covers about two orders of magnitude in time. A power law,

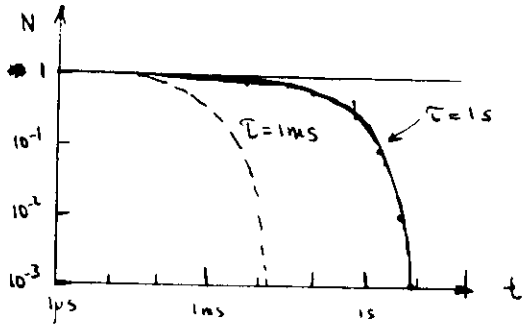

Fig. 26.9 Two single exponentials. The shape is invariant; a different mean time simply shifts the curve.

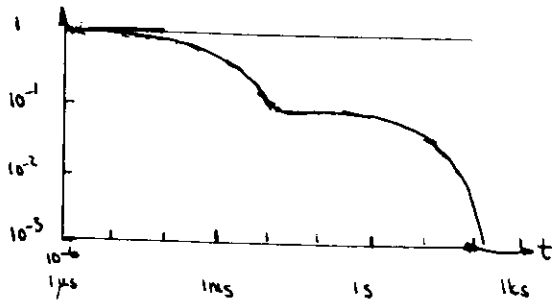

Fig. 26.10 A curve consisting of two exponentials with different rates.

$$N(t) = \text{const } t^{-n},$$

yields a straight line (Fig. 25.11); the slope gives the exponent n. Clearly, a power law cannot extend to minus infinity, it must bend over. A curve that does bend over is

$$N(t) = (1 + t/t_o)^{-n}.$$

This curve is constant at times small compared to t_o and represents a power law at times large compared to t_o.

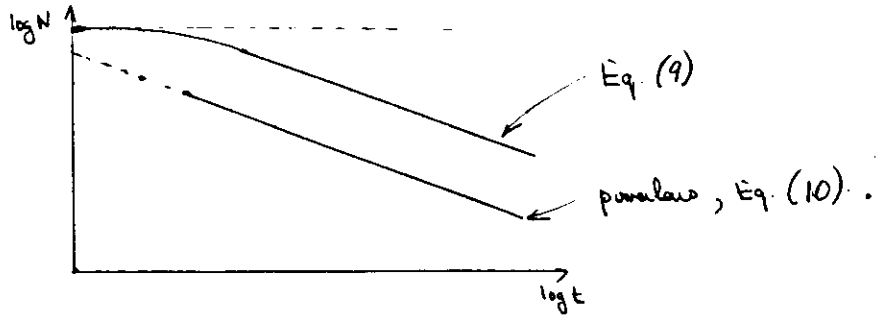

Fig. 26.11

For showing details: Plot part as lin N vs log t.

t and ω space.

Dielectric Relaxation.

NMR Relaxation.

26.3 Protein Relaxations

If Fig.23.14 is correct, we must expect protein motions to be very complicated and to depend strongly on temperature. At high T, motions may occur in all tiers of substates and the protein may undergo a wide variety of relaxations at the same. As T is lowered, motions in higher substates (CS^0, CS^1) may become so slow that they are frozen on any biologically relevant time scale. As T is further lowered, motion in other tiers may freeze out. Some motions may, however, persist to even very low temperatures; otherwise the specific heat would show the well-known dependence proportional to T^3. In any case, we can expect a rich spectrum of motions and these motions will tell us more about the energy landscape, because they depend on the barriers between substates. To explore the wide range of expected motions, every available tool will have to be used. We describe here only a small sample. Importance for function.

Motions in Tier 0. In Section 23.5 we discussed substates of tier 0 and showed that these CS in myoglobin can be characterized by their CO stretch wavenumbers as shown in Fig. 23.16. Fig. 23.17 demonstrates that the ratio of CS^0 populations depends on temperature and pressure and that the exchange between the substates ceases near 200 K. These observations together suggest how FIM 0, the motion between substates of tier 0, can be explored: Use a P or T jump to perturb the equilibrium among substates and follow the subsequent approach to the new equilibrium by monitoring the IR stretch bands.[13] [14] [15] Fig. 23.17 implies that such experiments are most easily done near 200 K.

In a pressure release experiment, a MbCO sample is placed into a pressure cell. Pressure of the order of 100 MPa (1 kbar) is applied well above the glass temperature. (Pressures much higher than 100 MPa denature proteins.) The sample is then cooled to the desired temperature and the pressure is released as quickly as possible and the IR spectrum is observed as a function of time after release. The result of such an experiment is shown in Fig. 26.12.

Fig. 26.12 shows that in MbCO near 200 K, exchange between CS^0 indeed occurs with measurable rates and we denote this motion by FIM 0. Comparison with Fig. 26.1 indicates that elastic relaxation does not take place. This observation is understandable : The different CS_0 correspond to rather different protein structures and elastic effects do not change the structure. The relaxation function for FIM 0 is shown in

---

[13] A. Ansari et al., Biophys. Chem. **26**, 337-355 (1987).

[14] I.E.T. Iben et al., Phys. Rev. Letters **62**, 1916-1919 (1989).

[15] H. Frauenfelder et al., J. Phys. Chem. 94, 1024 (1990).

Fig.26.13 c: ~~The data show a that~~ FIM 0 is biphasic; a slow and a fast component are observable.

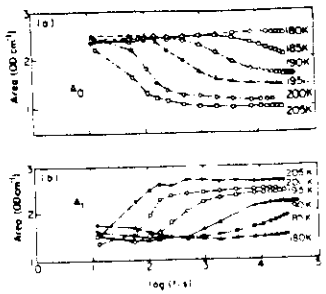

A_0 decreases

A_1 increases

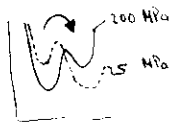

Fig. 26.12 The areas of the CO IR stretch bands A_0 and A_1 as a function of time after a pressure release from 200 to 25 MPa. Sperm whale myoglobin in 75% glycerol/water at pH 6.6.

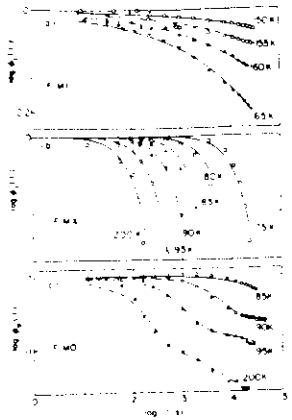

Fig. 26.13 Relaxation functions $\Phi(t;T)$ for sperm whale myoglobin. FIM 0 describes the change in CS^0 populations. FIM 1 is measured by observing the width of A_0. FIM X is characterized by the shift in the peak wavenumber of A_1.

The meaning of the two phases is not yet clear. The data can be fitted by a superposition of two stretched exponentials, Eq.(25.38), with β(fast) ≈ 1, β(slow) ≈ 0.2. Since the temperature dependence is only observed over a small range in T, k(T) in Eq. (25.38) can be fitted with an Arrhenius relation, yielding A(fast) ≈ 10^{27} s^{-1}, E(fast) ≈ 110 kJ/mol and A(slow) ≈ 10^{70} s^{-1}, E(slow) ≈ 280 kJ/mol. These values are similar to the values quoted for glycerol in Subsection 25.7 and demonstrate that the observed relaxation phenomena are collective in nature and cannot be described by an Arrhenius relations.

A fit to Eq.(25.40) for the data at pH 6.9 in the temperature range from 185 to 200 K gives[16] $\log(A_F/s^{-1})$ = 13, E_F = 10 kJ/mol. Thus the Ferry equation gives a fit to the data with a reasonable preexponential factor. The temperature range is very narrow: Below 185, the relaxation is too slow to be observed; above 200 K, it is too fast for the very slow technique used here. We will see later that a very different approach permits the determination of the rate for the exchange $A_0 \leftrightarrow A_1$ at considerably higher temperature.

FIM 0 poses a question : Its major component shows a non-Arrhenius temperature dependence, but an exponential time dependence. Stein et al have shown that such a behavior can occur in a transition if the barrier fluctuates.[17]

The non-Arrhenius temperature dependence, in particular the very large value of A for an Arrhenius fit, suggests that FIM 0 involves large-scale motions. Further evidence for this model comes from the viscosity dependence of FIM 0.[16] Fig. 26.14 shows the two FIM 0 processes $A_0 \leftrightarrow A_1$ and $A_1 \leftrightarrow A_3$ in two solvents with very different viscosities. The result is clear : the external viscosity affects the protein motions extremely strongly.

We expect that substates of tier 0 will occur in many proteins. The exploration of their dynamic properties is only at a beginning and much more work is required before a consistent picture can be painted.

[16] R. Scholl Thesis UI 1991

[17] D.L. Stein, R.G. Palmer, J.L. Van Hemmen, and C.R. Doering, Phys. Lett. A **136**, 353 (1989).

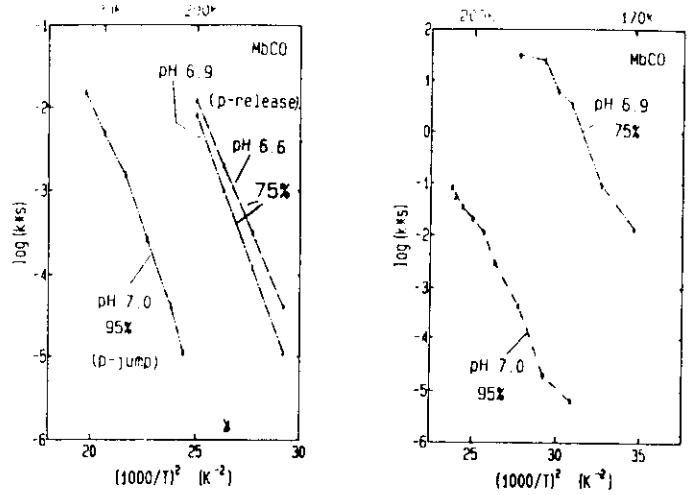

Fig. 26.14 The viscosity dependence of the motions in tier 0.

Rate coefficients vs. $(1000/T)^2$ in MbCO from p-relaxation experiments. Left: Fast process of FIM0($A_0 \rightarrow A_1$) - relaxation. Right: FIM0($A_1 \rightarrow A_3$) - relaxation. Samples: MbCO in 75% glycerol/buffer at pH 6.6 and pH 6.9; MbCO in 95% glycerol/buffer at pH 7.0.

Motions in Tier 1. The pressure release data[14 15] show that other changes occur in the temperature range between about 160 and 200 K : The IR stretch bands shift and change their width. At pH below 7, two different relaxation processes can be distinguished. At all temperatures, even down to 10 K, the band A_1 shows a fast elastic shift. At about 150 K, a conformational shift becomes visible and we assign the shift to tier 1, because the areas of the bands do not change. The motion must consequently occur within the substates of tier 0. The relaxation function for FIM 1, shown in Fig. 26.13 a, is nonexponential in time (β ≈ 0.3) and its Arrhenius parameters are approximately A ≈ 10^{20} s^{-1}, E ≈ 80 kJ/mol. FIM 1 consequently also has a non-Arrhenius T dependence and must describe collective motions.

The viscosity dependence of the motions in tier 1, shown in Fig. 26.15, shows that also these motions are strongly influenced by the external solvent.

The evaluation of the pressure jump and release experiments is performed by first fitting a stretched exponential to the data at a given temperature. The results yield values for β(T) and k(T). Usually, β(T) depends only weakly on T and is therefore assumed to be constant. Measurement at all values of T then give β

and k(T). A fit of an Arrhenius relation to k(T) indicates if this choice is correct : If the preexponential is of the order of 10^{13} s^{-1} or less, an Arrhenius relation **may** be adequate. If A is much larger, an equation adequate for collective motions, such as Eq. (25.39) or (25.40), should be used. (We can ask : what is the difference? The answer is extrapolation. To use the entire approach for biological phenomena, extrapolation from around 200 to 300 K is necessary. The difference between an Arrhenius relation and one of the others can be very large!)

Motions in Tier 2. The best evidence for motions within each of the different CS 1 comes from studies of ligand binding, to be discussed in Chapter 27.

Motions in Lower Tiers. Small scale motions occur well below 200 K. The anomalous specific heat implies that some motion occurs even below 1 K.

Open Problems. The brief description of the relaxation phenomena in proteins demonstrates clearly that only the surface of this rich field has been scratched so far. Work should progress along a number of lines :

i. Development of better techniques to study relaxation phenomena. The present techniques still have many "holes", i.e. regions in time, temperature, and pressure that cannot be studied easily. P, T, and **E** jump techniques can be extended. Modulation techniques may prove to be equally or even more useful.

ii. A systematic survey of the existing data to combine what is known from all dynamic tools.

iii. Measurements of the various relaxation phenomena in a small number of proteins of different overall structure (α helices, β sheet,...). Get as complete a data base as possible. Use very different probes to study different parts of the same protein.

iv. Study the relaxation phenomena in one selected protein as function of solvent, solvent viscosity, pressure,... .

v. Extend the experiments to mutants to see how specific mutations affect a particular motion.

27. DYNAMICS AND FUNCTION

We are now at the point where we can assemble what we have learned to treat a simple biological function, namely the binding of small ligands to myoglobin. The phenomenological features of ligand binding have been treated in Subsection 25.6. To discuss the process in molecular terms, we need nearly everything that we learned, flash photolysis (26.2), conformational substates (23.2), inhomogeneous spectral lines (23.2) , the hierarchy of substates (23.4), reaction theory (25), and glass relaxation (25.7).

We will treat this problem in steps, to show how an apparently extremely simple biological process is in fact extremely complex. Even now, after many years of work and a very large number of papers, some of the fundamental problems are still either unclear , undecided, or not solved. In treating ligand binding, we omit a number of important contributions.

27.1 Background and the Simplest Model.

The standard description of the binding of a small ligand such as CO or O_2 to Mb is described in Section 24.1. The essential coefficients characterizing association and dissociation at a given temperature and pressure are λ_{on}, λ_{off}, and $\Lambda_a = \lambda_{on}/\lambda_{off}$. It is customary in the literature to quote the association rate coefficient as a pseudo-first order coefficient, with dimension mol^{-1} s^{-1}. Collman et al. [1] pointed out that this definition leads to values of λ_{on} and Λ that depend on the solubility of the ligand in the solvent and that consequently comparisons in different solvent or of different ligands are ambiguous. It is better to give these coefficients in terms of s^{-1} for a given partial pressure of the ligand above the solvent and in equilibrium with the solvent. The initial state of the reaction is then unambiguously defined.

Approximate numbers for the various coefficients are given in the following table.

Table. Binding of ligands to sperm whale Mb

	λ_{off}/s^{-1}	$\lambda_{on}/s^{-1}{}_{mol}{}^{-1}$	λ_{on}/s^{-1} , 1 bar
Mb - CO	0.015	5.4×10^5	600
Mb - O_2	10	1.5×10^7	26 000

[1] J.P. Collman, J.I. Brauman, and K.M. Doxsee, PNAS **76**, 6035 (1979).

The coefficients in the table show that O_2 binds about 40 times faster than CO, but is much less tightly bound. The data, and many other observations, raise questions such as : Where does the protein discriminate against CO ? How does the binding process proceed?

The simplest model, accepted till about 20 years ago, described the binding as a one-step process, represented by a static double well. S denotes the solvent and A the bound state at the heme iron. Such a model does not answer the questions. An improved model came from experiments performed over wide ranges in temperature and time.

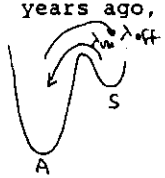

27.2 The "Single-Particle" Three-Well Model.

We have discussed the low-temperature rebinding data in Section 23.2. A set of rebinding data after flash photolysis are given in Fig. 23.5. The curves shown extend up to 160 K. Data for the binding of CO to Mb at higher temperatures are given in Fig. 27.1.[2]

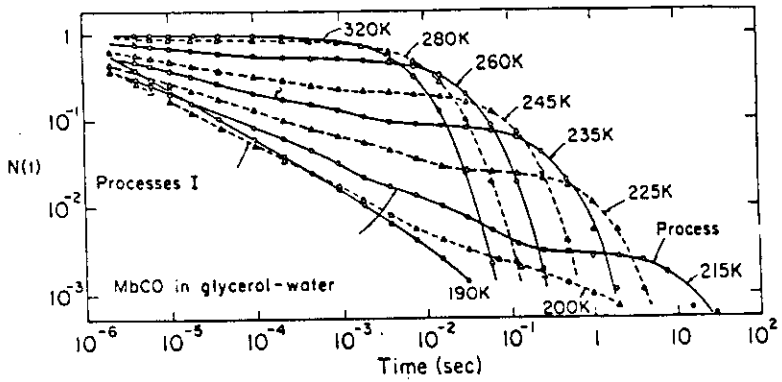

Fig. 27.1. Rebinding of CO to Mb after flash photolysis.[2] Data at lower T are shown in Fig. 23.5.

The figures 23.5, 27.1 and 27.2 together show that rebinding after photodissociation is more complicated than anticipated; a two-well model cannot describe the various processes seen in these data. We must therefore expand the two-well model.

Physicists love model building. A model is not a full theory, but a picture that encompasses the known experimental facts and permits a **quantitative** description of the observations. A model also must have predictive power and suggest new experiments. Some of the predictions will check with the

[2] R.H. Austin et al., Biochemistry **14**, 5355 (1975).

additional measurements, some will not. In steps, a model is then improved and strengthened, or disproven and forgotten. Here we build an initial model based on a combination of the flash photolysis results with structural features obtained by X-ray and neutron diffraction and also with molecular dynamics calculations.

We first consider the **flash photolysis** data. While Figs. 23.5 and 27.1 show "fine structure", the essential features can be summarized as shown in Fig. 27.2. Two different processes

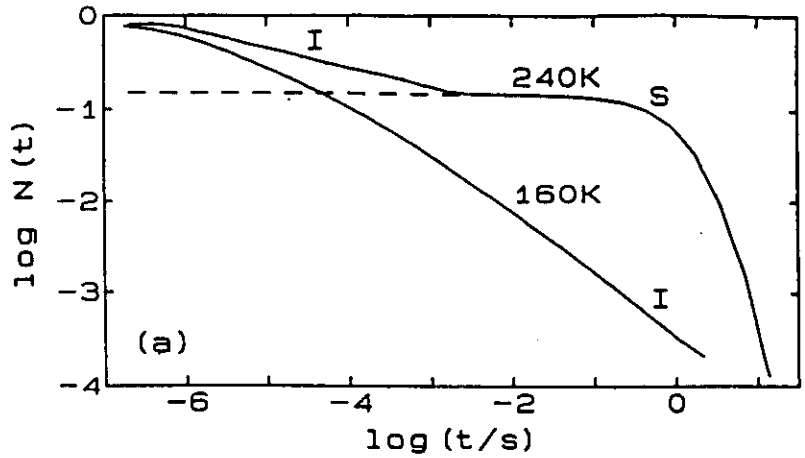

Fig. 27.2. The dominant features of the flash photolysis data at low and at high T.

can be recognized, I and S:

Process I (for Internal) occurs alone below about 180 K. A typical curve at 160 K is shown in Fig. 27.2. Process I is nonexponential in time; an explanation of the nonexponential characteristics has in terms of substates of tier 1 has been given in Section 23.2. The temperature dependence between about 40 and 160 K can be described by an Arrhenius relation. Below about 40 K, tunneling becomes important. Above about 160 K, relaxation sets it. Tunneling has already been treated in Section 25.4; relaxation will be considered below in Section 27.5.

Process S (for Solvent) is visible at long times at 240K in Fig. 27.2. S is approximately exponential in time and it is proportional to the ligand (C)) concentration in the solvent after the photoflash. As we will see later, the temperature dependence of S cannot be described by an Arrhenius law.

Next we consider the structure of Mb. A crude cross section through Mb is given in Fig. 4.8; the general arrangement of the α helices and the heme group is shown in Fig. 4.11. The electron density map near the heme as seen by X rays is reproduced in Fig. 27.3. [3] [4] (Note, however, that the protein is not Mb, but the separated beta chain of hemoglobin.)

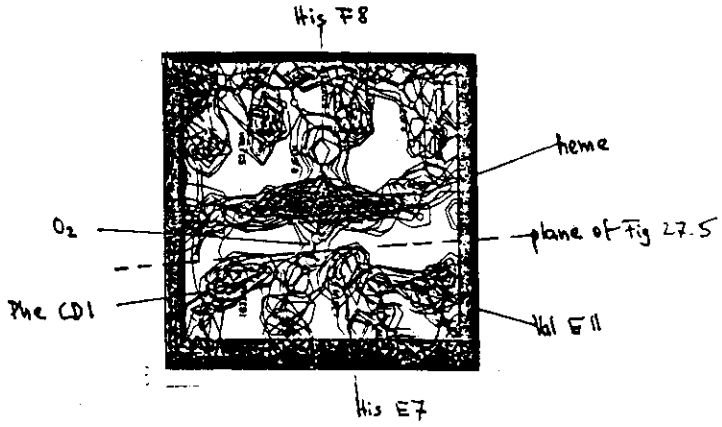

Fig. 27.3 Electron density map around the heme group in the separated beta chain of hemoglobin.[3] The bound $)_2$ can be recognized.

Fig. 27.4 displays the electron density map of MbCO, as obtained by neutron diffraction.[5] Both the X-ray and the neutron structure demonstrate that the bound ligand sits in a pocket and is prevented from easily moving to the outside by the protein structure.

While the electron density maps give an impression of the structural arrangement , they do not tell us directly about the barriers that a ligand encounters while moving through the protein. An understanding of this aspect is obtained through molecular mechanics. In this approach, the motion of a ligand is simulated on a computer. Fig. 27.5 , from calculations of Case

[3] S.E.V. Phillips, J. Mol. Biol. **142**, 531 (1980).

[4] B. Shaanan, J. Mol. Biol. **171**, 31 (1983).

[5] X. Cheng and B. P. Schoenborn, J. Mol. Biol. **220**, 381 (1991).

Fig.27.4 The heme environment in MbCO as determined by neutron diffraction.5

and Karplus[6], gives the nonbonded potential seen by a test particle in a plane parallel to the heme and displaced by 3.2 Å from it in the direction of the distal histidine. The approximate position of this plane is indicated in Fig. 27.3. The contour lines give the interaction energy between the free ligand and the protein. The open circles give the projection of nearby atoms onto the plane of the figure.

The flash photolysis data together with the structural information suggest a "multi-barrier" model for the association and dissociation of small molecules.[2] Binding at low T implies the existence of a barrier at the heme. The closed protein structure around the heme pocket points to the existence of a second barrier between solvent and heme pocket. A ligand, on binding from the solvent, should consequently move on a reaction potential as shown in Fig. 27.6.

S in Fig. 27.6 represents the situation with the ligand in the solvent,B with the ligand in the heme pocket, and A with the ligand covalently bound to the heme iron. In this simplest

[6] D.A. Case and M. Karplus, J. Mol. Biol. **132**, 343 (1979).

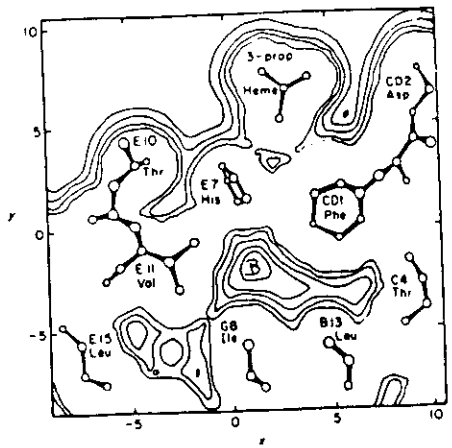

Fig. 27.5. Myoglobin contour map of the plane parallel to the heme and displaced 3.2 Å from it toward the distal histidine. Contours are at 376, 188, 42, 0, and -12 kJ/mol relative to the ligand at infinity. The highest contours are closest to the atoms. (Case and Karplus [6]).

realistic model, we assume that the reaction energy surface is fixed and independent of time and temperature. In physicists terms, it is a single-particle model. Such models are usually the first step to an understanding and to more sophisticated models.

The situation in Fig. 27.6 is described by the scheme

$$A \underset{k_{BA}}{\overset{k_{AB}}{\rightleftharpoons}} B \underset{k_{SB}}{\overset{k_{BS}}{\rightleftharpoons}} S \ . \tag{27.1}$$

The differential equations describing the motion of a ligand are

$$\begin{aligned}
\frac{dN_A(t)}{dt} &= -k_{AB}N_A(t) + k_{BA}N_B(t) \\
\frac{dN_B(t)}{dt} &= k_{AB}N_A(t) - k_{BA}N_B(t) - k_{BS}N_B(t) + k_{SB}N_S(t) \\
\frac{dN_S(t)}{dt} &= k_{BS}N_B(t) - k_{SB}N_S(t) \ ,
\end{aligned} \tag{27.2}$$

with the normalization

$$N_A(t) + N_B(t) + N_S(t) = 1. \tag{27.3}$$

Immediately after photodissociation, the ligand is assumed to be in the heme pocket, B , so that the initial conditions for ligand binding are

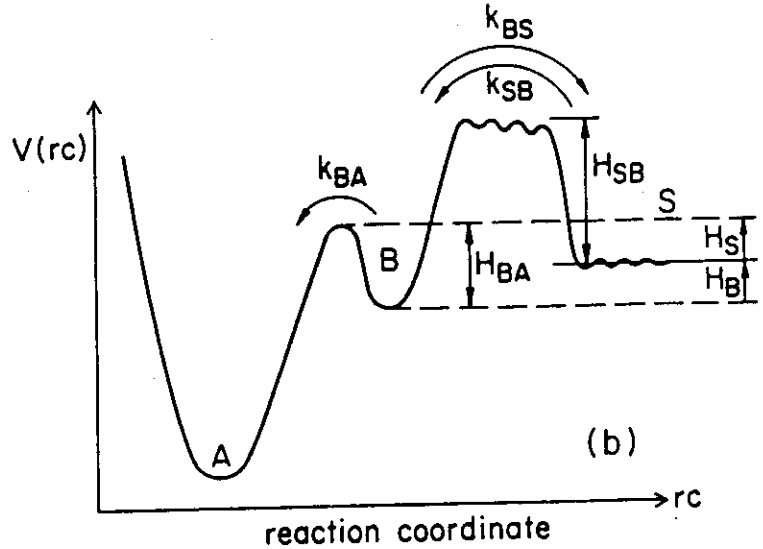

Fig. 27.6 The reaction energy landscape for motion of a ligand in a fixed (static) potential.

$$N_B(0) = 1, \ N_A(0) = N_S(0) = 0. \tag{27.4}$$

These conditions are valid at the ligand concentrations used in most experiments. The general solution of Eq. (27.2) is straightforward, but lengthy.[7] In most heme proteins, ligand in well A are tightly bound and thermal dissociation is much slower than any other reaction so that we can set

$$k_{AB} \approx 0. \tag{27.5}$$

Moreover, binding from the solvent is much slower than any other step so that we can also set

$$k_{SB} \ll k_{BA} \ , \ k_{BS} \ . \tag{27.6}$$

7 A.A. Frost and R.G. Pearson. **Kinetics and Mechanism** (John Wiley, NY) (1953).

Experimentally one observes the survival probability N(t), i.e. the fraction of proteins without bound ligand at time t after photodissociation,

$$N(t) = 1 - N_A(t) = N_B(t) + N_S(t). \qquad (27.7)$$

With Eqs.(27.3) - (27.7), N(t) becomes

$$N(t) = N_I \exp\{-\lambda_I t\} + N_S \exp\{-\lambda_{on} t\}, \qquad (27.8)$$

where

$$N_I = k_{BA}/(k_{BA} + k_{BS}) \ , \ N_S = k_{BS}/(k_{BA} + k_{BS}), \qquad (27.9)$$

$$\lambda_I = k_{BA} + k_{BS} \ , \qquad \lambda_{on} = k_{SB}\, k_{BA}/(k_{BA} + k_{BS}). \qquad (27.10)$$

We interpret the first term in Eq.(27.8) as describing the internal process I in Fig. 27.7, the second term as characterizing the solvent process S.

The rate coefficients k_{SB} and λ_{on} are second-order rate coefficients and depend on the CO concentration in the solvent. As pointed out above, it is best to use pseudo-first-order rate coefficients, with units s^{-1}, for a given partial pressure of the ligand gas above the solvent and in equilibrium with the solvent.

Use of the Eqs. (27.7) to (27.10) is straightforward. Nevertheless, it is helpful to have a simple picture from which one can obtain physical insight. Fig. 27.7 gives such a picture. It describes the three-well system in terms of

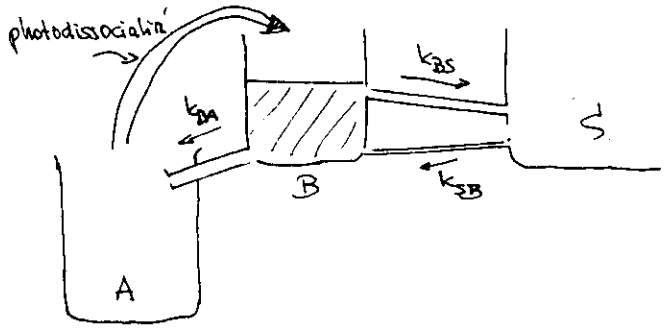

Fig. 27.7 A model for the three-well system.

three water reservoirs . At time t=0, all water is pumped from A to B. Water will then flow from B back to A and also to S. The total outflow consequently is given by the rate coefficient λ_I. The fraction that flows back to A is given by $k_{BA}/(k_{BA} + k_{BS}) = N_I$. The first term in Eq.(27.8) thus is explained. The fraction that flows out to S is given by N_S, and it returns with the rate coefficient k_{SB} to B. From B, the fraction N_I rebinds so that λ_{on} is indeed given by Eq.(27.10).

Control of Association-General Remarks. We can now ask the question : what controls the association rate λ_{on}, the step B→A at the heme or the transition S→B from the solvent to the heme pocket? The question can be answered unambiguously by measuring N_S. N_S is given by the value of $N_S(t)$, extrapolated back to t = 0. With Eqs.(27.9) and (27.10), the two limiting cases for $N_S(0)$ are

$$\text{i)} \quad N_S \approx 1 \ \rightarrow \ k_{BA} \ll k_{BS} \ \rightarrow \ \lambda_{on} \approx k_{BA}\left(\frac{k_{SB}}{k_{BS}}\right). \qquad (27.12)$$

$$\text{ii)} \quad N_S \ll 1 \ \rightarrow \ k_{BA} \gg k_{BS} \ \rightarrow \ \lambda_{on} \approx k_{SB}.$$

In case i, three rate coefficients control the association rate and a single measurement alone cannot determine all of them. In case ii, the rate limiting step is at the entrance to the heme pocket and the rate coefficient k_{SB} can be determined unambiguously.

The static three-well model can be used to evaluate the flash photolysis data. However, a number of problems remain:

1. The rate coefficient k_{BA} is, at least below about 180 K, not single-valued. As shown in Section 23.2, in particular in Fig. 23.5, the barrier between B and A must be described by a distribution. This fact must be taken into account in evaluating the experimental data.

2. Using linear differential equations as in Eq.(27.2) is valid as long as the ligand concentration in the solvent is large enough so that it can be considered constant during the binding process, but not so large that the probability of finding two or more ligands inside the protein becomes appreciable. If [L] is small, binding from the solvent is not exponential in time. If [L] is very large, a stochastic theory must be used.[7 8 9 10]

---

[8] N. Alberding, H. Frauenfelder, and P. Hanggi, PNAS **75**, 26 (1978).

[9] P. Hanggi, J. Theor. Biol. **74**, 337 (1978).

[10] R.D. Young, J. Chem. Phys. **80**, 554 (1984).

3. In Fig. 27.2, the internal process I is slower at 240 K than at 160 K. This result is puzzling and it was initially explained as being due to at least one additional deep well along the reaction coordinate in Fig. 27.6.[2] We will see later that relaxation accounts for the slowing of process I.

4. We have pointed out a few times that the protein does not show an entrance or exit path in its static structure. Motion into and out of the heme pocket must therefore be a dynamic process and a static reaction energy landscape is inadequate.

5. One other puzzle occurs when the photodissociation and rebinding of CO and O_2 are compared. The quantum yield of CO is essentially 1, but appears to be only about 0.4 for O_2.

6. Viscosity, which could be expected to play a major role if large motions determine entrance and exit, appears to have only a small effect on ligand binding at room temperature.

7. In Hb, the Bohr effect , namely the dependence of O_2 binding on pH, is well known. Mb, in contrast, has long been assumed not to show a pH dependence. It does, however. Why?

These are just a number of questions that are not answered by the model of Fig. 27.6. In the following, we clear up some of the problems, but add already a word of warning here. Many problems are not fully solved, and some of the answers given here remain to be verified.

27.3 Kinetic Hole Burning.

As pointed out in Section 23.2, spectral lines are inhomogeneously broadened and the peak of a homogeneous component may be a marker for a CS. The situation is sketched in Fig. 27.8. Substates thus may be mapped onto a particular wavenumber as indicated in panels a and b. However, CS also map onto the distribution g(H) of the activation barrier at the heme iron, a ↔ c. The particular activation energy g(H), in turn, gives rise to a rebinding rate k_{BA}, as indicated in c → d. If correct, we should thus be able to establish the entire mapping shown in Fig. 27.8 and connect CS (a), spectroscopy (b), structure (c), and function (d). Such a mapping is indeed possible.[11 12 13] The first problem is to find a suitable spectral marker. Fortunately, in Mb such a marker exists- band III. Band III, a charge-transfer transition near 760 nm (13 000 cm^{-1}) shows up only in the deligated Mb, for instance in deoxy Mb and in Mb^*. Here Mb^* denotes the state of MbCO immediately after photodissociation. With the band selected, mapping involves a few separate steps:[13]

---

[11] B.F. Campbell, M.R. Chance, and J.M. Friedman, Science **238**, 373 (1987).

[12] N. Agmon, Biochemistry **27**, 3507 (1988).

[13] P. J. Steinbach et al., Biochemistry **30**, 3988 (1991).

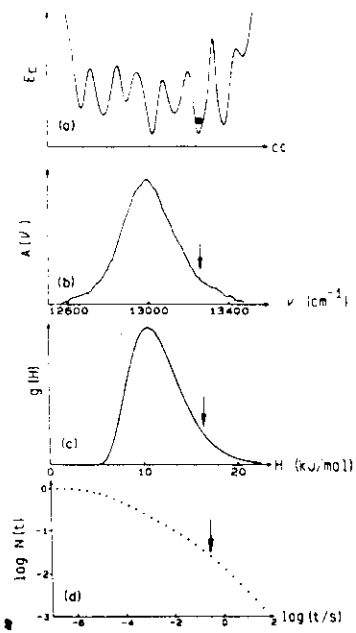

FIGURE 27.8 Connections among the conformational energy landscape (a), the inhomogeneously broadened spectral band III (b), the activation enthalpy distribution $g(H_{BA})$ (c), and the nonexponential rebinding $N(t,T)$ (d).

1. Connect k_{BA} and v'. Here v' is the first moment (peak wave number) of a homogeneous component of band III. To do so, the inhomogeneous band is measured as a function of time after photodissociation. The proteins that rebinding between times t1 and t_2 rebind with a rate approximately given by $2/(t_1 + t_2)$. The difference spectrum, shown in Fig. 27.9 , of the spectra of band III at the times t_1 and t_2 yields the corresponding peak wave number v'.

2. Connect k_{BA} and H. At temperatures where tunneling is unimportant, H and k are simply related by the Arrhenius relation. At lower T, tunneling must be taken into account.[17] The result of such a procedure is shown in Fig. 27.10.

3. Connect H_{BA} and v'. This connection is now straightforward and the result is shown in Fig. 27.11.

It is by no means trivial that H and v are so clearly and linearly related. The reason may actually be simple: The barrier for rebinding may depend on the out-of-plane distance of the heme iron. The position v' may depend on the same distance.

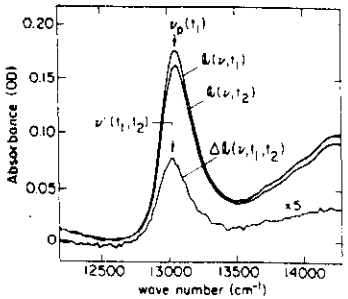

FIGURE 4: Rebinding of an inhomogeneous band. $a(\nu,t_1)$ is the average of five scans of band III taken consecutively after photodissociation of MbCO in pH 7, 75% glycerol/buffer (v/v) at 42 K. $a(\nu,t_2)$ is the average of five scans taken immediately after $a(\nu,t_1)$. The peak wavenumber $\nu'(t_1,t_2)$ of the difference spectrum $\Delta a(\nu,t_1,t_2)$ differs from $\nu_p(t_1)$.

Fig. 27.9

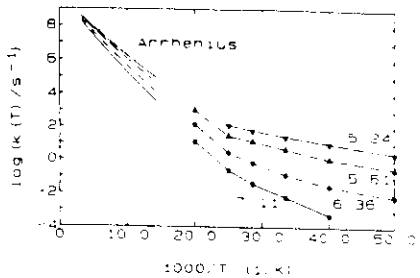

FIGURE 7: Rate coefficient $k(H,T)$ for the binding of CO at the heme iron, parametrized by the barrier height H, as a function of $10^3/T$. Data above 70 K assume an Arrhenius relation, eq 6.

Fig. 27.10

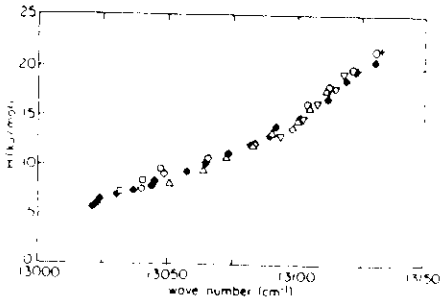

FIGURE 8: Connection between the barrier height H for the binding at the heme iron and the corresponding band position ν' of the homogeneous component of band III. Sample: MbCO in 75% glycerol/buffer solution at pH 7. Filled symbols denote data obtained from fitting the OLIS–Cary measurements, open symbols denote flash photolysis data. Uncertainties are typically less than ±5 cm⁻¹.

Fig. 27.11

27.4 Relaxation and Barrier Height

The connection between H and v' displayed in Fig. 27.11 provides us with a clue to the solution of another puzzle. The puzzle is shown in Fig. 27.2 where process I at 240 K is faster than at 160 K. The clue is connected to an observation by Iizuka and collaborators who first noticed that the band III in Mb* is red-shifted by about 10 nm from its position in Mb[14]. The shift actually depends on pH and for the sample represented by Fig. 27.11 it is somewhat smaller, about 120 cm^{-1}. The simplest interpretation is now as follows. Mb* and Mb have a slightly different structure. The structure influences the position of band III and of the barrier H_{BA}. As Mb* relaxes towards Mb, band III blue-shifts by about 120 cm^{-1}. Fig.27.11 then implies that the barrier H_{BA} increases by about 12 kJ/mol! The spectroscopic evidence predicts that the barrier for rebinding of CO in the fully relaxed deoxy structure should be about 11 kJ/mol higher than measured at low T. Fig. 23.6 shows that the peak of the distribution g(H) for CO binding to Mb is about 11 kJ/mol. At room temperature, the peak consequently should be at about 22 kJ/mol and rebinding to the heme iron from the pocket should be slower than extrapolated from the low temperature data.

Such a relaxation of the protein with concomitant increase in barrier height has been predicted by Agmon and Hopfield.[15] Does this relaxation with shift in the barrier energies really occur? And if so, how can it be described? To answer this question, we look carefully at the rebinding data between 160 and 210 K, shown in Fig. 27.12.

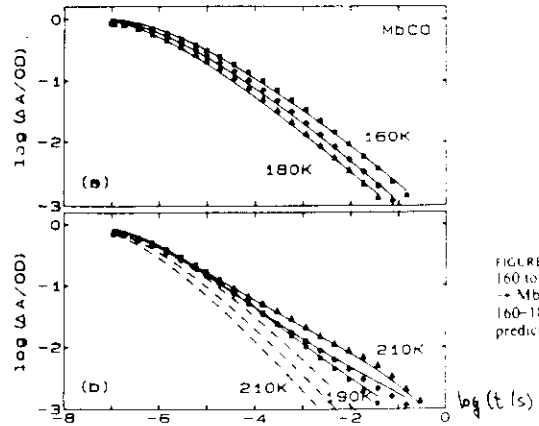

27.12

FIGURE 9: Data and fit to the relaxation model for MbCO from 160 to 210 K. The *solid lines* show the fit with the *relaxation* Mb* → Mb taken into account by using eq 23. (a) Internal process I at 160–180 K. (b) Process I at 190–210 K. The *dashed lines* give the prediction for process I if *no relaxation* Mb* → Mb occurs.

[14] T. Iizuka, H. Yamamoto, M. Kotani, and T. Yonetani, Biochim. Biophys. Acta 371, 1715 (1974).

[15] N. Agmon and J.J. Hopfield, J. Chem. Phys. 79, 2042 (1983).

The solid lines in Fig. 27.12 a are fits to the low-temperature $g(H_{BA})$; they fit the data very well. Above 180 K, however, rebinding is slower than predicted by extrapolating the low-T data. At 210K, for instance, rebinding at N(t) = 0.01 is about 100 times slower than expected. However, rebinding is still nonexponential in time! This observation suggests that the entire distribution shifts to higher activation enthalpies. To describe the shift in the activation energy spectrum caused by the relaxation $Mb^* \rightarrow Mb$, we use the analogy to glasses.

We consider first the relaxation $Mb^* \rightarrow Mb$ in which process I slows as the barrier H_{BA} increases. In analogy to the relaxation phenomena in glasses, we describe the change in H_{BA} by a relaxation function $\Phi^*(t,T)$ and write

$$H_{BA}(t,T) = H_0 + \Delta H^*[1 - \Phi^*(t,T)], \qquad (27.13)$$

where t is the time after photodissociation. The rate coefficient for CO rebinding, becomes time dependent,

$$k_{BA}(H(t,T),T) = A_{BA}(T/T_0)\exp[-H_{BA}(t,T)/RT]. \qquad (27.14)$$

The differential equation for binding, $dN_I(t,T) = -k_{BA}(H(t,T),T)\,N_I(t,T)dt$, leads to the survival probability $N_I(t,T)$ for a single barrier $H_{BA}(t,T)$,

$$N_I(t,T) = \exp[-\int_0^t dt' k_{BA}(H(t',T),T)]. \qquad (27.15)$$

The survival probability for a protein ensemble becomes

$$N_I(t,T) = \int dH_0\, g(H_0) \exp[-\int_0^t dt' k_{BA}(H(t',T),T)]. \qquad (27.16)$$

Eq. (16) is valid if $k_{BA} >> k_{BS}$. This condition holds below about 220 K. The distribution function $g(H_0)$ is time and temperature independent, but the rate coefficient $k_{BA}(H(t',T),T)$ depends on time. As relaxation function $\Phi^*(t,T)$, we use Eq. (25.38) with $\kappa^*(T)$ given by Eq. (25.40). The fit of Eq. (17) to the data up to 210 K, shown in Figure 17.12, yields $\Delta H^* \approx 11$ kJ/mol, $A^* \approx 10^{18} s^{-1}$, $E^* \approx 10$ kJ/mol, and $\beta^* \approx 0.21$. The model describes the behavior of process I between 160 and 210 K very well and ΔH^* agrees approximately with the value of $\Delta H = 12$ kJ/mol obtained from the shift of the band III. The extrapolation to room temperature gives $\kappa^*(293\ K) \approx 5 \times 10^{10}\ s^{-1}$, consistent with the observations that the resonance Raman spectrum of Mb^* is not relaxed within 30 ps (Dasgupta et al., 1985)[16], and that band III has shifted to the deoxy position by 10 ns (Sassaroli & Rousseau, 1987)[17]. The relaxation function $\Phi^*(t,293\ K)$, calculated with the parameters given above, is consistent with the molecular dynamics computation of the iron motion by Karplus and collaborators (Petrich et al., 1990)[18]. Similar relaxation processes have been observed by Friedman (1985)[19] in hemoglobin. The parameters for the rate coefficient $\kappa^*(T)$ are similar to those for glass relaxations. The value of β^* demonstrates that the shift is nonexponential in time. We justify the use of Eq. (25.40) for the temperature dependence by also fitting the data around T = 200 K to an Arrhenius relation. The result, $A \approx 10^{33}\ s^{-1}$ and $E \approx 120$ kJ/mol, implies that an Arrhenius relation is inappropriate.

---

[16] S. Dasgupta et al., Biochemistry **24**, 5295 (1985).

[17] M. Sassaroli and D.L. Rousseau, Biochemistry **26**, 3092 (1987)

[18] J.W. Petrich et al., Biochemistry **30**, 39 (1991).

[19] J.M. Friedman, Science **228**, 1273 (1985).

The result given in Fig. 27.12 is surprising: The distribution shifts without collapsing. Such a behavior supports the notion of a hierarchy of substates and implies that the shift $Mb^* \rightarrow Mb$ occurs in a different tier of the hierarchy than the one responsible for the nonexponential rebinding. We assign the motion $Mb^* \rightarrow Mb$ to tier 2, the distribution $g(H_{BA})$ to tier 1.

27.5 Entrance and Exit of Ligands.

We now return to the question how ligands enter and leave Mb. Consider first photodissociation. After the Fe-L bond is broken, the CO or O_2 molecule sits in the potential well B, shown in Figs. 27.5 and 27.6. How can it escape to the outside? The obvious path is between His E7 and Val E11, but the potential barrier calculated by Case and Karplus[6] for a static protein is of the order of 400 kJ/mol, much too high to be overcome by thermal activation. The problem has been known for along time: The X-ray structures of Mb and Hb show no obvious opening or channel.[20] [21] [22] Ligand binding can only occur through dynamic effects. The protein must breathe in order to let the ligand escape.

The fact that ligand binding involves protein motions is made dramatically clear by the binding of isonitrile, which are rather large. Consider for instance n-butyl,

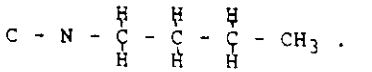

This ligand binds not much slower than CO.[23] Rebinding data are shown in Fig. 27.13. The behavior below about 260 K is rather different from that of Co or O_2 binding : Binding is much slower, but there appears to be an absorbance change that is much smaller than expected. This small change suggest that a very fast process takes place even at low T at times shorter than 1 µs. Such fast processes occur in a variety of situations and we return to them in Section 27. 8. At temperatures above about 280 K, a solvent process S appears. At 300 K, the association rate coefficient is about $\lambda_{on} \approx 200\ s^{-1}$, only about three times smaller than that of CO (Table 27.1). To admit ligands as large

---

[20] J.C. Kendrew et al., Nature **185**, 422 (1960).

[21] M. F. Perutz and F. S. Matthews, J. Mol. Biol. 21, 199 (1966).

[22] T. Takano, J. Mol. Biol. **110**, 537 (1977).

[23] P. I. Reisberg and J. S. Olson, J. Biol. Chem. 255, 4151 (1980).

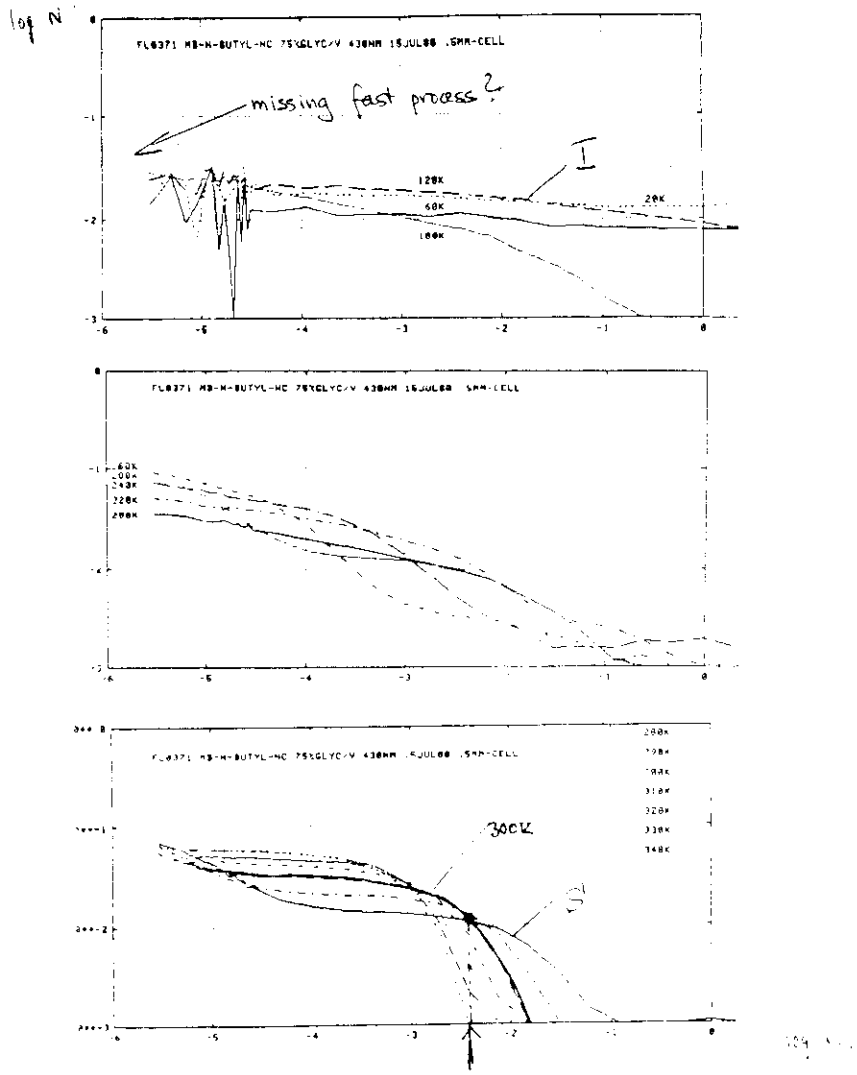

Fig. 27.13 Rebinding of n-butyl to Mb after photodissociation.

as n-butyl, Mb must open a rather large channel. The binding if isonitriles therefore is another fact that testifies to the importance of protein motions.

Fig. 27.13 suggests that the binding of isonitriles poses a number of challenging questions. The nonexponential rebinding at temperatures as high as 280 K extends to at least 10 μs, implying the existence of very slow conformational motions. Much work remains to be done to explore the binding of isonitriles.

The contour map in Fig. 27.5 raises the question : Where is the pathway for entry and exit? There is likely to be more than one escape route, but a major pathway has been found in an elegant X-ray diffraction experiment by Dagmar Ringe and collaborators.[24] Their approach can be called "Ariadne's thread".[25]

To find the pathway, they use a doorstop, a molecule large enough to keep the protein path open. Phenylhydrazine binds to myoglobin. On binding, the molecule loses its tail and the phenyl ring remains. The ring is large

Phenylhydrazine 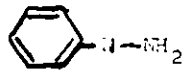

enough to "keep the door open". The results of the diffraction experiment are given in Fig. 27.14. The data indicate that two groups rotate out of the way to provide access to the binding site: The first is the isopropyl group of Val 68 (E 11), the second the imidazole group of His 64 (E 7). In both cases, the new position of the group is accommodated by an existing cavity in the structure. The rotation of the imidazole group of His E 7 forces the side chain of Arg 45 (CD3) to rotate outward. These motions together form a channel from the surface to the interior of the protein. The channel is almost parallel to the heme plane.

[24] D. Ringe, G.A. Petsko, D.A. Kerr, and P. R. Ortiz de Montellano, Biochemistry **23**, 2 (1984).

[25] Ariadne, a daughter of Minos, gave Theseus a thread to find his way out of the labyrinth.

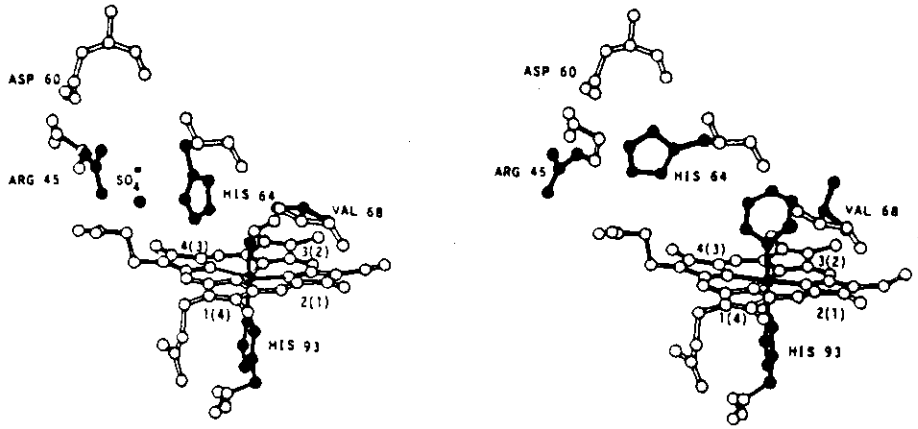

A. Drawing of the residues around the heme in metmyoglobin that are involved in the formation of a channel when phenylhydrazine is added. The iron atom, bound water molecule, sulfate ion, and amino acid side chains undergoing changes are indicated in black. The pyrrole numbering is given according to the two conventions: Protein Data Bank (metalloprophyrin).

B. Drawing of the residues around the heme in myoglo with phenyl bound to the iron atom. Asp-60(E3) and Arg-45(CI are close enough to each other to form an ion pair. The iron at phenyl group, and amino acid side chains, which have moved a consequence of the phenyl group, are indicated in black.

Fig. 27.14. From Ringe et al., ref. 24.

27.6 The Effect of Viscosity.

Additional evidence for the dynamic character of the entrance and exit comes from the dependence of the corresponding rate coefficients on viscosity. Some groups claimed that viscosity did not influence CO binding. They had measured λ_{on} at room temperature and found essentially no effect of viscosity. We can understand the absence of a viscosity effect easily. Near room temperature, $N_S \approx 1$ and the association rate is given by Eq.(27.12) as

$$\lambda_{on} = (k_{SB}/k_{BS})\, k_{BA}.$$

Binding at the heme is not influenced by viscosity. Opening of the pocket is a gating process described in Section 25.5. The rate of the gate opening is affected by viscosity, but the ratio of the in and out rates is viscosity independent.[26]

The viscosity dependence can be studied at high viscosities and/or low temperatures where $N_S \ll 1$. Eq. (27.9) then gives

$$\frac{\lambda_{on}}{N_S} \approx k_{SB} / k_{BS}\, k_{BA}.$$

[26] D. Beece et al., Biochemistry **19**, 5147 (1980).

These relations indicate that the viscosity dependence of k_{SB} and k_{BS} can be studied, assuming that k_{BA} is viscosity independent.[13] As an example, we show in Fig. 27.15 the dependence of N_S, and hence k_{BS}, on the solvent viscosity. It is obvious that N_S

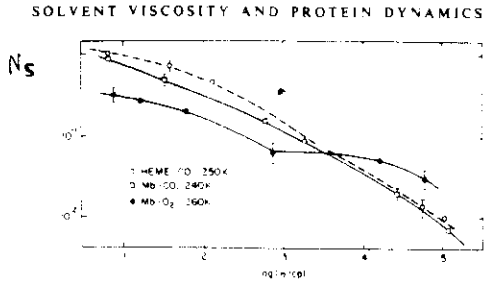

Fig. 27.15. Viscosity dependence of the fraction N_S.[26] The curve gives the viscosity dependence of k_{BS}.

depends on viscosity. The quantitative description, however, yields some new results. The Kramers equation (Section 25.3) predicts a dependence proportional to $1/\eta$ in the high-viscosity regime. The curves in Fig. 27.15 show a weaker dependence. In the high-viscosity regime, the rate coefficients can be parametrized by[26]

$$k = \text{const}\ \eta^{-\alpha} \qquad (27.17)$$

with $\alpha = 0.5$. The solvent viscosity appears to be damped. Some theoretical attempts to explain such a dependence[27], but far more experimental and theoretical work is needed to understand the problems fully.

More work is also required to connect the observed rates to the characteristics of the energy landscape and to decide in which tiers the various motions occur. There also exist an number of other connections, for instance to allostery.

[27] W. Doster, Biophys. Chem. **17**, 97 (1988).

27.7 Reaction and conformation coordinate.

Explain reaction and conformational coordinate. Conformational energy landscape temperature independent? But reaction energy landscape, because of the influence of CC, highly temperature dependent.

Describe CO binding at all T. Changes in the reaction coordinate.

27.8 Substates of Tier 0

Recall A states, different rebinding.
TDS
The importance of CS0 for all kinds of protein functions.
The exchange $A_0 \leftrightarrow A_1$. Extension of the low T P jump data. Fit to the entire set. Data. Viscosity dependence.

27.9 Fast rebinding processes

The O2-CO puzzle.
I*
Explanation
Fast processes in Mb
Difference O_2 and CO
Steric and electronic control

27.10 Mutants

27.11 Neglected topics.

Raman
CD, MD,..
What causes and determines the barrier BA - B ?